INVESTIGATION OF A BIOMIMETIC HEAT PIPE DESIGN FOR IMPROVED HEAT TRANSFER IN SPACE RADIATORS

by

Owen Telford

Submitted in Partial Fulfillment
of the Requirements for the Degree of
Masters of Science in Mechanical Engineering.

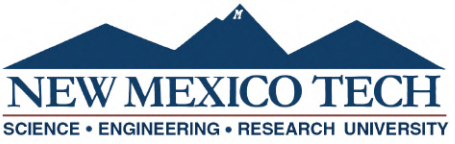

New Mexico Institute of Mining and Technology
Socorro, New Mexico
July, 2023

This thesis is dedicated to...

Every single person that has supported me through this. I have always underestimated my abilities in my academic career, but this work has proven to me that I am capable of doing hard things. I would like to dedicate this to a few special individuals that deserve proper recognition.

Kaitlyn Faith King-Telford. You are my wife, my best friend, my adventure partner. You sacrificed so much for me to come here. You took a leap of faith with me when we came out here, fully knowing what I am capable of and showing me how to get through even the most difficult of struggles. I know this has been just as hard for you, but we made it through this. We can do hard things together and as long as we're by each other side, we will achieve all of our dreams.

Thane and Lilian Telford, my amazing parents. I was literally born a miracle and you both have made me feel special my entire life. You have been nothing but supportive of my dreams and life goals, even if that takes me to places very far away. Leo and I are lucky to call you our parents. Even when each of you has been through life's struggles yourself, you are always there to listen and tell me that you're proud. Thank you for a great childhood and the tools to prepare me for adulthood.

Leo Telford, my brother. Even though we have always had a large gap in age, you made me feel like an equal. We have countless laughs and memories, that I will never forget. You taught me how to be a man and how to stand up for myself. You truly contributed to who I am and I'm proud to call you my brother.

To every member was a part of my carpool as I commuted over an hour from Albuquerque to New Mexico Tech three to four times a week. Shannon Ruyon, Dr. Christopher ChoGlueck, Dr. Youngman Lee, Mitchel Tappen, and Dr. Marina Choy. You all are amazing people through and through. Thank you for sharing your life stories and experience. I will cherish all of the early mornings and tired evenings together.

Brandon Turner, you were my first friend at Tech. That first semester was so difficult and I questioned a lot during that time. We spent a lot of time studying, and I would have never made it out of that semester without our teamwork. Thank you for showing me how to be a graduate student.

Thank you to all of the great people I've met at NMT during my time, including the professors and students I was able to get to know while a student, TA, and STEM Fellow.

Owen Telford
New Mexico Institute of Mining and Technology
July, 2023

ACKNOWLEDGMENTS

I would like to express gratitude to my Advisor. Dr. Ashok Ghosh for giving me the opportunity to attend NMT as well as his support throughout my time here. I would also like to thank my committee members, Dr. Cheol Park and Dr. Donghyeon Ryu for agreeing to join my committee along with their insights and knowledge. I want to thank Ryan Flynn for all of his help in conducting experiments and creating the testing apparatus as well as his thoughts and suggestions during the project. He has become a close friend and I wish him the best as he starts his own graduate journey. Dr. Ali Siahpush for giving advice and encouragement throughout. I want to mention a few departments at NMT that loaned supplies and other help. The NMT Mechanical Engineering Department for ordering supplies and for the data logging device. The NMT Civil Engineering Department for letting us use their Flir Thermal Camera. The NMT Chemistry Department for the hot plate and beakers. The NMT Physics Department for the anemometer. The NMT Fab Lab for various tools, advice, 3D printing assistance, and allowing access to the machine shop. Finally, this thesis was based upon work supported by the New Mexico Space Grant Consortium Research Initiation Grant (RIG) through the National Aeronautics and Space Administration (NASA) Cooperative Agreement No. NM-80NSSC20M0034.

This thesis was typeset with LaTeX[1] by the author.

[1]The LaTeX document preparation system was developed by Leslie Lamport as a special version of Donald Knuth's TeX program for computer typesetting. TeX is a trademark of the American Mathematical Society. The LaTeX macro package for the New Mexico Institute of Mining and Technology thesis format was written by John W. Shipman.

ABSTRACT

This thesis focuses on the investigation of biomimetic heat pipes for space radiator applications. Biomimetic heat pipes employ structures inspired by natural systems to enhance heat transfer efficiency where vapor is present. The research aims to address the need for improved heat dissipation mechanisms in nuclear space systems, where efficient thermal management is crucial. Heat pipes are passive heat transfer devices that enhance thermal management in various industries. The objective of this study is to evaluate the efficacy of a biomimetic heat pipe design compared to a traditional design, while also validating the fabrication process through comparison with an industry-made heat pipe. The methodology involves the fabrication and testing of biomimetic and traditional heat pipes using innovative hot oil bath testing methods. Thorough thermal analysis, physical experiments, and validation techniques are employed to assess the heat transfer capabilities of the biomimetic heat pipe. The tests are conducted at different temperature levels to examine the behavior and thermal performance of the heat pipes. The results indicate that the biomimetic heat pipe demonstrates superior heat dissipation capabilities, across the length. The thermal analysis and experimental data provide evidence supporting the effectiveness of the biomimetic structure in enhancing heat transfer. The findings suggest that the biomimetic heat pipe design has the potential to improve thermal management in space radiator applications. The study highlights the benefits of biomimetic design principles and their potential for future heat pipe advancements. Further study recommendations include exploring alternative materials, optimizing the testing apparatus, and improving the fabrication process.

Keywords: Heat Transfer; Heat Pipes; Space Radiator; Porous Fluid Transport; Bio-inspired;

CONTENTS

LIST OF TABLES

LIST OF FIGURES

LIST OF ABBREVIATIONS

RIG	New Mexico Space Grant Consortium Research Initiation Grant
NASA	National Aeronautics and Space Administration
LANL	Los Alamos National Lab
HP	Heat Pipe
THP	Traditional Heat Pipe
BioHP	Biomimetic Heat Pipe
MHP	Manufactured Heat Pipe
ASTM	American Society for Testing and Materials
ISS	International Space Station
NEP	Nuclear-Electric Propulsion
HVAC	Heating, Ventilation, and Air Conditioning
FEA	Finite Element Analysis

NOMENCLATURE

ΔP_1	Pressure drop that drives wick flow
ΔP_g	Pressure drop due to orientation of gravity
ΔP_v	Pressure drop that drive vapor flow
$\Delta P_{c,max}$	Pressure difference between the two sides of the HP
ΔP_{va}	Pressure difference in the adiabatic zone
ΔP_{vc}	Pressure difference in the condenser
ΔP_{ve}	Pressure difference in the evaporator
$\dot{m}$	Mass flow rate
$\dot{Q}$	Heat flux
$\dot{Q}_e$	Entrainment limit
$\dot{Q}_s$	Sonic limit
$\dot{Q}_b$	Burnout limit
$\dot{Q}_{in}$	Heat flux into the evaporator
$\dot{Q}_{out}$	Heat flux out of the condenser
ϵ	Porosity
η	Efficiency
γ	Specific Heat Ratio
λ	Diameter of the wick plus the distance between voids.
μ_1	Dynamic viscosity
μ_v	Dynamic viscosity
ϕ	Incline angle of the heat pipe
ρ_1	Density of the working fluid as a liquid

ρ_v	Density of working fluid as a vapor
σ_1	Surface tension coefficient
θ_e	Wetting value of the wick working fluid interface
A	cross-sectional area of the entire heat pipe
A_f	Flow cross-section of the wick
A_t	Area submerged in silicone oil
A_v	Cross-sectional area of the vapor region
A_w	Cross-section of the wick
A_d	Cross-sectional area of cooling duct
C_p	Heat Capacity
g	Acceleration due to gravity
h	Overall heat transfer coefficient
h_o	Coefficient of heat transfer for silicone oil
K	Wick permeability
L	Latent heat of vaporization
l_a	Length of adiabatic zone
l_e	Length of evaporator
l_{eff}	Effective length of a heat pipe
R	Thermal resistivity
r_e	Pore radius
r_v	Inner radius of the wick
r_v	Radius of vapor region
r_w	Outer radius of the wick
t_w	Thickness of wick
T_{evap}	Temperature of the evaporator
T_{oil}	Temperature of silicone oil
V_s	Speed of sound through working fluid
V_d	Velocity of air in the cooling duct

This thesis is accepted on behalf of the faculty of the Institute by the following committee:

Ashok Ghosh

Academic and Research Advisor

Cheol Park

Donghyeon Ryu

I release this document to the New Mexico Institute of Mining and Technology.

Owen Telford July 18, 2023

CHAPTER 1

INTRODUCTION

1.1 Purpose and Overview

The objective of this research, supported by the New Mexico Space Grant Consortium Research Initiation Grant (RIG), is to conduct a comprehensive comparison between a traditional two-phase heat pipe developed at Los Alamos National Laboratory (LANL) and a biomimetic heat pipe, to determine the potential for enhanced heat dissipation in the latter. To achieve this goal, physical testing was employed to directly compare the performance of the two designs. In-house heat pipe fabrication processes are utilized and verified through various tests. A comparison of an off-the-shelf manufactured heat pipe is compared to verify the adequate operation of fabricated heat pipes. The ultimate goal is to provide empirical evidence supporting the viability of the new biomimetic heat pipe design as a promising proof of concept.

The main objective of this endeavor is to develop a high-performance heat pipe capable of reliably operating at elevated temperatures up to 300 °C. Although the experimental assessments conducted within this project will not specifically reach such extreme temperatures, they will serve as a rigorous evaluation of the design's effectiveness and suitability for demanding thermal environments. Should the comparative analysis demonstrate a substantial improvement in efficiency compared to conventional heat pipes, the design can be readily adapted and scaled up by leveraging different materials while maintaining the core design principles intact. This scalability potential underscores the significance of achieving superior performance in this study, as it lays the foundation for future advancements in heat pipe technology.

The pursuit of high-temperature capabilities in this research project stems from the intention to integrate the developed heat pipe design into future thermal rejection systems for space exploration. As the demand for advanced propulsion systems, including nuclear systems, becomes prominent in deep space travel, a significant challenge arises in effectively managing the extreme temperatures associated with such systems. Conventional heat rejection methods prove inadequate in handling these elevated temperatures [1–3]. Thus, the primary aim of this research is to address this challenge by demonstrating the ability of the proposed design to withstand and efficiently dissipate heat at the anticipated temperature levels when implemented on a larger scale. By overcoming this chal-

lenge, the potential for incorporating heat pipes into advanced space missions involving nuclear systems can be realized, enabling safer and more efficient exploration of deep space.

The experimental investigation of the heat pipes involves the fabrication of two heat pipes in-house, namely the Traditional Heat Pipe (THP) and the Biomimetic Heat Pipe (BioHP), along with acquiring a manufactured heat pipe (MHP) for baseline testing. The development of the Biomimetic structure was an iterative process that took many attempts before the design that was used was finalized. The intricate details and technological aspects of heat pipe designs, operation requirements, and limits, as well as analysis techniques, including their distinguishing features, are extensively discussed in Chapter 2. It is important to note that the Biomimetic Heat Pipe incorporates a bone-inspired structure within its design, strategically placed to facilitate vapor collisions and phase change [4]. This innovative addition is theorized to contribute to the enhanced performance of the new heat pipe design.

Chapter 3 introduces the fabrication design process and the need to develop a comprehensive testing plan due to the lack of American Society for Testing and Materials (ASTM) standards for heat pipes. The chapter presents a step-by-step description of the heat pipe fabrication process, including material selection, assembly, and verification techniques.

Chapter 4 delves into the testing procedures and experimentation, outlining the data collection and compilation process using the Pico TC-08 thermocouples Data Logger. It provides insights into the experimental protocols and validation results.

In Chapter 5, detailed analysis and comparison of the results between the different heat pipe designs are presented. The chapter highlights key observations, trends, and potential errors, disparities, and efficacy of the THP and BioHP. It comprehensively evaluates the advantages and limitations of each design, shedding light on their respective strengths and areas for improvement.

Finally, Chapter 6 serves as the conclusive section of the research, summarizing the key findings and contributions. It offers a comprehensive discussion of the insights gained, implications for future applications, and recommendations for further optimization and validation of the design, fabrication, and testing processes. The chapter emphasizes the significance of the research and outlines potential avenues for future investigation in the field.

CHAPTER 2

LITERATURE REVIEW

2.1 Background

2.1.1 Space Radiator Relevance

Humanity has accomplished remarkable feats in the realm of space travel, including the launch of numerous satellites into the Earth's orbit and the historic moon landing. Furthermore, the International Space Station (ISS) serves as a testament to our ability to conduct extensive tests and research in space. Now, with our local neighborhood explored, the focus has shifted toward the vastness of deep space.

Deep space exploration has seen the deployment of various spacecraft, with Voyager 1 being a prominent example [5]. While this achievement is awe-inspiring, the prospect of sending human beings on such spacecraft remains a distant goal. Venturing beyond Earth's orbit and into deep space poses numerous challenges that must be addressed. Chief among these challenges is the need to sustain a power source capable of supporting long-duration space journeys. Unlike satellites, which require minimal power for basic operations and communication, human deep space missions demand significantly higher power levels to ensure the safety and well-being of the crew. Conventional power systems are ill-equipped to meet these demands, necessitating the development of alternative power solutions [1].

One such solution is the utilization of nuclear fission power sources. Nuclear power technology has been under development for decades and has even been incorporated into spacecraft, exemplified by NASA's SNAP-10A mission [6] However, due to funding constraints and societal concerns regarding nuclear power safety, research in this area was curtailed [6].

Looking ahead, nuclear power holds immense potential to expand the capabilities of space power systems and enable human exploration of deep space. Among the various nuclear power options, Nuclear-Electric Propulsion (NEP) emerges as the most promising for this purpose [3]. Nevertheless, NEP systems face a significant challenge in effectively managing high heat output [3].

NASA's Power and Energy Storage Roadmap [1] highlights the necessity for deep-space nuclear radiator designs capable of handling substantial heat flux while remaining lightweight.

2.1.2 Heat Pipe Technology

Heat pipes (HPs) were initially conceptualized in the early 1940s [2], but it wasn't until the late 1960s that the theory behind them started to be extensively investigated. The first published paper on the current design of a traditional two-phase heat pipe was presented by T.P. Cotter, a Los Alamos scientist, in "Theory of Heat Pipes" [2, 7]. Within a decade, Cotter's paper had garnered over 1000 references, and two international heat pipe conferences had taken place [2]. Since then, heat pipe conferences have been held regularly, and Cotter's publication remains the cornerstone of this expansive field of study.

Besides space applications, HPs find applications in a wide range of industries and possess numerous configurations [2]. They serve as effective heat management systems in both commercial and industrial settings. One of their primary functions is to cool down electrical components, ensuring optimal performance and longevity[2]. Additionally, they are employed in HVAC (Heating, Ventilation, and Air Conditioning) systems for efficient heat transfer.

One of the key advantages of heat pipes compared to other types of thermal control like heat exchangers is their ability to passively dissipate heat, eliminating the need for an external power source to operate effectively. As depicted in fig. 2.1, a traditional heat pipe exhibits four main components: the evaporator side, the condenser side, the adiabatic zone, and the wick. These elements work in harmony to facilitate efficient heat transfer and thermal management.

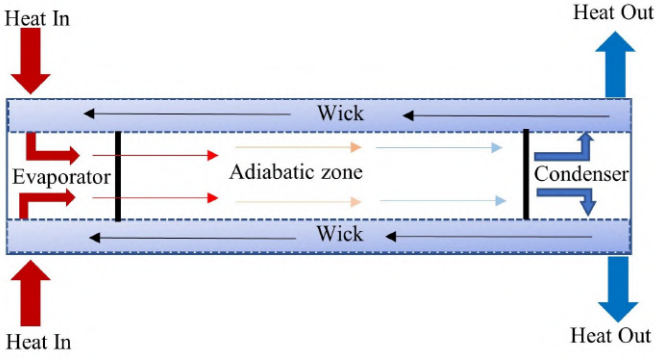

Figure 2.1: Cross-section of a Two-Phase Heat Pipe

HPs operate through a cyclic process that facilitates efficient heat transfer. The heat pipe is heated on one side. In the evaporator section, heat is transferred from the external source casing into the working fluid in the center. The working fluid within the evaporator absorbs this heat, undergoing a phase change from liquid to vapor. The vapor is then transported through the adiabatic section to the condenser side. As the vapor reaches the condenser, it undergoes another phase change back into a liquid state [8]. The condensed liquid is then transported back to the evaporator side by the wick, utilizing capillary action and pressure

differences to move the liquid. This continuous cycle allows for sustained heat dissipation, as long as the heat input remains within the design specifications of the heat pipe.

The specific requirements for the functioning of a heat pipe depend on various factors, including the choice of the working fluid, housing material, wick type, and internal structure geometry. Figure 2.1, also illustrates the standard geometry of a heat pipe, although there exist numerous variations that can alter its appearance and functionality. This is true when looking at the difference in the HPs used on the ISS [9].

Heat pipes offer a great solution that aligns with NASA's requirements [1]. These versatile passive heat radiators have already found extensive use in various space applications, most notably on the ISS. The ISS heat pipe design incorporates an aluminum housing, aluminum honeycomb wick, and ammonium as the working fluid [9]. As the ISS operates in space, water cannot be utilized as a working fluid due to the extremely low temperatures that would cause it to freeze. Additionally, the absence of natural convection in microgravity conditions poses a challenge. Fortunately, the surface tension of the fluid within the heat pipe enables sufficient flow to ensure its proper functioning, a phenomenon known as "Marangoni Convection" [10].

The Japanese ISS team conducted studies that involved creating a temperature gradient across the length of a fluid. As a result, a phenomenon known as a "Liquid Bridge" formed due to the cohesive forces within the liquid. This led to the establishment of a cycle and the observation of a convection current [10]. However, when the temperature gradient became excessively large, the current started generating eddies due to the turbulent nature of the liquid, causing the cycle to cease. This study highlights the effectiveness of heat pipes in space applications, as they rely on convective currents for their operation [10]. In relation to high-powered space applications, a detailed description showing more of the design implementations into a NEP system is shown in Appendix B.1

2.1.3 Biomimetic Influence

The goal of this research has been to investigate a bio-inspired heat pipe design that incorporates an internal structure that takes the idea from the spongy section of the bone. This smooth porous material promotes a flow cross-section that eliminates any small pockets where flow could get trapped. Figure 2.2 shows a rendering of this porous area of the bone.

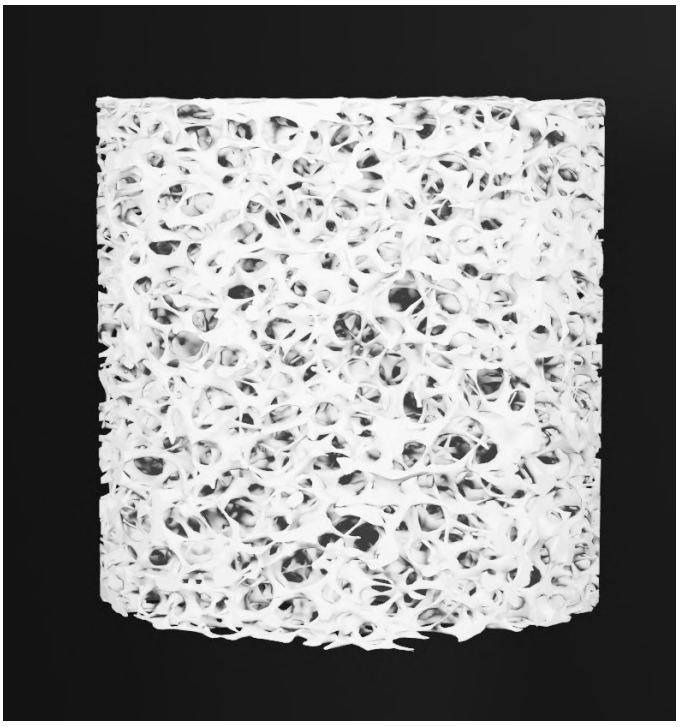

Figure 2.2: Rendering of the Spongy Porous Zone of the Bone

The inclusion of an internal structure, along with a fin design and slotted wick structure, enhances heat dissipation throughout the entire length of the heat pipe, rather than solely at the condenser end. This design concept, discussed in section 3.2, is further depicted in Figure 2.3, showcasing the final proposed version of the Biomimetic heat pipe with a fin and slotted wick design.

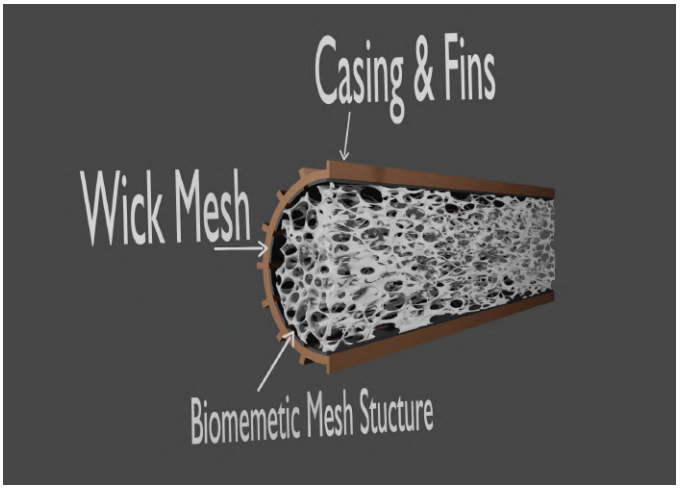

Figure 2.3: Cross-section Rendering of Biomimetic Heat Pipe With Fin and Slotted Wick Design

The incorporation of the biomimetic structure, coupled with the slotted wick and fin design, provides a larger surface area for improved heat dissipation across the entire length of the heat pipe. To better visualize the slotted wick fig. 2.4 shows the cross-section of the slotted wick aligned with the fins.

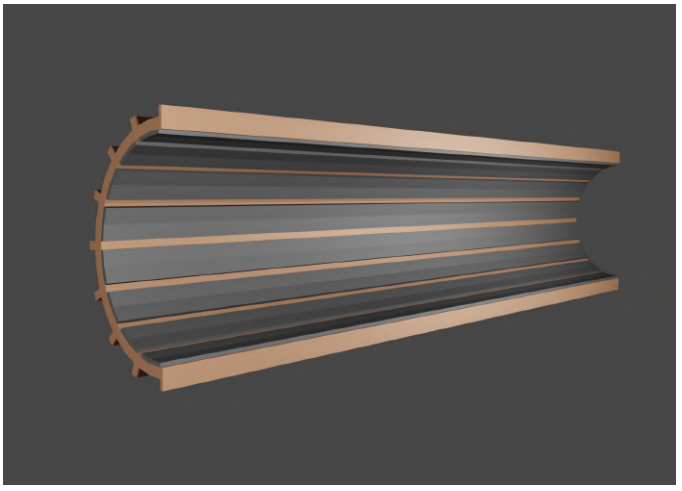

Figure 2.4: Render of Slotted Wick Design Aligned with Fins

This innovative approach promotes phase change of the vapor in the adiabatic zone, facilitating effective heat transfer throughout the heat pipe, rather than being limited to the condenser end alone.

Past research conducted by Ghosh [11] investigated how heat is distributed through a fluid-filled porous media. They were able to show that a localized heat flux caused the fluid to flow through the porous media and distribute heat across the length of the testing apparatus [11]. Ghosh's research brought large motivation to the biomimetic design, as the internal structure can transfer heat more effectively through a porous media as it comes into contact with the structure. Further evidence for vapor flow through a porous media is discussed in section 2.7.

2.2 Fluid Transport In Heat Pipes

Flow is an integral part when designing a heat pipe. There will be a difference in flow in both the adiabatic section and through the wick. Flow occurs due to a difference in pressure between the evaporator section and the condenser section, as well as from the condenser to the wick and then from the wick to the evaporator. The difference in pressure needs to be found to ensure the correct operation of the HP. These differences are relatively small, causing the flow to be slow. This is why the flow will always be considered to be laminar throughout. This is also correlated to the small difference in pressure at both ends of the HP. [2].

2.2.1 Wick of the Heat Pipe

Wicks can have multiple configurations that have the same function but vary in geometry. A wick is a porous media that matches the length of the tube. It transports fluid in only one direction. There are various materials that are used for the wick but all have the same general structure. These are known as homogeneous wicks. Homogeneous means the wick is of uniform geometry throughout. This type also has the wick lining the inner circumference of the heat pipe and is directly attached to the casing. A variation of this general design changes the category to a non-homogeneous type, meaning the wick's geometry changes based on pore size within each layer. The wick is also no longer required to be attached to the casing of the HP in this situation. Each of these wick configurations will be discussed in detail in Chapter 3.

Capillary action and surface tension of the working fluid is the driving force of the cycle. Capillary action occurs when a fluid is being transported through a narrow area. The surface tension pulls the liquid through the structure with the help of adhesive forces. The interaction with the wick layers causes the liquid to be transported from the condenser side to the evaporator side.

The temperature and pressure difference between these two sides also aids in the HP operating properly. The pressure difference between the two sides of the HP, $\Delta P_{c,max}$ is known as the capillary pumping pressure. Equation 2.1 [7] gives the maximum capillary pumping pressure.

$$\Delta P_{c,max} \geq \Delta P_1 + \Delta P_v + \Delta P_g \tag{2.1}$$

Where ΔP_1 is the pressure drop need to transport the liquid from the condenser to the evaporator. ΔP_v is the required pressure to cause vapor to flow from the evaporator side to the condenser side. ΔP_g is the pressure due to gravity. This inequality needs to be met to ensure the wick does not dry out on the evaporator side, causing the flow in the HP to not initiate or cease [2].

2.2.2 Capillary Pressure Difference

Capillary pressure plays a crucial role in the operation of heat pipes as it is responsible for driving the heat pipe cycle. It is an integral part of the underlying mechanisms that enable heat pipes to efficiently transfer heat. The capillary pressure arises due to the combined effects of surface tension and capillary action.

Surface tension is a phenomenon that occurs at the interface between a liquid and a solid, resulting in cohesive forces within the liquid. It causes the liquid to form a curved meniscus at the solid surface, trying to minimize its surface area. In the context of heat pipes, surface tension allows the condensed liquid to form a continuous film or wetting layer on the inner walls of the heat pipe's wick structure.

Capillary action, also known as capillary rise, is the ability of a liquid to flow against gravity within narrow spaces or capillaries. In the case of heat pipes, capillary action enables the condensed liquid to be drawn into the wick structure. The capillary action arises from the combination of intermolecular forces, such as cohesion and adhesion, along with the geometry and pore size of the wick material.

The capillary pressure, resulting from the combined effects of surface tension and capillary action, allows the liquid to be effectively transported and distributed throughout the wick structure of the heat pipe. It facilitates the movement of the working fluid from the between the condenser and the evaporator, where it absorbs heat, undergoes a phase change, and then returns to the condenser for the cycle to continue. Equation 2.2 shows the pressure difference of the capillary action[2]

$$\Delta P_{c,max} = 2\sigma_1 \frac{cos\theta_e}{r_e} \tag{2.2}$$

where σ_1 is the surface tension coefficient, θ_e wetting value of the wick, and r_e is pore radius.

Understanding and optimizing the capillary pressure in the heat pipe design is crucial for ensuring efficient heat transfer. Proper selection of wick materials, pore size, and geometry, as well as consideration of surface properties and operating conditions, are important factors in achieving optimal capillary pressure and overall heat pipe performance. By harnessing the principles of surface tension and capillary action, heat pipes are able to effectively transfer heat over long distances making them valuable components [2].

2.2.3 Gravitational Pressure Change

The gravitational pressure difference is a direct function of the incline angle of the heat pipe. This is shown in equation 2.3.

$$\Delta P_g = \rho_1 g l \sin\phi \tag{2.3}$$

In the equation, where ρ_1 represents the density of the liquid (kg/m^3), g denotes the acceleration due to gravity (9.81 m/s^2), l is the length of the HP, and ϕ signifies the angle at which the heat pipe is positioned relative to the horizontal with positive values indicating that the evaporator is positioned higher than the condenser [2].

When the evaporator rises above the horizontal position, the condensed fluid within the heat pipe begins to counteract the force of gravity. As a result, a stronger pressure difference is required to sustain optimal performance, as the capillary pressure needs to overcome the opposing gravitational force. On the other hand, when the condenser approaches a vertical position, gravity aids the flow of the fluid in the wick, leading to an increase in heat dissipation within the heat pipe.

2.2.4 Pressure Change in Wick

The pressure drop needed to move the liquid to the evaporator from the condenser requires a few considerations. The first is to know whether or not the wick is considered to be homogeneous or non-homogeneous. If a homogeneous wick is used, the area in which the fluid will flow through the wick needs to be found. Equation 2.4 shows A_f which is the flow cross-section of the wick [7].

$$A_f = A_w\epsilon = \pi(r_w^2 - r_v^2)\epsilon \tag{2.4}$$

Where r_w is the outer radius of the wick and r_v is the inner radius of the wick. ϵ is the fraction of the area available for the fluid to pass through. A_w is the area of the wick and can be calculated to find the optimal size of the wick depending on how much heat is being put into the system. The effective length l_{eff} is found using eq.2.5 and is used in the to find ΔP_1.

$$l_{eff} = l_a + \frac{l_e + l_c}{2} \tag{2.5}$$

where l_a is the length of the adiabatic zone, l_e is the length of the evaporator, and l_c is the length of the condenser.

The difference in pressure through the wick can now be described and is found in eq. 2.6 [2, 8].

$$\Delta P_1 = \frac{\mu_1 \dot{Q} l_{eff}}{\rho_1 L A_w K} \tag{2.6}$$

Where μ_1 is the dynamic viscosity of the liquid. L is the latent heat, K is wick permeability, $\dot{Q}$ is heat transfer ($\frac{KJ}{Kg}$).

2.2.5 Pressure Change Due To Vapor

The pressure difference from both ends in the vapor section of the pipe requires an analysis of 1-dimensional incompressible flow that is comparably more involved than the previously discussed pressure difference. Reay-Key-M^cGlen derives this analysis by breaking up each section of the pipe into three pressure areas. ΔP_{ve}, ΔP_{va}, and ΔP_{vc} for the adiabatic section, condenser and evaporator respectively [2]. The sum of these pressure differences equals ΔP_v. Equations 2.7 and 2.8 show this [2]:

$$\Delta P_{va} = \frac{8\mu_v \dot{m}}{\rho_v \pi r_{vv}^4} l_a \tag{2.7}$$

where l_a is the length of the adiabatic section, ρ_v is the density of the working fluid as a vapor, r_v is the radius of the vapor region, and $\dot{m}$ is the mass flow rate of the vapor.

$$\Delta P_{ve} = \frac{4\mu_v \dot{Q} l_e}{\rho \pi r_v^4 L} \tag{2.8}$$

where l_e is the length of the evaporator section, μ_v is the dynamic viscosity of the working fluid, and L is the latent heat of vaporization.

$$\Delta P_{vc} = \frac{-4}{\pi^2} \frac{\dot{m}^2}{8\rho_v r_v^4} \tag{2.9}$$

The above three equations can be summed up to find the total pressure difference between each of these sections [2]. This is shown in eq. 2.10.

$$\Delta P_v = \left(1 - \frac{4}{\pi^2}\right)\left(\frac{\dot{m}}{8\rho_v r_v^4}\right) + \frac{8\mu_v \dot{m} l_a}{\pi \rho_v r_v^4} \tag{2.10}$$

Busse has literature that has solved this analysis using the Navier-Stokes equations and has come to a similar solution [12]. Tower-Hainley also has different ways of calculating the pressure drop in the vapor section as well as different geometry configurations to help solve various types of heat pipes [13].

2.2.6 Gravity Assisted Heat Pipe Considerations

Gravity-assisted heat pipes operate with the condenser section positioned above the evaporator, relying on the gravitational pressure difference as discussed in section 2.2.3. When a gravity-assisted heat pipe is designed without a wick structure, it is referred to as a Thermosyphon. In Thermosyphons, the absence of a wick means that the condensed liquid is not actively pulled back to the evaporator. Instead, the pressure difference created by gravity alone is sufficient to drive the cyclic process.

In contrast, a gravity-assisted heat pipe incorporates a wick that aids in the transport of condensed liquid (as discussed in section 2.2.4), increasing the flow of the condensed liquid back to the evaporator and thus increasing its performance. This increase in performance allows the heat pipe to operate up to its maximum potential.

Kemme has extensively studied the performance of gravity-assisted heat pipes [14]. The research identified certain limitations that occur in gravity-assisted mode, particularly focusing on the sonic limit and entrainment. Limitations associated with heat pipes are discussed in section 2.4. Using the force of gravity allows the investigated heat pipe design to operate at ideal conditions [2].

However, it's important to note that most of the research conducted thus far has been limited to liquid metal heat pipes, which exhibit different behaviors compared to non-liquid metal heat pipes. There has been limited research on water-based gravity-assisted heat pipes [2]. Additionally, Kemme's extensive studies did not include testing procedures related to gravity-assisted heat pipes. This omission is understandable, as the tests were conducted at LANL, and much of the testing was confidential at that time [14]. While the documentation has since been released, it still lacks detailed testing procedures for gravity-assisted heat pipes. This serves as additional motivation for our current project, highlighting the need to develop a comprehensive method for testing gravity-assisted heat pipes.

2.3 Heat Transfer Analysis

2.3.1 Heat Transfer in Evaporator

Heat will begin to raise the temperature of the liquid that is contained inside of the evaporator, first through conduction of the walls and then through convection as it is transported through the liquid not in contact with the wall. As the temperature reaches the boiling point of the liquid, it will become superheated and voids will start to form inside the liquid. These bubbles that have formed will increase the convection of the system. If the heat flux continues to increase too much, however, it will reach a limit that will cause the wick to dry out. Dry out happens when the returning liquid in the wick is unable to reach the evaporator end. This stops the cyclic process, causing the HP to cease operation. This is also known as the *Burnout Limit*. The limit can be estimated and will be incorporated into the design. A critical heat flux value was found by Griffith and Rohsenow [15]. This value will be critical to the design and is found by eq. 2.11:

$$\dot{Q}_b = -0.012 L \rho_v A_v \left(\frac{\rho_1 - \rho_v}{\rho_v} \right)^{0.6} \tag{2.11}$$

where $\dot{Q}_b$ is the heat flux threshold to cause burnout. Further explanation and other limitations are discussed in section 2.4.

2.3.2 Heat Transfer in Wick

Heat transfer has various effects on the wick as well. Research has shown critical heat flux can be influenced based on the surface finish and the type of mesh being used. The finer the mesh the more linear the heat flux. [16, 17]. This extensive research shows how the critical value will be influenced by these characteristics by using many different mesh configurations. Temperature, pressure, and choice of working fluid also play a large role since they directly influence heat transfer rate.

2.3.3 Heat Transfer in Condenser

Condensation of the working fluid occurs in one of two ways, the vapor condenses into a continuous liquid or the vapor forms into many large droplets. In our case, the first will take place due to the working fluid that will be used. The major difference between the analysis, when considering the condenser side compared to the evaporator, is the non-compressible gas present in the HP. The remaining air in the HP will collect on the end of the condenser making the area filled with this gas unattainable for the working fluid. This is why a HP needs to have pressures close to a vacuum environment for it to work properly. The temperature difference will be considered in the same manner as the evaporator region of the pipe, refer to 2.3.1 for more detail.

2.4 Operating Limits

Understanding the limitations of heat pipes is crucial to ensure their reliable start-up and continuous operation without encountering avoidable errors in the data. Numerous studies and reports have been published, extensively documenting various limitations associated with heat pipes. By taking these limitations into account, informed decisions can be made during the design process [2].

2.4.1 Capillary Limit

The capillary limit or wick limit was described using eq. 2.1 and needs to be satisfied to prevent the wick from drying out as described earlier.

2.4.2 Sonic Limit

Kemme has done extensive research on the effects of the supersonic flow of the vapor during start-up and steady-state operation of heat pipes [18]. This occurs when the velocity of the vapor reaches the speed of sound through the vapor. This results in a decrease in pressure across the length of the pipe. The heat flux rate that will cause sonic flow in the vapor ($\dot{Q}_s$) can be readily calculated by using eq. 2.12

$$\dot{Q}_s = \frac{\rho_v V_s L}{\sqrt{2(\gamma+1)}} * A_v \tag{2.12}$$

Here, A_v represents the cross-sectional area of the vapor space, V_s denotes the speed of sound in the vapor at the operating temperature, and γ represents the ratio of the specific heats of the vapor.

It is important to note that the vapor's velocity increases as it traverses the length of the pipe. This behavior resembles that of a converging-diverging nozzle [2]. Kemme's study investigated a similar heat pipe configuration using liquid metal heat pipes, where a layered mesh was incorporated in the adiabatic section with a concentric annulus surrounding the center [18]. Their findings indicated that the heat pipe can operate at heat fluxes exceeding the sonic limit; however, the heat pipe's efficiency decreases once the vapor transitions into the supersonic flow. This aspect is significant to consider in the context of biomimetic heat pipes due to the porous nature of the internal structure, which causes the acceleration of vapor in the adiabatic zone [19]. The value is calculated using eq. 2.12 is the limit of heat flux that needs to be avoided to cause inefficiencies.

2.4.3 Entrainment Limit

Entrainment is a phenomenon that occurs inside when the shear forces between the vapor and the liquid returning through the wick are so great that it slows or stops the wick from returning to the evaporator section. The condensed liquid gets pulled from the wick and flows in the other direction with the vapor [20]. Kemme has studied entrainment limitations and the maximum heat flux can be calculated using eq. 2.13 [2]

$$\dot{Q}_e = A_v L \left[\frac{\rho_v}{A} \left(\frac{2\pi\gamma}{\lambda} + \rho_1 g D \right) \right]^{0.5} \tag{2.13}$$

where A is the cross-sectional area of the entire heat pipe, γ is the ratio of specific heats of the working fluid, and λ is defined as the diameter of the wick plus the distance between voids.

One possible approach to mitigate entrainment in the heat pipe is to incorporate a concentric annulus design. This design features a solid barrier positioned between the adiabatic zone and the wick, effectively preventing the occurrence of shear forces at the boundary. By introducing this barrier, the risk of entrainment can be significantly reduced, enhancing the overall performance and reliability of the heat pipe system.

2.4.4 Boiling Limit

Nucleation growth in the working fluid at the evaporator is a normal behavior in heat pipe operation. Issues, however, can start to appear when bubbles start to form in the wick of the heat pipe. This can be an obstacle to the circulation of the working fluid with hot spots also appearing along the length. This limit is fundamentally different from the previous limits due to it being caused by radial heat flux and not axial [20]. The boiling limit is also the value that causes what is known as burnout. The equation for this is shown in 2.11.

2.5 Heat Pipe Elements

2.5.1 Working fluid Compatibility

The working fluid that is chosen needs to be able to be compatible with the HP housing and selected mesh in order to have sustainable longevity of operation. Reay-Key-M^cGlen gives a list of requirements to help ensure compatibility [2]. Lifetime failures usually occur when the material is incompatible with the working fluid. Material Considerations and selection are discussed in Chapter 3.

2.5.2 Correlation to Length in HPs

Heat pipes are often very long and relative to their diameter. This, however, is used because of the applications and not due to a performance increase. In reality, the longer the heat pipe the higher the thermal resistance, and this results in less heat reaching the condenser zone. This is shown from the dependency of l_{eff} in eq 2.5. The shorter the heat pipe the less resistance there is, and the faster it will begin rejecting heat. Figure 2.5 shows a comparison of the maximum heat transport of two heat pipe designs.

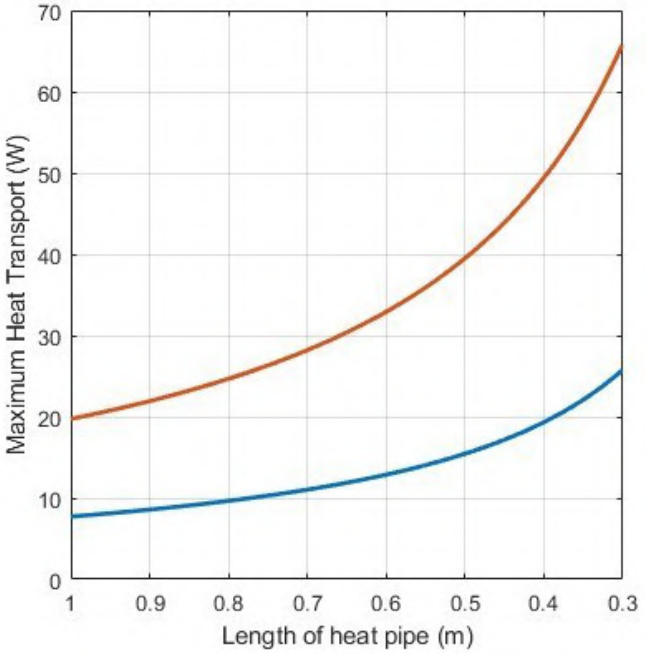

Figure 2.5: How Length Affects the Maximum Overall Heat Transport

As the length decreases, the overall maximum heat transport increases. While this may initially seem like an advantageous design decision it comes with a trade-off. The reduction in length also decreases the fluid transport capability in the adiabatic and wick sections of the heat pipe. If the heat pipe becomes too short, the evaporated vapor will not travel a sufficient distance from the heated zone to condense back into a liquid, leading to burnout. Appendix B.1 goes into more detail about this analysis and how its influence has an impact on design.

2.6 Wick Geometry

The geometry and structure of the wick in a heat pipe vary depending on the specific application. Generally, there are three main types of wick structures used.

The first type is employed in horizontal and gravity-assisted heat pipes, where larger pore sizes are typically used. The smaller pressure differences between both ends of the heat pipe in these configurations make smaller pore sizes unnecessary.

The second type is used when gravity opposes the operation of the heat pipe. In such cases, smaller pore sizes are required to ensure that the flow can overcome the gravitational force.

The third type involves non-homogeneous wicks, where the wick's geometry and mesh structure vary, not only based on pore size but also on its placement within the heat pipe. Arterial wicks are an example of this type. Instead of being placed against the wall of the heat pipe, the wick extends through the adiabatic section of the pipe away from the wall. However, this design presents a challenge: gas bubbles have the potential to block the arteries, thereby reducing or completely blocking the transport of fluid [2].

2.7 Vapor Flow through Porous Media

A recent study investigated how vapor travels through porous media. These studies call into question the original ideas proposed by Philippe and de Freeze on how steam through a porous media increases in velocity [19, 21]. This phenomenon was studied when water vapor flow was noticed to have a higher velocity than predicted values used by Fick's law for flow through porous media. This was especially apparent when a temperature gradient was present and condensation of liquid forms on the media interface [19].

Several new ideas have been proposed to address the problems of previous models and explain the difference between predicted and observed steam motion [4]. These new explanations focus on the importance of the pathways of interconnected pores. The purpose of this study was to measure the specific role

of liquid bridges, as well as local temperature differences and capillary forces in vapor transport through porous media.

To understand this phenomenon, models were built to measure how vapor propagates through partially liquid-filled porous media [19]. Through both simulations and physical experimentation, it was shown that vapor travels faster in the presence of an isolated liquid bridge caused by condensation. It is also suggested this is actually due to the shorter distance the vapor has to travel. The presence of a temperature difference can help if the gradient is aligned with the direction of the capillary force. As more liquid fills the media, capillary forces become more important, and, as suggested by Philippe and de Freeze, improvements in vapor movement are limited to situations where there is not much liquid [19, 21].

This investigation reveals compelling evidence that its internal porous structure significantly enhances heat dissipation effectiveness in the biomimetic design. As the saturated vapor traverses through the internal structure, specific regions of the vapor undergo condensation upon the porous media. This condensation process leads to an increase in vapor velocity, facilitating faster transportation of the vapor to the condenser. Simultaneously, the heat is dissipated across the entire length of the heat pipe due to the latent properties of the working fluid.

2.8 Biomimetic Effectiveness

As discussed in this chapter, there are several factors that can influence the efficiency of a heat pipe. When heat is absorbed in the evaporator, it transforms the liquid into vapor, initiating vapor flow driven by the pressure difference between the evaporator and the condenser [2]. As ΔP_v increases, the vapor velocity also increases, a characteristic common to all heat pipes. However, in the case of the biomimetic heat pipe, this velocity increase is more pronounced due to the influence of the structure.

Studies by Kemme [14] have revealed that heat pipes behave similarly to converging-diverging nozzles, a behavior directly tied to how the area changes as vapor flows through a given section [22]. Notably, the biomimetic heat pipe continuously varies its area along its length, which consequently affects the fluid's velocity, as discussed in section 2.7. In micro-gravity environments, as discussed in section 2.2.1, Marangoni Convection arises from the surface tension between two phases of the working fluid [10]. Experiments have shown that larger temperature gradients induce fluid turbulence, which the biomimetic structure can leverage to its advantage.

Under normal circumstances, eddies resulting from increased velocity and temperature gradients would hinder heat pipe effectiveness as the adiabatic zone remains open. However, the incorporation of the biomimetic structure enables interactions between the circulating turbulent fluid and the biomimetic features

[23]. These interactions promote phase change back into a liquid, facilitating more efficient heat dissipation along the entire length of the heat pipe [24]. These ideas will be taken into consideration as the results are analyzed to determine if the BioHP is more effective at dissipating heat.

CHAPTER 3

DESIGN PROCESS

3.1 Material Selection

Selecting the appropriate material for a heat pipe involves careful consideration of several factors. First and foremost, the material must be compatible with the working fluid, able to withstand the conditions the heat pipe may experience and be feasible for fabrication. These considerations are crucial in heat pipe design, as multiple materials must work together harmoniously. In the case of this research, the heat pipes need to operate within a temperature range of 30 to 200°C to align with the limitations of the testing equipment [2].

The choice of casing material is significant, especially for space applications. Aluminum alloys, such as 6061, are commonly used in industry due to their lightweight nature, malleability, and high thermal conductivity [2]. Aluminum heat pipes are often paired with gaseous working fluids like ammonia, which are compatible and suitable for space applications [2]. However, for this research, compatibility with the working fluid at room temperature and high thermal conductivity are crucial, leading to the selection of copper as the casing material. Copper offers excellent thermal conductivity and compatibility with various fluids, making it a suitable choice [2].

The choice of working fluid is equally important. While options like ammonia or silver are common in certain heat pipe applications, they do not cover the temperature range of 30 to 200°C. Consequently, water was chosen as the working fluid for this research. Water operates within the specified temperature range and is compatible with copper [2]. Additionally, water's high latent heat vaporization capacity allows it to hold significant energy during the phase change from liquid to vapor. This characteristic is advantageous in heat pipes as the released energy facilitates efficient heat transfer dissipation when water returns to the liquid phase [2].

While these heat pipe designs may not be specifically tailored to space design, their adaptability allows for customization to suit different requirements. It is worth noting that copper heat pipes with water as the working fluid are widely adopted in the industry as a standard configuration. This provides an opportunity for direct comparison between the fabricated heat pipes and established industry products, enabling a thorough evaluation of their performance and effectiveness. The flexibility of these designs allows for potential modifications and

optimizations to meet specific application needs.

3.2 Biomimetic Design Process

The development of the Biomimetic Design involved an iterative process, undergoing numerous design changes and configurations to achieve the optimal geometry. The initial concept, shown in Figure 3.1, employed a cylindrical structure with various-sized holes cut through it using Solidworks software. The aim was to incorporate an arterial wick within the biomimetic zone, eliminating the need for an external wick and enhancing heat transfer to the outer walls. However, this design encountered challenges due to isolated flow areas and software limitations, leading to significant time-consuming processes and inefficiencies.

Figure 3.1: First Biomimetic Design Concept

To address these issues, the design evolved to a "Pronged Plate" concept, as depicted in Figure 3.2, aimed at reducing the solid portions of the structure while focusing on the arterial wick design. Despite this improvement, limitations arose concerning the uniformity of the wick structure along the length of the heat pipe.

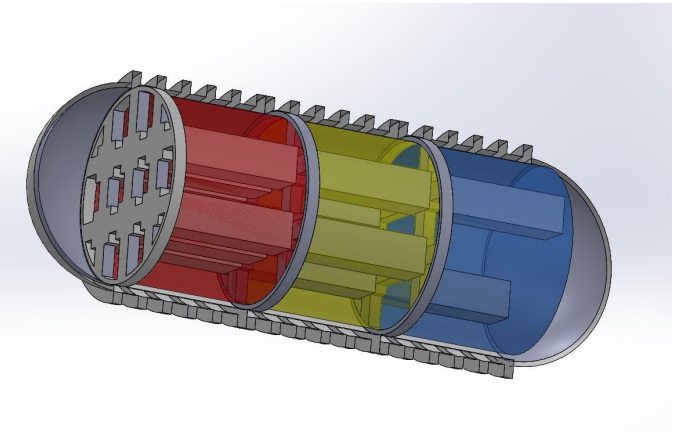

Figure 3.2: Pronged Plate Design

Subsequently, a lattice structure design was explored, incorporating rotated sections to increase porosity. Figure 3.3 illustrates this concept, which showcased potential but did not align with the desired arterial concept due to the absence of continuous passageways throughout the entire length. Therefore, a revised lattice structure was developed, maintaining the same geometry while inserting wicks into different sections, as shown in Figure 3.4. However, this design proved ineffective for heat dissipation, with excessive open areas impeding vapor collisions and velocity enhancement.

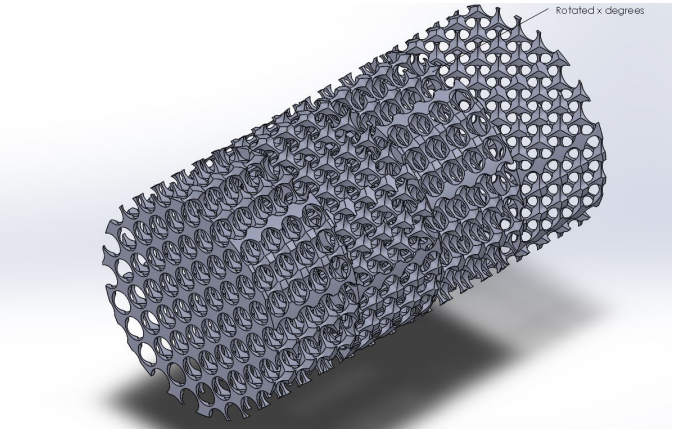

Figure 3.3: Render of Rotated Structures

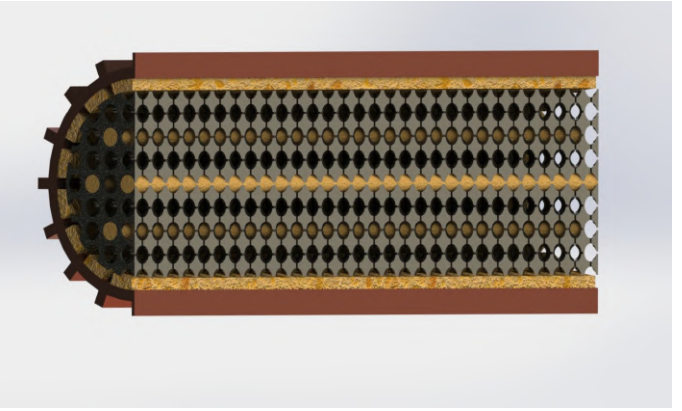

Figure 3.4: Render of Final Lattice Concept

Recognizing the need for a fresh approach, a complete restart was warranted. The slotted wick and fin concepts remained feasible, but a re-imagining of the biomimetic structure was necessary. Solidworks, the software utilized thus far, had limitations in representing the desired real-life bone-inspired structure. As a result, Blender, an open-source software capable of handling intricate and manipulable geometry, was explored as an alternative.

By leveraging online resources and learning Blender, a primitive model of the bone-inspired structure was obtained, as seen in Figure 2.2. Subsequent manipulation and refinement within Blender led to the final design of the heat pipe, depicted in Figure 3.9, showcasing the culmination of the Biomimetic Design process. The final concept needed to forgo the arterial wick concept due to the structure, but still has the potential to help increase performance and can be introduced in future design concepts.

3.3 Need For Testing and Fabrication Standards

A comprehensive search for relevant American Society for Testing and Materials (ASTM) standards pertaining to the thermal management characteristics of heat pipes was conducted. Although several ASTM standards were found, none specifically addressed the unique requirements of heat pipe testing. Among the identified standards were ASTM C335-05 Standard Test Method for Steady-State Heat Transfer Properties of Pipe Insulation [25], ASTM E1530-06: Standard Test Method for Evaluating the Resistance to Thermal Transmission of Materials by Guarded Heat Flow Meter Technique [26], and ASTM Standard E1952-06: Standard Test Method for Thermal Conductivity and Thermal Diffusivity by Modulated Temperature Differential Scanning Calorimetry [27].

However, none of these standards provided a suitable framework for determining the thermal management characteristics of the heat pipes under investigation. As a result, it became necessary to develop a new testing procedure

tailored specifically to assess the thermal performance of these heat pipes. The development of a new testing procedure is a crucial step in evaluating the thermal performance and efficiency of heat pipes. It not only provided valuable insights into their heat transfer capabilities but also established a foundation for further research and development in the field of heat pipe technology. The utilization of a standardized and reliable testing method ensures accurate and comparable results, enabling meaningful comparisons and advancements in heat pipe design and optimization.

3.4 Fabrication of Heat Pipes

Three heat pipes are utilized for testing, with two of them being constructed in-house and the third one was obtained from Wakefield Thermal [28] for comparison purposes. The Wakefield Heat Pipe will be referred as the Manufactured Heat Pipe (MHP). This approach will establish a baseline test to validate the fabrication process of the manufactured heat pipes. All heat pipes consist of a copper casing housing a copper wick inside. The primary distinction lies in the type of wick employed: the MHP features a sintered wick, while the fabricated heat pipes will incorporate a copper mesh wick. Sintered wicks offer pore sizes that cannot be achieved through foam methods[2], leading to higher capillary pressure and improved efficiency. By subjecting the manufactured heat pipe to the same testing procedure, we can establish a baseline for comparison with the fabricated heat pipes and evaluate their performance. The geometry of the manufactured heat pipe was also considered in the dimensions decisions as well as understanding the limitations of standardized shelf material dimensions.

The two in-house heat pipes include the Traditional Heat Pipe (THP) and the Biomimetic Heat Pipe (BioHP). The fabrication procedures for both designs are largely similar, but the BioHP incorporates an additional internal structure. To construct the heat pipes, a copper pipe with a diameter of 0.55 inches (0.014 meters) and a length of 5 feet (1.524 meters), along with copper end caps of the same diameter. The copper pipe was cut into sections measuring 6 inches (0.1524 meters) in length, deburred, and sanded smooth. Figure 3.5 shows one of the cut tubes.

Figure 3.5: Six inch Cut Copper Tube

The wick for these tests is a thin copper mesh with a porosity of 95% and a pore size of 50 μm with a single mesh thickness of 0.1mm. The circumference

using the ID of the tube is calculated to determine the dimensions of the wick. The analysis to find the optimal wick layers is discussed in section 4.3. The copper foam is then cut into coupons and rolled using a 3D-printed cylinder that is the size the mesh needs to be in order to be inserted against the wall of the heat pipe. Figure 3.6 shows three of the copper foam coupons before rolling and insertion.

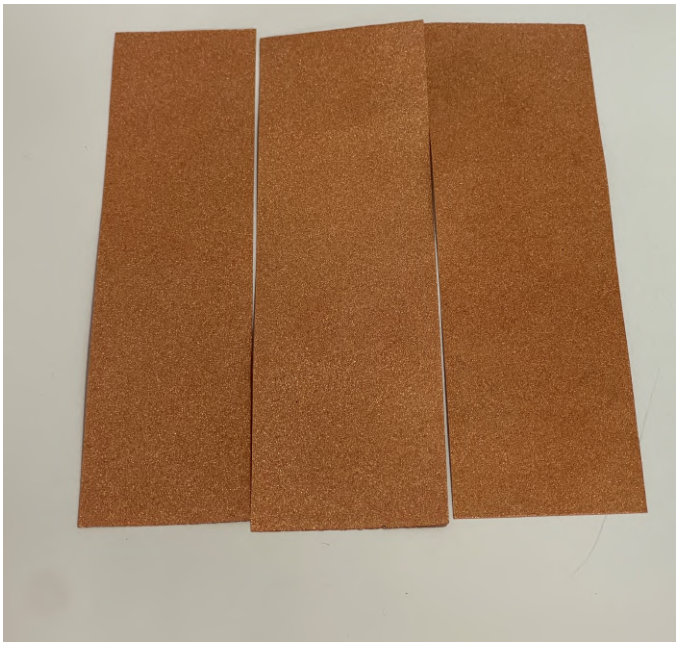

Figure 3.6: Cut Copper Foam

Construction of the in-house fabricated heat pipes is described as follows. To achieve a smooth finish, the exterior of the tubes and the inner surface of the end caps are sanded. The outer surface of one end of the pipe and the inner surface of the cap were treated with soldering flux. Subsequently, one cap is positioned onto the tube and heated using a butane torch. The flux was heated until it underwent a color change, indicating its activation, following which a lead solder was applied to securely join the tube and the cap. The coupons are then rolled and carefully inserted against the inner wall of the casing. The copper tube with the wick structure inserted is shown below.

Figure 3.7: Traditional Heat Pipe with the Wick Inserted

The remaining cap has a 0.0238 mm hole drilled in and soldered onto the pipe. The process to properly seal the heat pipe is shown below.

3.4.1 Sealing Process

Optimal heat pipe performance requires minimizing the presence of air inside the pipe. Although a heat pipe can still function with air present, non-condensed air tends to accumulate at the condenser end, impeding the working vapor's reach to that area. As a result, the working fluid condenses prematurely before reaching the end, effectively reducing the effective length of the heat pipe [2]. To tackle this issue, an attempt was made to expel as much air as possible from the heat pipe.

To achieve this approach, a copper straw with a diameter of 3/32 inches (0.0238 meters) was utilized. The straw is then inserted 1" (approximately 0.0254 meters) into the drilled end cap hole. The full assembly is shown below:

Figure 3.8: Constructed Prototype with Soldered Cap and Straw

Once all the tubes were joined to complete the heat pipe assembly, 4mL of distilled water is inserted through the straw with a granulated syringe. This decision was made, based on research that determined how performance affected the amount of working fluid in the evaporator [29]. This is discussed further in section 4.3.1. The pipe is then partially submerged in a silicone oil bath at 100°C until the working fluid undergoes a phase change inside the pipe. When steam begins to exit through the straw at a consistent rate, a pair of pinch-off locking pliers were employed to crimp the end of the straw, ensuring a tight seal. The sealed heat pipe is then cooled down to room temperature and observed for a duration of 5 minutes to verify if water continued to exit the pipe, indicating a potential leak.

Following the sealing process, an additional leak test needs to be performed to ensure the integrity of the heat pipe and verify that no other components are allowing air ingress. A granulated cylinder is filled with 200 ml of water. The sealed heat pipe's mass is measured, then heated back up to 100°C in the oil bath. Next, it is fully immersed in a 200 ml graduated cylinder for a duration of 30 seconds. Subsequently, the heat pipe is carefully removed from the container, and the water level in the container and the total mass of the heat pipe were measured. If there was minimal to no change in the water volume or mass, it indicates the heat pipe had successfully passed the leak test. The heat pipe is now suitable for operation testing.

3.4.2 Fabrication of Biomimetic Design

The BioHP's fabrication procedure follows all of the same steps indicated in section 3.1, additionally, this design involves the insertion of the Biomimetic structure.

The BioHP design involves the exploration of an internal structure inspired by the spongy section of bone. This structure exhibits a porous-like arrangement with rounded beams that exhibit variations throughout the structure. The selection of this structure was based on its resemblance to the natural bone structure, offering advantages over a manufactured porous structure. The unique geometry of the bone structure ensures a continuous flow without any areas where fluid flow could be obstructed or trapped within channels. While also, maintaining contact with the wick, and casing. Figure 3.9 illustrates the geometry of the Biomimetic structure.

The discovery of this structure is a result of an investigation related to the osteoporosis model. A generalized version of the structure was identified and procured as a three-dimensional model. Subsequently, the model is imported into Blender, an open-source creation suite known for its versatile geometry manipulation capabilities. The initial geometry of the structure was in the form of a rectangular prism. However, since the structure is intended to be placed in the adiabatic zone of the heat pipe, it needs to conform to the shape of the heat pipe itself. This necessitates further modifications of the geometry within Blender to transform it into a cylindrical shape. Figure 3.9 shows the final shape of the structure.

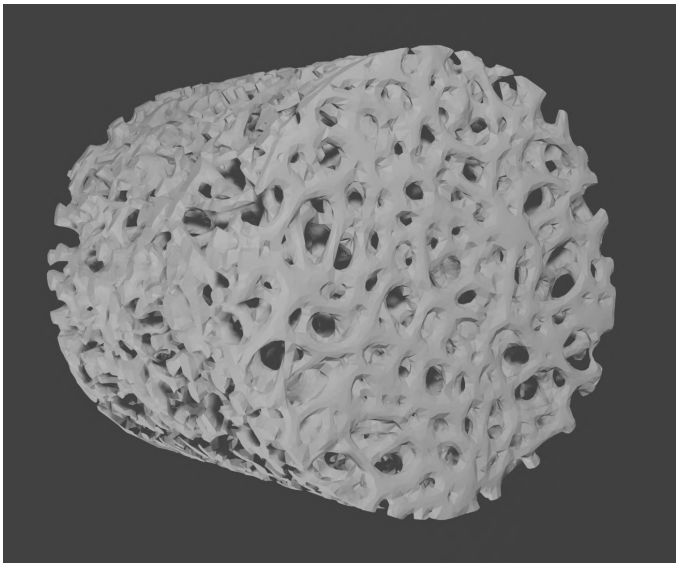

Figure 3.9: Biomimetic Bone Structure Visualization

After finalizing the geometry of the structure, the next challenge is determining the most suitable method for 3D printing the object. Due to the complexity

of the geometry, using a traditional filament layering 3D printer posed difficulties. The intricate structure requires internal supports and would require a double nozzle printer capable of using water-soluble materials for support. While this approach was technically feasible, exploring alternative options was deemed more advantageous.

The optimal solution identified involved utilizing a resin 3D printer for this particular model. Resin printing involves using a vat of UV-curable Aresin to create the desired geometry. The liquid environment allows for the creation of more intricate and detailed structures. New Mexico Tech's fab lab offers a resin printer, specifically the Form Labs 3+ resin printer, which is used for all the prints of the biomimetic model. The High Temp v2 Resin is selected to ensure the biomimetic structure maintained its integrity during BioHP operation.

To ensure successful printing, multiple test prints need to be conducted, involving variations in geometry and size. Scaling the geometry up to twice its original size is performed to assess the adequacy of the pore size. Figure 3.10 below showcases the first successful print of the biomimetic structure.

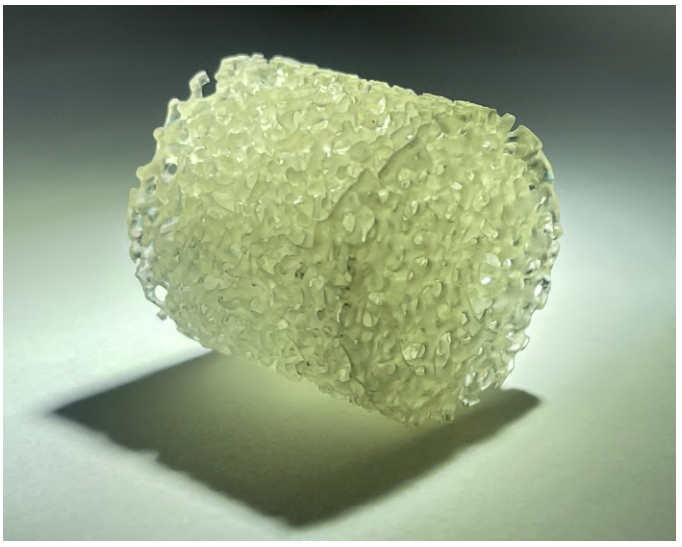

Figure 3.10: Print made from high-temperature resistant resin polymer.

With the successful test prints validating the feasibility of the biomimetic structure, the next step is to attempt printing a structure with the same diameter as the heat pipe. Initially, Blender scaled down the object to match the desired diameter. However, this approach encountered a challenge during the dripping phase of the print. After the printing process is complete, the model is positioned above the vat to allow excess resin to drip off, preventing resin from getting trapped inside the structure. Unfortunately, the smaller pore sizes of the model posed a problem. The combined effects of capillary pressures and surface tension of the liquid resin hindered the dripping process, regardless of the duration of the waiting period. As a result, the finished prints contained cured

resin inside the structure, rendering it nearly solid. The figure below illustrates an unsuccessful print.

Figure 3.11: Failed Test Print. It Can be Seen That the Resin is Cured Inside of the Structure, Making it Solid.

To overcome the challenge of resin curing inside the structure, a different approach is taken. Instead of scaling down the model, Blender is used once again to precisely cut the object to the desired diameter. With this modification, another attempt was made to print the structure at the correct diameter. This method proved to be successful. The final test print confirmed the effectiveness of this approach in creating the desired biomimetic structure. Figure **??** below showcases the final test print.

Figure 3.12: Two Successful Prints to the Correct Diameter. Left: Printed Vertically Right: Printed Horizontally

Two orientations of printing are explored to assess the impact on print quality in relation to the position of the structures. The investigation revealed that

there is minimal to no discernible change in print quality based on the orientation. This finding is significant as it indicates that the orientation can be optimized to minimize print time when producing the full-scale version of the structure. By understanding that the print quality is not significantly affected by orientation, time and resources can be efficiently allocated during the printing process.

With the refined approach and successful test prints, a full-scale print of the biomimetic structure can now be performed. Leveraging the same methods previously discussed, the structure was printed to match the complete length of the heat pipe. The iterative process of test prints proved to be highly valuable, as it ensured the necessary adjustments were made prior to the full-scale print. As a result, the first full-scale print of the biomimetic structure is a success, as depicted in the figure below.

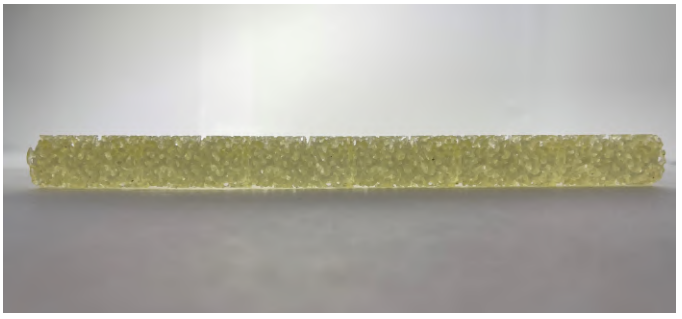

Figure 3.13: Full Scale print of the Biomimetic Structure

To ensure the High-Temperature Resin is able to hold its integrity while inside the BHP, a test was conducted to see if the printed structure will retain its structural integrity in a high-temperature environment. This ensures that the biomimetic structure will keep its shape inside the heat pipe. The silicone oil bath was set to a steady state temperature of 170 °C. A 22mmx9mm cylinder of the high-temperature resin was placed in the bath for 4 hours. It was then taken out and manipulated with the purpose of causing plastic deformation by applying pressure to the top and bottom surfaces in a vice grip.

It was found that the printed structure becomes slightly ductile when heated to this temperature, but the structure was able to retain its shape. The discoloration is apparent, caused by the resin material at higher temperatures, but this is only an aesthetic change. Figure 3.14 shows the structure after the test. It is worth mentioning that while this test did not draw any data, it was valuable for ensuring the printed structure can maintain its shape under a small amount of force.

Figure 3.14: Biomimetic Structure After Integrity Test

Following the fabrication process, both the THP and BioHP were successfully constructed using the described methods. The fabrication steps involved soldering one end cap, attaching the copper mesh wick to the inner casing wall, inserting the internal structure (in the case of the BioHP), inserting the working fluid, soldering the other end cap with a drilled hole using the straw for sealing, and finally, heating the pipe until vapor was observed exiting through the straw before sealing it. The submersion tests were conducted to ensure the integrity of the heat pipes. Results from this test are shown in Chapter 5.

CHAPTER 4

EXPERIMENTATION

4.1 Heat Transfer Analysis

To adequately test the heat pipe, the heat flux that of the fabricated heat pipes are based on multiple parameters. The heat transport can be found by using a pressure balance equation for a heat pipe, this is shown in equation 2.1. By using the definitions of each pressure that are shown in equations 2.2, 2.3, and 2.6 the vapor pressure drop is assumed to be negligible in this analysis.

$$\frac{2\sigma_1 cos\theta}{r_c} = \frac{\mu_1}{\rho_1 L} * \frac{\dot{Q} l_{eff}}{A_w K} + \rho_1 g l sin\phi \tag{4.1}$$

Where $A_w(m^2)$ is the cross-sectional area of the wick in the heat pipe.

The permeability of the wick, K (m^2) and is defined from a modified Blake-Kozeny equation [30] and is shown in eq. 4.2

$$K = \frac{t_w^2(1-\epsilon)^3}{66.6(1-\epsilon)^2} \tag{4.2}$$

where t_w(m) is the thickness of one wick layer multiplied by the number of layers.

After utilizing these definitions, Equation 4.1 can be rearranged to determine the mass flow rate in the wick ($\dot{m}$) as follows shown in eq. 4.3 [2]:

$$\dot{m} = \frac{\rho_1 K A_w}{\mu_1 l_{eff}} \left[\frac{2\sigma_1}{r_c} cos\theta - \rho_1 g l_{eff} sin\phi \right] \tag{4.3}$$

Now that the flow rate is determined, the heat flux can be calculated using the following relationship [31]:

$$\dot{Q} = L * \dot{m} \tag{4.4}$$

Knowing the maximum heat flux value allows easy comparison to the MHP. These calculations are based on the previously discussed geometry specifications.

However, to properly evaluate the heat pipe, additional parameters must be considered. The equation for convective heat transfer is presented in eq. 4.5 [31].

$$\dot{Q}_{in} = A_t h_o \left(T_{oil} - T_{evap}\right) \tag{4.5}$$

where A_t is the area of the heat pipe that is submerged in the oil, h is the convective heat transfer coefficient for the silicone oil, T_{oil} is the required oil temperature, and T_{evap} is the temperature of the heat pipe before being placed into the oil. It is important to note that because the tests were conducted in gravity assist mode, the heat flux is likely to exceed the rating, due to the large increase in effectiveness, this was considered in section 2.2.6.

Furthermore, this analysis provides insights into determining the optimal number of wick layers required in the heat pipe to achieve a heat flux that closely aligns with the manufactured heat pipe. Given that both the THP and BioHP possess the same wick geometry, the calculations for the heat flux are assumed to be identical, enabling a direct comparison of their performance based on experimental data.

4.2 Testing Procedure

4.2.1 Safety Considerations

To ensure testing is performed as efficiently and smoothly as possible minimizing the chance of injury, a detailed safety procedure must be followed before any testing can be conducted. This procedure is described below.

1. Personal Protective Equipment (PPE): All personnel involved in the testing procedures must wear appropriate PPE, including safety goggles, and heat-resistant gloves, to protect against potential hazards.

2. Training: All individuals participating in the experiment should receive proper training with the experimental setup, including understanding the associated risks, emergency procedures, and the location of safety equipment.

3. Emergency Preparedness: Clearly display emergency contact numbers, including 911 and relevant security personnel, near the experimental area. Ensure that at least one person is present during testing to call for emergency assistance if required.

4. Fire Safety: Keep fire extinguishers readily accessible near the experimental area and ensure that personnel are trained in their proper use. Maintain a clear and unobstructed path to emergency exits.

5. Ventilation: Ensure that the lab is adequately ventilated to prevent the accumulation of any harmful gases or vapors. Follow proper ventilation guidelines and conduct regular checks to ensure the ventilation system is functioning effectively.

6. Equipment Inspection and Maintenance: Regularly inspect all equipment, including the heat pipe, for any signs of damage or malfunction. Perform routine maintenance to ensure proper functionality and address any issues promptly.

7. Waste Disposal: Dispose of waste materials, such as used oils, in accordance with local regulations and guidelines. Use designated waste disposal containers and clearly label them.

By following these protocols, the risk of injury is as low as possible. The setup of the experiment is shown below.

4.2.2 Testing Set-up

To ensure accurate testing of the heat pipe, the entire setup is enclosed within an acrylic box, referred to as the heated box. This enclosure acts as an insulator, which helps minimize disturbances caused by fluctuations in ambient temperature. A VWR hot plate stirrer serves as the heat source for all the conducted tests, offering precise control over steady-state temperatures.

In preparation for testing, 100 ml of silicone oil is poured into a Pyrex beaker, and a magnetic stirrer is placed inside to enhance heat transfer within the fluid. The system is then monitored until it reaches a steady-state temperature.

Next, the heat pipe is partially submerged in the oil, and the temperatures of the heat pipe are carefully observed. Figure 4.1 shows the heated box, along with the instrumentation.

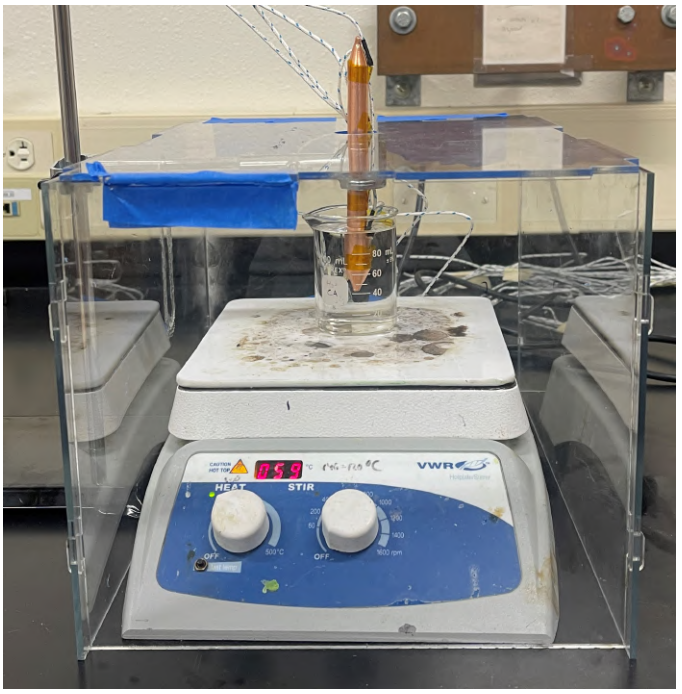

Figure 4.1: Testing Set-up with Heated Box

To capture temperature gradients across different regions of the heat pipe, thermocouples are attached at various locations, and a TC-08 Pico data logger is employed. This setup allows for precise temperature measurements and monitoring. A total of six thermocouples are employed for temperature measurement and monitoring. To ensure steady-state conditions, one thermal couple is positioned within the silicone oil. Another thermal couple is placed on the evaporator end of the heat pipe, submerged in the oil. Two additional thermocouples are positioned along the length of the heat pipe, outside of the oil but still within the heated box. Lastly, one thermal couple is placed on the condenser end, outside of the heated box.

Figure 4.2 shows the manufactured heat pipe and the placement of the four thermocouples. From left to right, they are referred to as the evaporator, node 1, node 2, and the condenser. The evaporator and condenser are placed 3 mm from the tip of the cone and 3 mm from the cap in the fabricated heat pipes. They are then even spaced 42.32 mm apart to cover the entire length of the heat pipes evenly. This ensures an accurate temperature gradient reading across the heat pipe during testing.

Figure 4.2: Thermocouples Taped on with Thermal Tape

Figure 4.3 displays the two thermocouples located inside the oil. Thermal tape is utilized to securely attach the thermocouples to the heat pipe, ensuring accurate temperature readings.

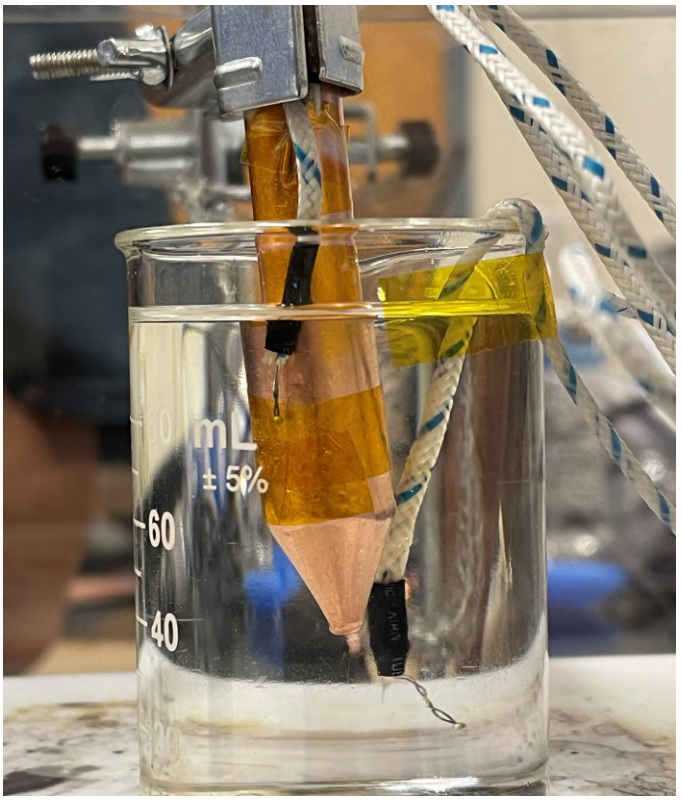

Figure 4.3: Close-up of the evaporator end of the heat pipe

As illustrated in Figure 4.1, the condenser end of the heat pipe extends beyond the boundaries of the heated box. To further optimize the cooling process, an additional box, referred to as the cooling duct, is placed on top of the heated box. Figure 4.4 shows the cooling duct that is constructed from acrylic, it covers the exposed end of the heat pipe.

The cooling duct features a fan located at one end, which generates forced convective air currents. These air currents are directed over the condenser side of the heat pipe, enhancing its effectiveness. The forced airflow aids in the condensation of vapor on the condenser side, promoting phase change and facilitating the transfer of heat energy into the wick. This active cooling mechanism plays a crucial role in enabling the proper operation of the heat pipe.

Two additional thermocouples are strategically placed in the cooling duct to enhance the temperature monitoring process. The first thermal couple is positioned in front of the fan, while the second one is located towards the end of the duct, just in front of the heat pipe. By measuring the temperature difference between these two nodes, valuable insights can be gained, allowing for the determination of thermal rejection at the condenser section.

The fan speed is precisely controlled through the utilization of a voltage regulator. To accurately measure the speed, an anemometer is employed. By possessing knowledge of the duct's cross-sectional area and the fan's speed, the mass

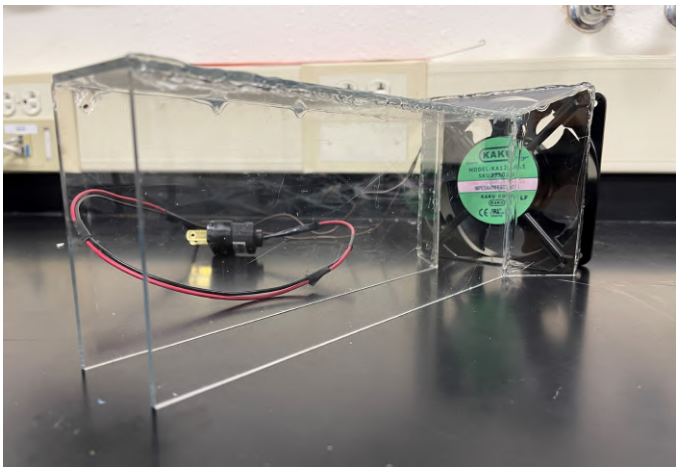

Figure 4.4: Cooling Duct Apparatus

flow rate can be calculated using the equation $\dot{m} = \rho_{Air} A_{duct} V_{Air}$, where ρ_{Air} represents the density of air, A_{duct} denotes the cross-sectional area of the duct, and V_{Air} signifies the velocity of the fan speed. Equation 4.6 enables the calculation of the amount of heat lost at the condenser section.

$$\dot{Q}_{out} = (T_{out} - T_{in}) C_p \dot{m} \tag{4.6}$$

Where T_{out} is the temperature at the end of the duct, T_{in} is the temperature next to the fan, and C_p is the heat capacity of air.

This equation plays a significant role in assessing the effectiveness of each heat pipe in terms of its capacity to efficiently transfer heat to the condenser. The analysis will leverage these measurements to compare and evaluate the heat transfer capabilities of each heat pipe.

4.2.3 Performance Evaluation

Analyzing the performance of a heat pipe is a complex task that involves multiple factors and considerations. Since there is no standardized testing or fabrication method for heat pipes, different research papers adopt various approaches to evaluate them. When examining heat pipe data, it is crucial to assess each heat pipe based on temperature measurements obtained during tests.

Two key aspects are important when assessing the performance of a heat pipe. First, the heat pipe must effectively transport heat, which occurs through the phase change of the working fluid from liquid to vapor. The vapor then reaches the condenser, where heat is released. Evaluating the thermal resistance

of the heat pipe is one way to assess this heat transfer capability. Thermal resistance quantifies the ease of heat flow across boundaries. A lower thermal resistance indicates more efficient heat transfer. Equation 4.7 illustrates the calculation of thermal resistance [31].

$$R = \frac{T_{evap} - T_{cond}}{Q_{in}} \tag{4.7}$$

where R is thermal resistivity(°C/W), T_{evap} is the steady state temperature of the evaporator, T_{cond} is the steady state temperature of the condenser and Q_{in} is the heat flux coming into the heat pipe from the oil. Equation 4.5 is utilized for this calculation.

The second important parameter in evaluating heat transfer effectiveness is the overall heat transfer coefficient h (W/m^2-°C). This coefficient quantifies the conductive heat transfer rate between the two ends of the heat pipe. Higher values indicate more efficient heat dissipation. Equation 4.8 demonstrates the calculation of the heat transfer coefficient.

$$h = \frac{Q_{in}}{A_t(T_{evap} - T_{cond})} \tag{4.8}$$

By finding both the thermal resistance and the overall heat transfer coefficient from each test, a direct comparison of each heat pipe can be made.

4.2.4 Testing Procedure

1. Start-up Analysis:
    - Observe temperature profiles of the evaporator and condenser ends during start-up.
    - Note the significant temperature difference between the two ends initially.
    - Monitor the temperature increase at the evaporator end as the test progresses.
    - Observe of the temperature change of the condenser section.
    - Wait until each section of the Heat Pipe has reached a steady state condition.
2. Steady-State Analysis:
    - Determine the desired steady-state temperature of the oil before testing begins.
    - Measure and evaluate temperature gradients along the heat pipe.

- Compare the observed gradients with the desired performance.
- Visualize the heat transfer characteristics through temperature profiles and heat transfer equations.

3. Q_{out} Analysis:
    - Observe the temperature difference between the two fan positions.
    - Ensure the placement of the fan thermocouples is correct.
    - Monitor the temperature response at each side closely.
    - Record Temperature difference
    - Use 4.6 to find the amount of heat dissipated at the condenser end.
    - Formulate and compare values
4. Data Interpretation:
    - Compare the performance of the MHP, and THP to validate design efficacy.
    - Analyze temperature patterns, gradients, and variations observed during testing.
    - Evaluate the effectiveness of the internal structure in the BioHP compared to the THP.
    - Draw meaningful conclusions regarding the performance, feasibility, and suitability of the BioHP.

By following the established fabrication process and utilizing the designated testing set-up and procedure, the BioHP can be thoroughly analyzed to determine its heat dissipation capabilities in comparison to other designs. The careful implementation of the fabrication techniques and precise execution of the testing procedures enable an accurate assessment of whether the BioHP exhibits superior heat transfer performance. These methods provide a solid foundation for evaluating the efficacy of the BioHP in dissipating heat and contribute to a comprehensive understanding of its potential advantages over alternative heat pipe designs.

4.3 Fabrication Requirement Analysis

Considerations for the heat transfer analysis were conducted using a Matlab script, providing an efficient means to verify values when making calculations, Appendix A shows said script. Table 4.1 presents the measured and constant values utilized in all calculations [2, 31].

Table 4.1: Measured Values and Constants

Constant	Value	Unit
σ	58.9×10^{-3}	N/m
L	2.26×10^{6}	J/kg
h_o	4100	W/(m^{2}K)
ρ_1	958	kg/m^3
ρ_v	0.597	kg/m^3
μ	0.282×10^{-3}	Pa s
d	0.013	m
t_w	0.20×10^{-3}	m
r_e	5×10^{-6}	m
ϵ	0.05	-
r_c	0.005	m
C_p	1.0	kJ/kg K
θ_e	1	-
l_c	0.038	m
l_e	0.038	m
l_a	0.054	m
l_{eff}	0.126	
Layers	3	-
A_t	0.0028	m^2
A_a	1.32×10^{-4}	m^2
A	1.54×10^{-4}	
r_c	5.0×10^{-4}	m
V_s	477.5	m/s
γ	1.33	-

Where σ is the surface tension of water, L is the latent heat of vaporization of water, h_o is the heat transfer coefficient of the silicone oil, ρ_1 is the density of water as a liquid, ρ_v is the density of water as a vapor, μ is the dynamic viscosity of water, d is the diameter of the vapor region, t_w is the thickness of the wick, r_e is the pore radius of the wick, ϵ is the porosity of the wick, r_c is the radius of the cap, C_p is the specific heat of water, and θ is the contact angle across the curved surface of the wick, l_c is the length of the condenser, l_e is the length of the evaporator, l_a is the length of the adiabatic zone, *Layers* is the number of wick layers, A_t is the surface area submerged in the oil, A_a is the cross-sectional area of the adiabatic zone,A is the total area of the pipe, V_s is the speed of sound in water, and γ is the specific heat ratio of water vapor.

Furthermore, the heat flux rate, $\dot{Q}$, for the manufactured heat pipe is specified as 150 W. To achieve a rating as close to 150 W as possible, the THP and BioHP are fabricated based on the description presented in section 4.1. Equations 4.2 4.3 4.4 shows the calculations for K, $\dot{m}$, and $\dot{Q}$ respectively.

The analysis led to the discovery that using three layers is the best option to achieve a heat transfer rate ($\dot{Q}$) that closely matches that of the manufactured heat pipe. Additionally, the study identified the optimal lengths for different sections of each of the custom-made heat pipes by comparing the final $\dot{Q}$ with the MHP and adjusting the parameter until the closest value was found. These calculations are shown below as well as in Appendix A1.

$$K = \frac{(0.0002 \cdot 3)^2 \cdot (1 - 0.05)^3}{66.6(1 - 0.05)^2} = 5.14 \times 10^{-9} \mathrm{m}^2$$

$$\dot{m} = \frac{958 \cdot 5.14 \times 10^{-9} \cdot 2.64 \cdot \times 10^{-5}}{0.282 \times 10^{-3} 0.126} \left[\frac{2 \cdot 58.9 \times 10^{-3}}{0.005} - (0.597 \cdot 9.81 \cdot 0.126 \cdot \sin(1)) \right]$$

$$\dot{m} = 1.31 \times 10^{-5} \, \frac{\mathrm{kg}}{\mathrm{s}}$$

$$\dot{Q} = (1.31 \times 10^{-5}) \cdot (2.258 \times 10^{6}) = 161.4 \, \mathrm{J/s}$$

Based on these findings, two BioHPs and two THPs were fabricated following the specifications derived from the analysis. The decision to create multiple heat pipes of each type was twofold. Firstly, it aimed to ensure that the fabrication techniques employed were consistent and reproducible. Secondly, it served to validate the reliability and consistency of the experimental tests conducted on these heat pipes.

By employing these measures, the study ensures that the fabricated heat pipes not only meet the desired performance criteria but also provide a reliable foundation for further investigations and practical applications.

4.3.1 Sealing Validation

Before conducting the sealing tests, it was necessary to determine the appropriate filling volume for the heat pipes. This is discussed in section 3.4.1. The optimal filling amount is 50% of the total volume of the evaporator section [**?**]. Considering the geometry of the evaporator, the volume needed to be calculated. Since the cap on the end needs to be considered, it was broken up into two sections. The length of the cap was found to be 14 mm and the diameter to be 18 mm. The tube was then measured and the diameter and length were determined to be 16mm and 20 mm respectively. The volume for both sections was then added and the total volume was found to be 7583.8 mm^3. By dividing the total volume of

the evaporator in half, it was determined that 3.8 mL of water should be inserted into each heat pipe.

To account for any mass loss during the sealing process, a total of 4 mL of water was added to each heat pipe. This slightly higher quantity ensures that the desired filling volume is achieved even after accounting for potential mass reduction during sealing.

Following the filling process, the mass of each heat pipe was measured. Subsequently, the sealing and submersion processes were performed according to the specified procedures discussed in section 3.4.1. The mass is then measured again, and the results from this test are shown in table 4.2

Table 4.2: Submerge Test Results (g)

Heat Pipe	Before Submersion	After Submersion
THP1	76.14	76.12
THP2	75.00	75.00
BioHP1	82.7	82.7
BioHP2	82.68	82.67

Based on the analysis conducted, it was ensured that each heat pipe tested was properly sealed, and the appropriate amount of water was placed inside. As part of the fabrication process, four wickless copper pipes were initially created to verify the feasibility of fabrication, sealing, and leak detection tests.

4.4 Limitation Calculations

The limitations are found to ensure the heat flux between the evaporator and the oil does not exceed any limits. If this does occur, the heat pipe's wick will dry out, causing errors in the testing data. Each limitation is discussed in section 2.4. Table 4.3 shows the calculated limits using equations 2.11,2.12, and 2.13 as well as values taken from 4.1. The calculations and table are shown below as well as in Appendix A.

$$\dot{Q}_b = -0.012 \cdot 2.26 \times 10^6 \cdot 0.597 \cdot 1.32 \times 10^{-4} \cdot \left(\frac{958 - 0.597}{0.597}\right)^{0.6} = 355.9kW$$

$$\dot{Q}_s = \frac{0.597 \cdot 477.5 \cdot 58.9 \times 10^{-3}}{\sqrt{2(1.33+1)}} \cdot 1.32 \times 10^{-4} = 45.8kW$$

$$\dot{Q}_e = 1.32 \times 10^{-4} \cdot 58.9 \times 10^{-3} \left[\frac{0.597}{1.32 \times 10^{-4}} \left(\frac{2\pi 1.33}{0.027} + (9589.810.0113)\right)\right]^{0.5} = 814.5kW$$

$$\Delta P_{c,max} = 2 \cdot 58.9 \times 10^{-3} \cdot \frac{cos(90)}{5 \times 10^{-6}} = 1274.1 Pa$$

Table 4.3: Limitations Calculations

Limit	**Value**	**Unit**
$\dot{Q}_b$	355.9	kW
$\dot{Q}_s$	45.8	kW
$\dot{Q}_e$	814.5	kW
$\Delta P_{c,max}$	1274.1	Pa

These limitations will be taken into consideration when the values for heat flux are calculated for the heat pipes. When considering the values to determine the capillary limit, the heat flux of each test is to be calculated and compared to values found in Table 4.3. It is important to note that it is assumed the wick on both heat pipes is fully wetted, meaning, there the contact angle across the curved surface of the wick (θ_e) is zero.

CHAPTER 5

DATA ANALYSIS

There were a total of 22 tests conducted. Each test was grouped into a range of temperatures based on the steady-state temperature of the oil during the test. Temperatures from 26-45 °C are denoted as ”Low”. Temperatures from 45-80 °C are denoted as ”Mid”, and temperatures above 80 °C are considered ”High”. The temperature of the oil was gradually increased until a steady state was achieved. Subsequently, each heat pipe was immersed in the oil, and the temperature was recorded until the heat pipe also reached a steady state. It is worth noting that all the ”High” temperature tests correspond to the upper limit of the silicone oil's temperature tolerance.

The calculations were performed using the average values from each temperature group, as well as the average temperature profiles for each design. This approach provides a more comprehensive understanding of the heat pipes' behavior across a range of temperatures, as opposed to relying solely on isolated test results.

5.1 Fabrication Validation

To validate the performance of the fabricated heat pipes, a comparison is made between the MHP and THP designs. This allows us to assess the effectiveness of the fabrication process and examine how well the designed HPs perform compared to a manufactured one. In order to help understand what is going on in each of the tests, the Q_{in} values need to be calculated using eq. 4.5, the average temperatures for each test were taken from the raw data found in appendix C. Constant values from 4.1 are used. The calculation below shows the Q_{in} for the averaged low temperatures for the MHP and THP, for the low values, the average temperature of the oil was found to be T_{oil} =36.98 $^{\circ}C$, the average temperature of the evaporator for the MHP and the THP were found to be T_{evap} =33.4 $^{\circ}C$ and T_{evap} = 32.8 $^{\circ}C$ respectively.

$$\dot{Q}_{in-MHP} = 0.0028 \cdot 4100 \cdot \big(36.98 - 33.4\big) = 43.76W$$

$$\dot{Q}_{in-THP} = 0.0028 \cdot 4100 \cdot \big(36.98 - 32.8\big) = 50.39W$$

Due to the large number of calculations needed for each range of tests, each calculation for each temperature average and heat pipe was written in a Matlab script and is presented in Appendix A. Table 5.1 shows all the calculated averages for the MHP and THP in each temperature range.

Table 5.1: Average $_{in}$(W) for MHP and THP

Temperature	**MHP**	**THP**	%**Difference**
Low	43.76	50.39	14.1%
Mid	113.6	121.1	6.4%
High	336.4	463.7	31.8%

Table 5.1 shows that at low and middle ranges, the amount of heat that each heat pipe receives very similar heat fluxes in the evaporator. At high temperatures, the THP has a larger value for Q_{in} about 32% more than the MHP.

To help better understand how each heat pipe performs relative to each end of the heat pipe. The thermal resistance and the overall heat transfer coefficient are calculated using eqs. 4.7 and 4.8 respectively. As described in section 4.2.3, thermal resistance (°C/W) quantifies the ease of heat flow across boundaries. The lower the values the better the heat pipe is at transferring heat from the evaporator to the condenser. The overall coefficient of heat transfer(W/m^2°C) subsequently quantifies the conducive heat transfer rate between the two ends. A higher value indicates more heat is being transferred per unit area. Calculations to find the thermal resistance and overall heat transfer coefficient for the low-temperature ranges are shown below. Values for Q_{in} and A_t are taken from table 4.1 and table 5.1 respectively. The average temperature of the condenser at low-temperature ranges, for the MHP and THP, are T_{cond}=28.8 °C and T_{cond}=30.03 °C respectively.

$$R_{low-MHP} = \frac{33.4 - 28.8}{43.76} = 0.011(^{\circ}C/W)$$

$$R_{low-THP} = \frac{32.8 - 30.03}{50.39} = 0.055(^{\circ}C/W)$$

$$h_{low-MHP} = \frac{43.76}{0.0028 \cdot (33.4 - 28.8)} = 3.27(W/m^{2^{\circ}}C)$$

$$h_{low-THP} = \frac{50.39}{0.0028 \cdot (32.8 - 30.3)} = 6.21(W/m^{2^{\circ}}C)$$

The values for each Thermal Resistance at their respective temperature are provided in Table 5.2.

Table 5.2: Average Thermal Resistance(°C/W) for MHP and THP

Temperature	**MHP**	**THP**	%**Difference**
Low	0.11	0.055	61.7%
Mid	0.059	0.037	46.8%
High	0.088	0.031	96.1%

The thermal resistance values for the MHP and THP show a considerable difference at all three levels, the largest being at the high-temperature range. This means that at all temperature ranges, the THP is able to transfer heat from the evaporator to the condenser more effectively. This is a direct function of the temperature difference at each of the ends. In the MHP at the low level, the temperature difference is 4.6 while the THP only has a temperature difference of 2.5. They are slightly closer at the middle level but separate considerably at the high-temperature range.

Table 5.3 shows the results from the evaluation of calculating the overall heat transfer coefficient of the two heat pipes.

Table 5.3: Average Heat Transfer Coefficient(W/m^2-°C) for MHP and THP

Temperature	**MHP**	**THP**	%**Difference**
Low	3.27	6.21	62.02%
Mid	5.73	9.24	46.89%
High	3.4	11.0	105.1%

Based on the analysis of the heat transfer coefficient values presented in Table 5.3, the following observations can be made:

- The trend observed in the average thermal resistance data is consistent with the average heat transfer coefficient data.
- At the low-temperature range, the THP exhibits slightly larger heat transfer coefficient values compared to the MHP.
- At the mid-temperature range, the difference between the two is closer, but the THP is still considerably higher.
- At the high-temperature level, the THP demonstrates a significantly larger heat transfer coefficient compared to the MHP, with difference of approximately 105.1%.
- This suggests that the THP performs better than the MHP in dissipating heat at high temperatures.

The findings in tables 5.2, and 5.3 show that the THP consistently performs at a higher level compared to the MHP. At the high-temperature range, the THP performs considerably better than the MHP.

Overall, the comparison of heat transfer coefficient and thermal resistance data between the THP and MHP reveals that the THP performs better compared to the manufactured heat pipe. This validates the effectiveness of the THP design and fabrication process. The results highlight that the THP is capable of achieving comparable or even superior heat transfer performance compared to the MHP, particularly at high-temperature levels.

5.2 BioHP and THP Comparison

5.2.1 Thermal Performance

After validating the heat pipe fabrication process, a comparison between the BioHP and THP designs can be conducted to evaluate their respective heat transfer capabilities. This comparison is based on the heat flux values (Q_{in}) at each temperature level, which indicates how effectively the heat pipes receive heat in the evaporator zone. By using the same process for finding the Q_{in} values shown in section 5.1, Table 5.4 presents the results obtained using Equation 4.5.

Table 5.4: Average Q_{in} for BioHP and THP

Temperature	**BioHP (W)**	**THP (W)**	**%Difference**
Low	22.79	50.39	75.4%
Mid	159.4	121.1	27.3%
High	378.6	463.7	20.2%

The findings demonstrate a significant difference in the amount of heat being transferred into the system between the BioHP and THP designs. At two of the three temperature levels, the THP outperforms the BioHP. At low-temperature ranges, the THP is considerably high, at the middle range, however, the BioHP surpasses the THP, but only by 27.3%, and at the highest level, the THP passes the BioHP and is slightly higher. It is worth noting it is only 20.2%, which indicates that they are performing similarly.

The heat flux calculations in Equation 4.5 solely consider the amount of heat input at the evaporator of the heat pipe. This calculation relies on the temperature difference between the oil and the evaporator. When the temperatures are closer to each other, the heat flux decreases. In the case of the BioHP at the low-high ranges, the evaporator temperature is closer to the oil temperature compared to the THP tests. This information will be further discussed in section 4.4.4, providing a more comprehensive understanding of the observed results.

5.2.2 Limitation Validation

After determining the heat fluxes, the next step is to calculate the pressure differences at each section of the heat pipe using Equations 2.3, 2.6, and 2.10. These values are then compared with the inequality given in Equation 2.2 using the inequality shown in Equation 2.1. The sum of the pressure differences from the three sections is denoted as ΔP_{tot}. Table 5.5 presents the results of this evaluation.

Table 5.5: Pressure Comparison for BioHP and THP (Pa)

Temperature	ΔP_{tot}BioHP	ΔP_{tot}THP	%Difference
Low	510.0	511.3	0.26%
Mid	511.0	515.2	1.02%
High	518.8	521.1	0.44%

The findings in Table 5.5 indicate that the pressure differences obtained for both the BioHP and THP designs at each temperature level satisfy the inequality for $\Delta P_{c,max}$ as specified in table 4.3. This suggests that the pressure gradients within each section of the heat pipes are within acceptable limits.

Furthermore, the results demonstrate that the behavior of the heat pipes, in terms of pressure gradients at each section, is nearly identical for both the BioHP and THP designs. The percentage differences in pressure between the two designs are negligible, ranging from 0.26% to 1.02%. This indicates that the two designs are effective in maintaining the required pressure differences for proper heat transfer and fluid flow within the heat pipe system.

5.2.3 Q_{out} Analysis

The analysis conducted in this study involves the use of data collected from the Cooling duct fan to quantify the amount of heat dissipated in the evaporator zone during steady-state conditions, as determined by Equation 4.6.

It is important to mention that temperature readings were only taken using the fan for the high-level tests. This decision was made because the radiation emitted from the heat pipes at the low and middle levels is too low to accurately measure the temperature difference. Table 5.6 presents the constant values used in the analysis, while Table 5.7 presents the heat leaving the heat pipe at the condenser (Q_{out}) and compares it to the previously calculated Q_{in} values from section 5.2.1. The area of the box was measured to be 0.00516 m^2. The fan speed was regulated by a voltage controller and was set to 60 W. The speed of air through the duct was then measured by the anemometer and was found to be 1.5 m/s. The density of air and the specific heat of air at constant pressure were then used

to find the mass flow rate of the air in the duct [2]. The calculations are shown below. They are also tabulated in table 5.6.

$$\dot{m} = 1.196 \cdot 0.00516 \cdot 1.5 = 0.0093(kg/s)$$

Table 5.6: Measured Values for Evaluation for BioHP and THP

Parameter	Value	Unit
ρ_{air}	1.196	kg/m^3
A_d	0.00516	m^2
V_d	1.5	m/s
C_p	1.006	kJ/kgK
$\dot{m}$	0.0093	kg/s

This can now be used to find the amount of heat dissipated at the condenser end by using the data collected by the fan thermocouples at the high level. The raw data in the graph is shown in Appendix C. The respective temperatures for each test and their calculations are shown below. It was found that T_{in-bio} = 19.88 °C, T_{in-THP} = 18.24 °C, $T_{out-bio}$ = 52.17 °C, and $T_{out-THP}$ = 40.2 °C.

$$Q_{out-THP} = (40.2 - 18.24) \cdot 1.006 \cdot 0.0093 = 204.6W$$

$$Q_{out-Bio} = (52.17 - 19.88) \cdot 1.006 \cdot 0.0093 = 300.8W$$

Table 5.7 shows a comparison between the Q_{in} calculated in section 5.2.1 and the Q_{out} values that were just found.

Table 5.7: Q_{out} Evaluation for BioHP and THP (W)

Parameter	BioHP (W)	THP (W)
$\dot{Q}_{in}$	378.6	463.7
$\dot{Q}_{out}$	300.8	204.6
η	79.45%	44.12%

This comparison shows that the BioHP has more heat reaching the condenser than the THP at these elevated temperatures. Only 77.8 Watts of energy is lost across the BioHP, while for the THP, 259.1 Watts of energy is lost.

Considering that for the Q_{in}, ΔP_{tot} both the HPs showed similar behaviors at the high-temperature range, and are unlike the trend that was previously observed.

To better understand the performance comparison of the THP and BioHP, the thermal resistance was found and is shown in table 5.8

Table 5.8: Thermal Resistance Comparison for BioHP and THP (°C/W)

Temperature	**BioHP**	**THP**	%Difference
Low	0.347	0.104	107.7%
Mid	0.106	0.036	98.6%
High	0.045	0.031	36.8%

This evaluation shows that there is a large difference at both the low and middle levels, with both being close to 100% different from each other. This implies that at lower temperatures, the BioHP has a considerably larger temperature gradient between the evaporator and the condenser. At higher temperatures, similar to what was seen in table 5.4, the values are closer. This indicates that at lower, temperatures, there is a higher temperature gradient across the two sections, but at elevated temperatures, the temperature difference is smaller.

5.2.4 Temperature Gradients

To provide further insight into the behavior of the heat pipes, temperature gradient graphs were generated to illustrate the temperature changes along the length of the heat pipes. Figure 5.1 displays the temperature gradient for both the BioHP and THP at the low-temperature level. The x-axis represents the location along the heat pipe, from the evaporator to the condenser, and the y-axis represents the temperature.

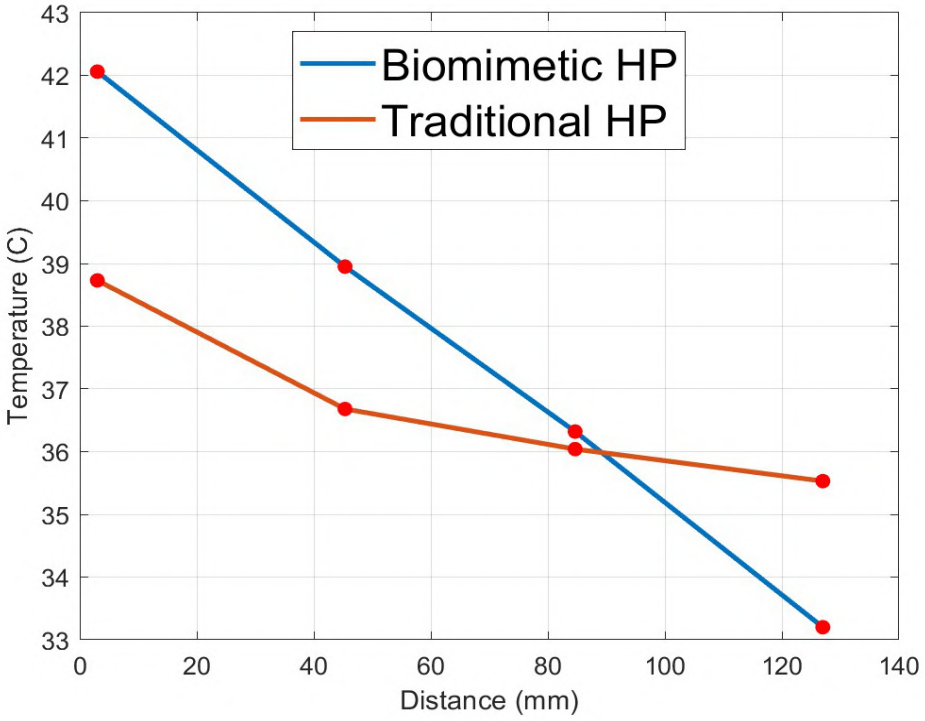

Figure 5.1: Temperature Gradient for BioHP and THP at Low Level

A traditional heat pipe should exhibit an almost isothermal relationship, with minimal temperature variations between each section of the heat pipe. As observed in Figure 5.1, the BioHP shows a nearly linear temperature profile, at each position, the temperature drops an average of three degrees. At steady state conditions, the BioHP drops a total of nine degrees. In contrast, the THP demonstrates relatively small temperature variations between different sections along the length of the heat pipe with a total temperature drop of 3.5 degrees. Due to the almost identical testing procedures of each heat pipe, it is possible that the biomimetic structure is playing a role in the large temperature drops.

Figure 5.2 illustrates the temperature gradients at the middle-temperature level. Similar to the low-temperature level, the BioHP still exhibits a predominantly linear temperature profile, albeit with a slight improvement toward an isothermal appearance. A total temperature drop of 21 degrees, over twice as large of a difference as the low test. This again, coupled with the data found in table 5.8 suggests the biomimetic structure is absorbing the heat, preventing the temperatures to reach levels similar to the THP. The temperature drop for the THP shows a smaller increase, with a total temperature difference of 5 degrees

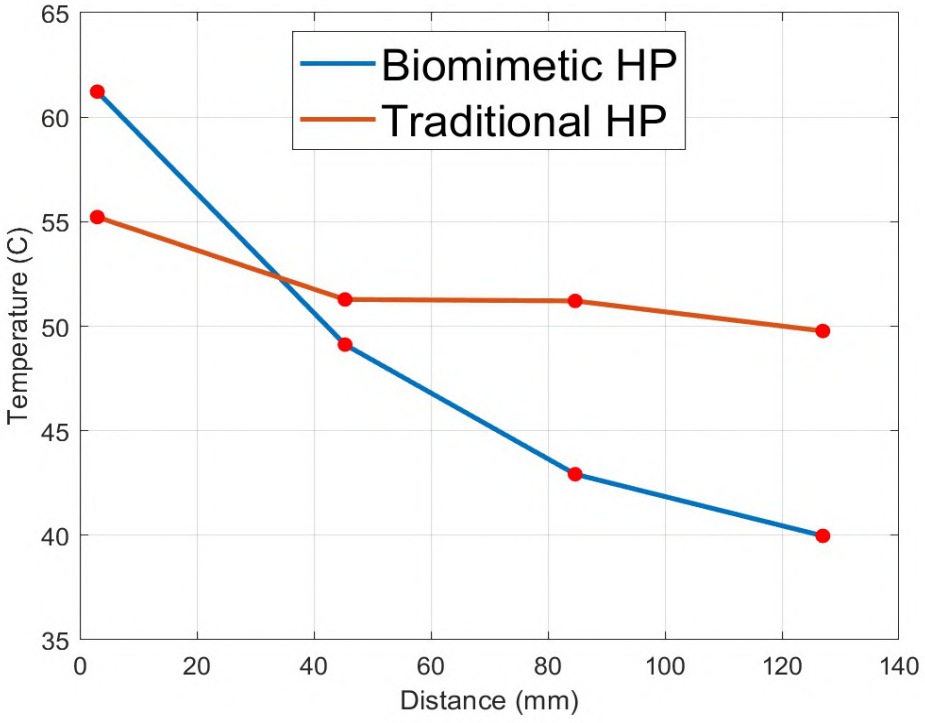

Figure 5.2: Temperature Gradient for BioHP and THP at Middle Level

Figure 5.3 presents the temperature gradients at the high-temperature level. At this level, a change is observed in the behavior of the BioHP. The total temperature drop for the BioHP is 14.5 degrees, suggesting that more heat flux is reaching the condenser end, resulting in a higher temperature at that end. This also is a similar observation that was made in earlier tests. At these elevated temperatures, the BioHP performs similarly to the THP.

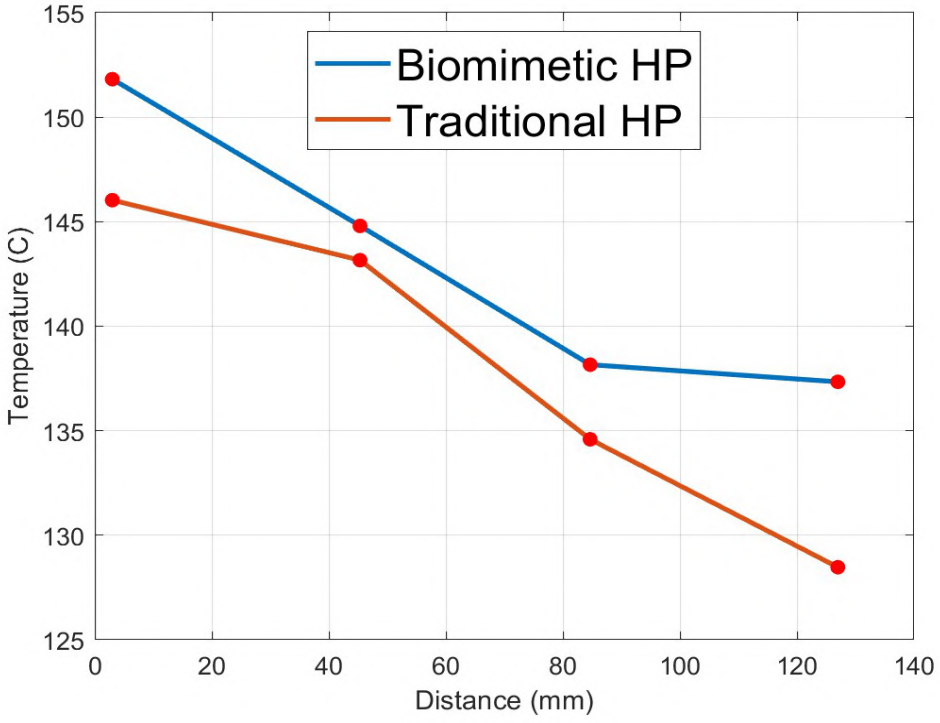

Figure 5.3: Temperature Gradient for BioHP and THP at High Level

Since each test was conducted under as close to identical conditions as possible, the primary variable between the two heat pipes is the biomimetic structure. The results strongly suggest that the material properties of the BioHP structure play a significant role in its performance at different temperature levels. At lower temperatures, the material appears to absorb a significant amount of heat, causing the vapor to condense into a liquid at an earlier section of the heat pipe.

As previously discussed in section 2.1.3 and section 3.2, vapor impacts on the biomimetic structure are theorized to influence condensation through the porous structure. From the performance evaluation, there is evidence that this is occurring. In both the resistance calculations, as well as what was seen in the temperature gradients, the temperatures of the BioHP reduce considerably across the length of the heat pipe. At higher temperatures, however, the BioHP shows a change in behavior that is not unlike the THP. This observation, coupled with the results found in table 5.7, show that at the high-temperature level, the heat is reaching the condenser and is not absorbing as much as what was shown in lower tests.

5.3 Integration Challenges

5.3.1 Temperature Measurements

After conducting the tests, it is important to address potential sources of error. One crucial consideration is the accuracy of thermal measurements during testing. The thermocouples used in the experiments followed the manufacturing standards outlined in IEC-584-2 [32], which allows for an error range of ±1.5°C within the temperature range of the tests. Although this error range is within acceptable bounds, it is essential to acknowledge its potential impact on heat pipe behaviors.

To validate the temperature measurements further, a Flir thermal camera was utilized to visualize the temperature gradients of the heat pipes. Figure 5.4 displays a thermal image of the THP at the high-temperature level. It is worth noting that these images were captured after the high-temperature tests, as the low and middle levels did not exhibit significant temperature changes compared to the environment. Because, there is no way to see the entire heat pipe during testing, due to the oil's heat preventing this the heat pipes were removed from the testing apparatus. Additionally, it is challenging to maintain stable temperatures once the heat pipes are removed from the oil, leading to reduced accuracy in capturing temperatures similar to those during the tests. Figure 5.4 show the thermal image of the THP in and demonstrates relatively consistent temperature distribution along the length of the heat pipe.

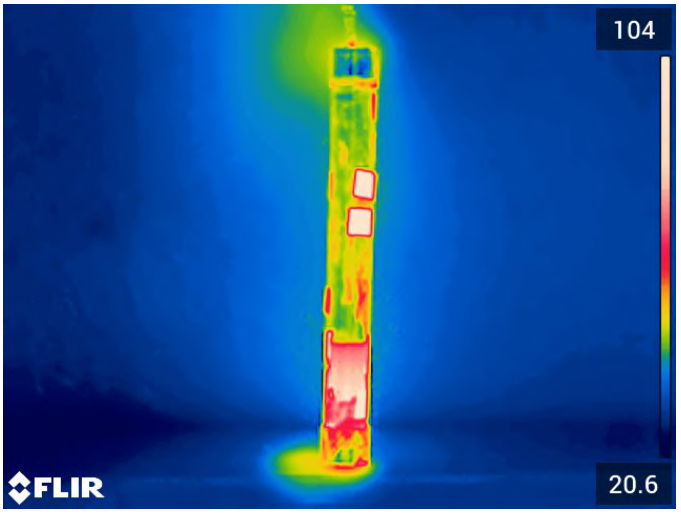

Figure 5.4: THP Thermal Image at High Temperature Level

The lower portion of the image corresponds to the hot region where the heat pipe was immersed in the oil. Residual oil is visible due to difficulties in removing it completely. The warm regions in the middle of the image are reflections

caused by thermal tape, creating an exaggerated appearance of higher temperatures when, in reality, they are at the same temperature as the heat pipe. Figure 5.5 showcases the thermal image of the BioHP, displaying a similar temperature distribution pattern.

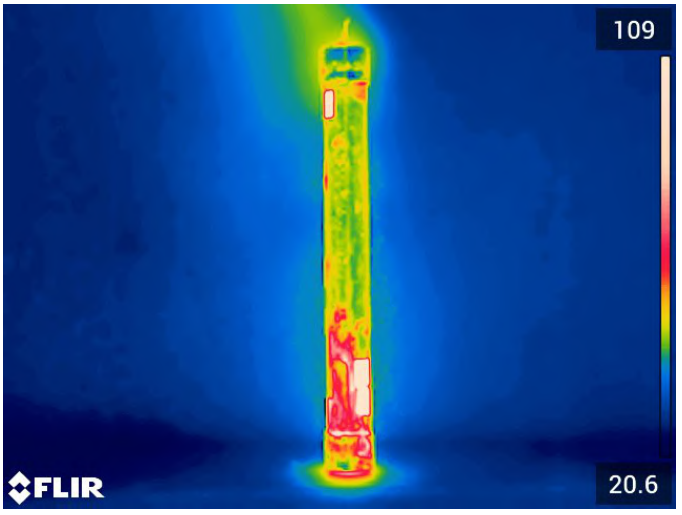

Figure 5.5: BioHP Thermal Image at High Temperature Level

The colder areas in the regions where the caps are located are attributed to the caps acting as additional barriers to heat transfer. Soldering the caps creates an additional medium that heat needs to pass through. These thermal images provide further validation of the thermal couple readings at high temperatures, especially when comparing them to the MHP. Figure 5.6 presents the thermal images of the MHP at high temperatures, demonstrating comparable temperature gradients to the other two heat pipes.

Although the thermal images cannot be directly compared to the thermal couple data, they confirm consistent temperature gradient behavior among the heat pipes at high-performance temperatures.

5.3.2 Testing Set-up

While each test was conducted with care, it's important to consider the potential sources of error that may have influenced the results. One such source is the fluctuation of ambient temperatures both in the testing room and within the heated box. Despite efforts to maintain a consistent environment, the lid box had issues completely sealing to the rest of the box, which could have caused fluctuations in the heat pipe temperatures. It should be noted, however, that the measurement values used in the results were obtained when the heat pipes reached steady-state conditions, and most of the temperature variations occurred during the transient phase of the tests.

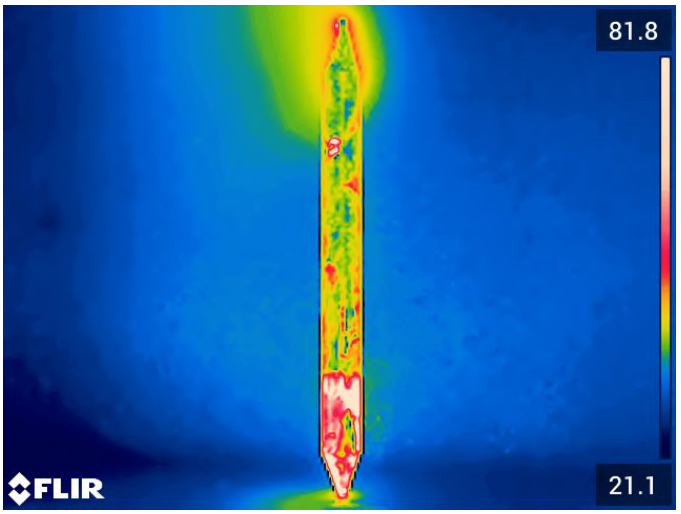

Figure 5.6: MHP Thermal Image at High Temperature Level

Another potential source of error is related to the placement and adhesion of the thermocouples on the heat pipes. Although great care was taken in positioning the thermocouples, measuring and marking their placement, and securing them with thermal tape, there were challenges associated with the properties of the silicone oil. The thermal tape sometimes had difficulty adhering to the heat pipe surface without coming into contact with the oil. Additionally, as multiple tests were performed on each heat pipe, thorough cleaning was necessary to remove any residual oil. Despite efforts to clean the heat pipes, some spots may have been missed, and the tape's adhesive properties could have been compromised, leading to a loss of thermal contact with the heat pipe. Whenever this was observed, the thermocouples were correctly reattached, and the issue was noted.

Regarding the oil used in the experiments, it's worth noting that there were variations in its temperature, as well as the temperature of the hot plate. Maintaining a consistent temperature for the oil between tests proved to be challenging. Silicone oil is known for its ability to retain heat once it reaches a steady state temperature, which is advantageous. However, achieving the desired steady-state temperature was not always straightforward, particularly when aiming for lower temperatures. During the tests, the oil temperature would eventually stabilize, but it could still be observed to exhibit slight fluctuations, with a gradual increase or decrease over time. To ensure the accuracy of the data collected, it was ensured that the oil temperature for each temperature level analysis remained consistent.

Lastly, it's important to acknowledge a potential limitation regarding the readings at the evaporator section. In the graphs displayed in section 5.2.4, it is evident that the evaporator temperature often appeared significantly higher than the temperatures at other sections, even when the other sections showed an almost isothermal relationship. This discrepancy is attributed to the thermal couple in the oil, which, despite being partially protected by thermal tape, still

experienced some heat flux from the hotter oil. Consequently, the temperature of the evaporator was influenced, and attempts to add additional thermal tape to mitigate this effect did not yield significant corrections.

5.3.3 Biomimetic Structure Integrity

To assess the physical integrity of the BioHP during the tests, a cross-section of the heat pipe was cut to examine the structure's condition, particularly after subjecting it to high temperatures. Since copper, the material used in the heat pipe is opaque, it is not possible to directly observe the internal state of the heat pipe during operation. However, by examining the cross-section, it can be determined if the structure maintained its shape and integrity throughout the testing. Figure 5.7 illustrates the result of cutting the BioHP.

Figure 5.7: Cross-section of BioHP After Testing

The image demonstrates that the biomimetic structure remained intact and unaffected by the rigorous testing it underwent. This observation along with the integrity test shown in fig. 3.14 provides validation to the results obtained for the BioHP and supports the conclusions drawn. It suggests that the structural design of the BioHP is capable of withstanding the testing conditions and retains its functionality even under high-temperature operating conditions.

5.3.4 Other Potential Sources

There are a few additional potential sources that need to be addressed and are not able to be categorized anywhere else.

Repeatability A total of 22 tests were conducted and used for this research with a total of 6 heat pipes tests, four of them being fabricated in-house. This approach was adopted to account for any variations in manufacturing and fabrication among the heat pipes. However, it should be noted that the number of tests conducted is still relatively low. To establish a robust understanding of the behavior of each heat pipe design in different situations, a larger number of tests would be ideal, preferably around twenty tests for each scenario across each heat pipe, about three times more than what was already done. Unfortunately, due to limitations in available resources, such a comprehensive test campaign was not feasible within the given time frame.

Nevertheless, conscious efforts were made to ensure consistency and reliability in the results. This was particularly emphasized during the fabrication and sealing processes of the THP and BioHP. As mentioned in section 4.1.1, five tests were performed to verify the effectiveness of the sealing process. Figure 5.8 provides thermal images captured during the sealing process, showing the formation of bubbles at the straw end as the working fluid begins to boil. These images served as indicators of the appropriate timing for sealing the heat pipe.

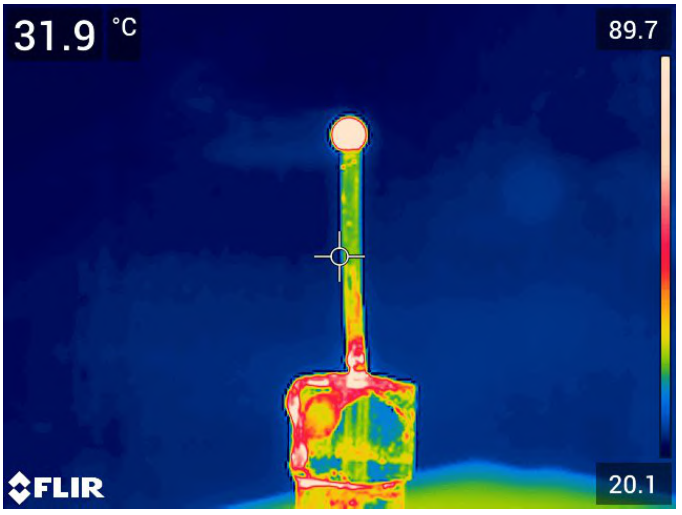

Figure 5.8: Thermal Images During Sealing Process

It is important to acknowledge that the sealing process itself may introduce some unforeseen errors. The amount of vapor lost during the process could not be precisely determined until after the sealing was completed. However, this

loss was expected to have a minimal impact on the test results, as the maximum amount of fluid lost during the tests was only 0.3 ml.

Additionally, challenges were encountered in maintaining a reliable seal at the straw end. The tool used for cold welding the straw effectively sealed the heat pipes, as demonstrated in section 4.1.1. However, the sealing process created a fragile area near the sealed end of the straw. Dislocations in the crystalline structure of the metal caused brittleness in this region. Special care was taken to prevent any bumps or disturbances to the end of the straw, as it could potentially introduce air or affect the integrity of the seal. It is worth mentioning that in the high-temperature tests, any failure in the seal would have been evident, as the temperatures exceeded the boiling point of water. No observations of unsealed heat pipes or the presence of water at the end of the heat pipes were made during the tests, indicating the integrity of the sealing process.

Potentials in Human Error It is crucial to acknowledge that human error is always a possibility when collecting and compiling data, as well as conducting experiments. Despite careful adherence to experimental procedures, there is always a chance of inaccuracies in readings, calculation errors, or even a limited understanding of the underlying physical phenomena. In an effort to minimize human error, a second individual was involved in cross-checking all collected data and calculations. However, it is important to recognize that random errors associated with human involvement should be considered as a potential source of uncertainty in the results.

CHAPTER 6

CONCLUSIONS AND RECOMMENDATIONS

6.1 Conclusions

This research compares the efficacy of a biomimetic design by comparing it with a traditional two-phase wick design. Through comprehensive thermal analysis, physical experiments, and rigorous validation techniques, evidence suggest the biomimetic structure disperses heat across the length of the heat pipe, notably at lower temperature ranges. The ideas discussed in section 2.1.3 lend credibility to the observed results. The heat distribution patterns and thermal analysis data observed at the lower temperature levels strongly suggest that the absorption of the internal structure influenced the findings in section 5.2.

When considering high temperatures, the concepts presented in Chapter 2, particularly in section 2.7, further support the notion that increasing vapor velocity at high temperatures improves heat distribution performance. There is evidence for this in section 5.2.3, but further research is necessary to observe similar trends. Additionally, the ideas discussed in section 2.1.3 lend credibility to the observed results. The heat distribution patterns observed at the lower temperature levels strongly suggest that the absorption of the internal structure influenced the findings in section 5.2.4.

6.2 Contributions

6.2.1 Heat Pipe Testing Methods

This research achieved a significant milestone by developing a unique testing method for heat pipes that has not been previously explored in the existing literature. The literature investigation conducted revealed a scarcity of research on gravity-assisted heat pipes utilizing water as the working fluid, and the methods devised in this study are not documented in other published works. Section 3.3 further discusses the need for an ASTM standard, and the need to create a detailed testing procedure.

6.2.2 Heat Pipe Fabrication

This research introduces novel fabrication techniques that are distinct from those commonly found in the existing literature and industrial practices. Conventional fabrication techniques for heat pipes often involve complex processes and the use of specialized equipment, which may not be feasible for individual researchers or small research groups. The techniques detailed in Chapter 3 enable researchers to achieve satisfactory results using readily available materials that can be purchased off the shelf. By presenting these techniques, this research opens up opportunities for future researchers to effectively fabricate heat pipes without the need for extensive resources or specialized equipment, thereby facilitating further investigations in this field. It is also worth noting that like the testing methods detailed above, there is no ASTM standard for the fabrication of heat pipes.

6.2.3 Space Application

The research findings indicate that the biomimetic heat pipe design has the potential to enhance heat dissipation, particularly at high temperatures. However, further investigation is required to determine its applicability in nuclear environments, especially at significantly higher temperatures. Additionally, the integration of fins and modifications to the wick design could further enhance heat dissipation capabilities.

Testing heat pipes in space-like conditions poses significant challenges. However, considering the successful utilization of heat pipes on the ISS, it is plausible to adapt heat pipe designs for space applications with appropriate modifications. Suggestions for improved materials in space applications include the use of aluminum casings. Aluminum is renowned for its lightweight properties and is commonly employed in space-related endeavors. Moreover, selecting a working fluid capable of withstanding both high and low temperatures is crucial. Dynaline, a molten salt material, exhibits these desired properties and is proposed as a potential working fluid for future heat pipe designs intended for space applications [33]. By incorporating these advancements, heat pipe technology can be further optimized for space-based thermal management systems.

6.3 Future Work

Exploring alternative biomimetic structures constructed from metal materials to enhance the thermal conductivity of the heat pipe is recommended. Metal structures would facilitate more efficient heat transfer across all temperature ranges. However, extensive research and development would be required to establish effective manufacturing techniques for such complex structures. Metal 3D printing is a potential avenue, although precise tolerances must be ensured.

Improving the testing apparatus is another important recommendation. While the current apparatus served its purpose, it can be further optimized. Addressing gaps in the box to prevent heat leakage would enhance the accuracy of the tests. Additionally, implementing a cooling jacket system at the condenser end, instead of relying on the fan method, would provide better temperature regulation and enable more reliable low-temperature testing.

The results from Figure 5.3 deviate from the expected heat dissipation pattern observed in Figures 5.1 and 5.2, where heat is distributed uniformly across the length of the Biomimetic Heat Pipe (BioHP). This discrepancy is likely due to the vapor velocity increasing and reaching the condenser end of the heat pipe. Evidence for this phenomenon was further discussed in section 2.7.

To achieve efficient heat dissipation across the entire length of the BioHP at higher temperatures, it is recommended that the biomimetic structure gradually increases in pore size along its length. This configuration would mimic the behavior of a converging-diverging nozzle for the vapor flow [2, 22]. This was discussed in section 2.8. By gradually enlarging the pores, the vapor flow would decelerate, preventing it from reaching the condenser section prematurely, as observed in the high-temperature tests [22]. It is important to note, that this is only a possibility if the flow is under sonic conditions [14].

Furthermore, conducting a more extensive series of tests, particularly at higher temperatures, would shed more light on how the biomimetic structure behaves. Due to limitations imposed by the properties of the oil, the maximum heat flux that could cause the heat pipe to cease operation was not determined. While significant evidence supports the superior heat dissipation capabilities of the biomimetic structure, expanding the sample size would provide a more comprehensive understanding of its performance. Moreover, exploring design modifications such as geometry alterations, increased wick porosity, and refined cap designs could further optimize the heat pipe's effectiveness.

Lastly, performing simulation analysis, specifically Finite Element Analysis (FEA), is recommended. Although the original research intended to include comprehensive simulations detailing the internal behaviors of the biomimetic heat pipe, constraints related to licensing and funding prevented their execution. Conducting FEA simulations would provide valuable insights and validation of the effects of the biomimetic structure, enabling a deeper understanding of its behavior and performance that may not be observable through physical testing alone. This simulation analysis was originally a part of the scope of this research, and many hours were put into developing a detailed FEA simulation. Unfortunately, NMT only holds a classroom license, and once it was known that research was being performed on that license by the software company, all simulations relating to the Heat Pipes were ended. An attempt to buy a research license was attempted, but due to a limitation in funding, it was not purchased.

6.4 Final Thoughts

In conclusion, this research has provided valuable insights into the field of heat pipes and their potential for passive heat dissipation. The findings demonstrate the effectiveness of heat pipes as a reliable method for heat transfer, owing to the unique properties of the working fluid. Furthermore, the investigation of biomimetic heat pipes has shown promising results and suggests that they have the potential to be the heat pipes of the future.

Although the research conducted in this study did not uncover all the desired outcomes, it has laid a solid foundation for future investigations. There are still numerous avenues for further exploration, including the development of more robust fabrication techniques and the careful consideration of diverse applications. By refining the manufacturing processes and exploring different materials, the performance of heat pipes can be further optimized.

The evidence gathered through this research supports the notion that biomimetic heat pipes are capable of dissipating heat across the entire length. However, more studies and grants are required to delve deeper into this field and fully explore its potential. The research conducted here serves as a stepping stone, providing valuable insights and opening up new possibilities for future advancements in heat pipe technology.

Overall, this research has contributed to the growing body of knowledge in the field of heat pipes and has set the stage for further investigations. With continued efforts and support, it is thought that heat pipes, particularly biomimetic designs, could play a role in addressing future heat dissipation challenges.

REFERENCES

[1] Anon. "NASA Space Technology Roadmaps and Priorities". Technical report, 6 2012.

[2] D. A. Reay, P. A. Kew, and R. J. McGlen. *Heat pipes: theory, design and applications*. Butterworth-Heinemann, 2014.

[3] Briana N. Tomboulian. *Lightweight, High-Temperature Radiator for In-Space Nuclear-Electric Power and Propulsion*. PhD thesis, University of Massachusetts Amherst, 2014.

[4] Nima Shokri, Peter Lehmann, and Dani Or. "Critical evaluation of enhancement factors for vapor transport through unsaturated porous media". *Water Resources Research*, 45(10), 2009.

[5] C. E. Kohlhase and P. A. Penzo. "Voyager mission description". *Space Science Reviews*, 21(2):77–101, 1977.

[6] C. L. Stokely and Eileen K. Stansbery. "Identification of a debris cloud from the nuclear powered snapshot satellite with haystack radar measurements". *Advances in Space Research*, 41(7):1004–1009, 1 2008.

[7] T.P. Cotter. "Theory of Heat Pipes". Technical report, Los Alamos Scientific Laboratory of the University of California, 1965.

[8] Brian Dunbar. "Keeping Cool with Heat Pipes on the Space Station". NASA's Glenn Research Center, 2011. https://www.nasa.gov/mission-pages/station/research/news/heat-pipes.html. (accessed May 25, 2022).

[9] Lee Mason and Dave Poston. "Fission Surface Power System Initial Concept Definition". Technical report, National Aeronautics and Space Administration and Department of Energy, 2008.

[10] Hiroshi Kawamura and Koichi Nishino. "Chaos, Turbulence and its Transition Process in Marangoni Convection". Japan Aerospace Exploration Agency, 2013.

[11] A.K. Ghosh. "Thermal Management Characteristics of a Fluid Filled Porous Composite - An Experimental Investigation". 23^{rd} Nat. Heat And Mass Transfer Conf. and the 1^{st} Int. ISHMT-ASTFE Heat And Mass Transfer Conf., Thiruvanthapuram, India, December 17-20, 2015.

[12] C. A. Busse. "Theory of the Ultimate Heat Transfer Limit of Cylindrical Heat Pipes". *International Journal of Heat and Mass Transfer*, 16:169–186, 1973.

[13] L.K. Tower and D.C. Hainley. "An Improved Algorithm for the Modelling of Vapour Flow in Heat Pipes". 9^{th} International Heat Transfer Conference, Minsk, USSR, 21-25 May 1990.

[14] F.C. Prenger, J.E. Kemme, M. Groll, and T. Spendel. "Performance limits for smooth-wall gravity-assisted heat pipes". AIAA Thermophysics Conference, Monteral, Canada, 1 June 1983.

[15] W M Rohsenow and P Griffith. "Correlation of Maximum Heat Flux Data for Boiling of Saturated Liquids". Technical report, Massachusetts Inst. of Tech., Cambridge. Div. of Industrial Cooperation, 1955.

[16] Andreas H. Brautsch. "Heat Transfer Mechanisms During the Evaporation Process From Mesh Screen Porous Structures". Heriot Watt University, Dept. Engineering Physical Sciences, Edinburgh, United Kingdom, 1970.

[17] F. Reiss and K. Schretzmann. "Pressure balance and maximum power density at the evaporation". 2^{nd} Intern. Conf. on Thermionic Electrical Power Generation, Stresa, Italy, May 1963.

[18] Joseph E. Kemme. "Ultimate heat-pipe performance". *IEEE Transactions on Electron Devices*, 16:717–723, 1969.

[19] Ebrahim Shahraeeni and Dani Or. "Pore Scale Mechanisms for Enhanced Vapor Transport Through Partially Saturated Porous Media". *Water Resources Research*, 48, 2012.

[20] Vyacheslav Cheverda, I. S. Vozhakov, and F. V. Ronshin. "Heat pipe: a Simple One-dimensional Model and an Experimental Study". *Journal of Physics: Conference Series*, 1369:12–54, 2019.

[21] J. R. Philip and D. A. De Vries. "Moisture movement in porous materials under temperature gradients". *Eos. Transactions American Geophysical Union*, 38:222–232, 1957.

[22] John David Anderson. *Modern Compressible Flow: With Historical Perspective*. McGraw-Hill, 4 edition, 2021.

[23] David Jon Furbish. *Fluid Physics in Geology: An Introduction to Fluid Motions on Earth's Surface and within Its Crust*. Oxford University Press, 1996.

[24] Patrick E. Fleming, and Tom Neils, "Physical and Theoretical Chemistry Textbook" ChemistryLibreTexts, 2022. [Online]. Available: https://chem.libretexts.org. Accessed: June 10, 2023.

[25] ASTM International. "Standard Test Method for Steady-State Heat Transfer Properties of Pipe Insulation". ASTM C335-05, 2005.

[26] ASTM International. "Standard Test Method for Evaluating the Resistance to Thermal Transmission of Materials by Guarded Heat Flow Meter Technique". ASTM E1530-06, 2006.

[27] ASTM International. "Standard Test Method for Thermal Conductivity and Thermal Diffusivity by Modulated Temperature Differential Scanning Calorimetry". ASTM E1952-06, 2006.

[28] Anon. "Wakefield-Vette 124672". https://www.digikey.com/en/products/detail/wakefield-vette/124672/9356471(accessed May 20,2023).

[29] Aloke Kumar Mozumder, Abul Fahad Akon, Mahbub M. U. Chowdhury, and Sajal Chandra Banik. "Performance of Heat Pipe for Different Working Fluids and Fill Ratios". *Journal of the Institution of Engineers Bangladesh*, 41(2):96–102, 2011.

[30] Sicong Tan, Cong Guo, Yuyan Jiang, Tao Wang, and Chengzhan Li. "Investigation on Permeability of Ultra-thin Screen Wick with Free Surface Using Gravity Flow and Numerical Simulation Methods". *International Communications in Heat and Mass Transfer*, 131:58–79, 2 2022.

[31] Yunus A. Çengel and Afshin J. Ghajar. *Heat and mass transfer: fundamentals & applications*. McGraw Hill Education, fifth edition edition, 2015.

[32] Anon. "Thermocouples - Part 2: Tolerances". Technical Report IEC-584-2, 1982.

[33] Anon. "Dynalene Molten Salts". https://www.dynalene.com/product-category/heat-transfer-fluids/dynalene-molten-salts/. (accessed: July, 7 2022).

APPENDIX A

MATLAB SCRIPT

A.1 Constants and Q dot Calculations

```
1
2  clear; clc;
3
4  sig=58.9e-3; %surface tension of water
5  L=2.258e6; %Latent heat of water
6  rho1=958;%density of liquid water
7  rho2=.5974;  %density of vapor water
8  l=.16;%total length of pipe
9  mu=.282e-3;
10 % numoflayers1=2
11 % numoflayers2=1
12 w_d1=0.0045% cm
13 w_d2=0.0025;
14 la=.092;
15 le=.034;
16 lc=.034;
17 leff=la+((lc+le)/2)
18 D1=1;
19 D2=0.7;
20 d=.014;%m diameter of the tube
21 t_1w=.0002;% Wick thickness
22 ps=5e-6;%poresize
23 e=0.05;%Porosity
24 layers=3%Number of layers of copper mesh
25 t_w=t_1w*layers%Total thickness of wick
26 d_a=d-t_w %diameter of adiabatic zone
27 rt=0.018/2%total radius submerged in oil00
28 r_manu_t=0.012/2;%radius of manufatured HP
29 h=0.04;%Height submerged in tube
30 Aw=t_w*pi*d;%cross-sectional area of wick.
31 h_cyl=0.02;
32 lcap=0.014;%length of cap
```

```
le1=le-lcap;%length of pipe not connected to cap
rc=0.009;%radius of cap
%%
% surface area of tube submerged in oil

At=((2*pi*rt^2)+(2*pi*rt*le1))+((2*pi*rc^2)+(2*pi*rc*lcap));
Aa=pi*(d_a/2)^2;%area of adiabatic zone
ho=4100;%w/(m^2K) Thermal conductivity of Silicone


%%
% %AVERAGE Low temperature values

T_oil_low = 36.98;
T_evap_low_bio = 35.09;
T_con_low_bio = 27.19;
T_evap_low_thp = 32.8;
T_con_low_thp = 30.0324;
T_evap_low_mhp = 33.35;
T_con_low_mhp = 28.8;

%%
% % AVERAGE Mid temperature values

T_oil_mid = 70.1;
T_evap_mid_bio = 56.88;
T_con_mid_bio =39.97;
T_evap_mid_thp =60.052;
T_con_mid_thp = 55.593;
T_evap_mid_mhp = 60.68;
T_con_mid_mhp = 53.94;

%%
% % AVERAGE High temperature values

T_oil_high = 171.6;
T_evap_high_bio = 140.2;
T_con_high_bio = 123.1;
T_evap_high_thp = 133.14;
T_con_high_thp = 118.83;
T_evap_high_mhp = 143.7;
T_con_high_mhp = 110.33;

%%
```

```
% % Low temperature Heat Flux calculations

Q_bio_low = At * ho * (T_oil_low - T_evap_low_bio)
Q_thp_low = At * ho * (T_oil_low - T_evap_low_thp)
Q_mhp_low = At * ho * (T_oil_low - T_evap_low_mhp)
%%
% %Low Temperature Thermal Resistance

R_low = [
    (T_evap_low_bio - T_con_low_bio)/Q_bio_low
    (T_evap_low_thp - T_con_low_thp)/Q_thp_low
    (T_evap_low_mhp - T_con_low_mhp)/Q_mhp_low
]
%%
% % Low Temperature Heat Transfer Coefficent

h_low = [
     Q_bio_low / (At * (T_evap_low_bio - T_con_low_bio))
     Q_thp_low / (At * (T_evap_low_thp - T_con_low_thp))
     Q_mhp_low / (At * (T_evap_low_mhp - T_con_low_mhp))
]
%%
%
%
% % Mid temperature Heat Fluxcalculations

Q_bio_mid = At * ho * (T_oil_mid - T_evap_mid_bio)
Q_thp_mid = At * ho * (T_oil_mid - T_evap_mid_thp)
Q_mhp_mid = At * ho * (T_oil_mid - T_evap_mid_mhp)
%%
% %Mid Temp. Resistance

R_mid = [
    (T_evap_mid_bio - T_con_mid_bio)/Q_bio_mid
    (T_evap_mid_thp - T_con_mid_thp)/Q_thp_mid
    (T_evap_mid_mhp - T_con_mid_mhp)/Q_mhp_mid
]
%%
% %Mid Temp HT Coefficent

h_mid = [
     Q_bio_mid / (At * (T_evap_mid_bio - T_con_mid_bio))
     Q_thp_mid / (At * (T_evap_mid_thp - T_con_mid_thp))
     Q_mhp_mid / (At * (T_evap_mid_mhp - T_con_mid_mhp))
```

```
]

%%
% % High temperature Heat Flux calculations

Q_bio_high = At * ho * (T_oil_high - T_evap_high_bio)
Q_thp_high = At * ho * (T_oil_high - T_evap_high_thp)
Q_mhp_high = At * ho * (T_oil_high - T_evap_high_mhp)
%%
% %High Temperature Thermal Resistance

R_high = [
    (T_evap_high_bio - T_con_high_bio)/Q_bio_high
    (T_evap_high_thp - T_con_high_thp)/Q_thp_high
    (T_evap_high_mhp - T_con_high_mhp)/Q_bio_high
]
%%
% %High Temperature HT Coefficent

h_high = [
    Q_bio_high / (At * (T_evap_high_bio - T_con_high_bio))
    Q_thp_high / (At * (T_evap_high_thp - T_con_high_thp))
    Q_mhp_high / (At * (T_evap_high_mhp - T_con_high_mhp))
]
Q_low = [Q_bio_low, Q_thp_low, Q_mhp_low]
Q_mid = [Q_bio_mid, Q_thp_mid, Q_mhp_mid]
Q_high = [Q_bio_high, Q_thp_high, Q_mhp_high]
%%
% % Rearrange the data for plotting

R_values = [R_low, R_mid, R_high]'
h_values = [h_low, h_mid, h_high]'
Q_values = [Q_low; Q_mid; Q_high]

%%
% % Create bar graphs

degrees = char(176);
parameters = {'R ( C /W) ', 'h (W/m^2- C ) ', 'Q (W) '};
parameters2 = {'Resistance', 'HT Coeficent', 'Heat Flux'};
temperatures = {'Low', 'Mid', 'High'};
heatpipes = {'Bio', 'THP', 'MHP'};
values = {R_values, h_values, Q_values};

```

```
%%
% MHP to THP compairson

heatpipes = {'MHP', 'THP'};  % Updated to include only MHP
    and THP
values = {R_values(:, [3, 2]), h_values(:, [3, 2]),
    Q_values(:, [3, 2])};
parameters = {'R ( C /W) ', 'h (W/m^2- C ) ', 'Q (W) '};

% Create the first figure for Resistance (R)
figure;
for j = 1:3
    subplot(3, 1, j);
    bar(values{1}(j, :), 'BarWidth', 0.7);
    ylabel(parameters2{1});
    title([parameters{1} '-' temperatures{j}]);
    set(gca, 'XTickLabel', heatpipes);
%     grid on;
%

end
sgtitle('Heat Pipe Resistance');

% Create the second figure for Heat Transfer Coefficient (h)
figure;
for j = 1:3
    subplot(3, 1, j);
    bar(values{2}(j, :), 'BarWidth', 0.6);
    ylabel(parameters2{2});
    title([parameters{2} '-' temperatures{j}]);
    set(gca, 'XTickLabel', heatpipes);

end
sgtitle('Heat Pipe Heat Transfer Coefficient');

% Create the third figure for Heat Flux (Q)
figure;
for j = 1:3
    subplot(3, 1, j);
    bar(values{3}(j, :), 'BarWidth', 0.6);
    ylabel(parameters2{3});
    title([parameters{3} '-' temperatures{j}]);
    set(gca, 'XTickLabel', heatpipes);

```

```
%     grid on;

end
sgtitle('Heat Flux at Steady State');

subplot(3,1,1)
set(gca,"XGrid","off","YGrid","on")
subplot(3,1,2)
set(gca,"XGrid","off","YGrid","on")
subplot(3,1,3)
set(gca,"XGrid","off","YGrid","on")

%%
% Bio VS THP Compairsion

heatpipes = {'Bio', 'THP'};  % Updated to include only MHP
   and THP
values = {R_values(:, [1, 2]), h_values(:, [1, 2]),
   Q_values(:, [1, 2])};
parameters = {'R ( C /W) ', 'h (W/m^2- C ) ', 'Q (W) '};

% Create the first figure for Resistance (R)
figure;
for j = 1:3
    subplot(3, 1, j);
    bar(values{1}(j, :), 'BarWidth', 0.6);  % Set the
       'BarWidth' property to 0.6
    ylabel(parameters2{1});
    title([parameters{1} '-' temperatures{j}]);
    set(gca, 'XTickLabel', heatpipes);
%     grid on;

end
sgtitle('Heat Pipe Resistance');

% Create the second figure for Heat Transfer Coefficient (h)
figure;
for j = 1:3
    subplot(3, 1, j);
    bar(values{2}(j, :), 'BarWidth', 0.6);  % Set the
       'BarWidth' property to 0.6
    ylabel(parameters2{2});
    title([parameters{2} '-' temperatures{j}]);
%     set(gca, 'XTickLabel', heatpipes);
```

```
%     grid on;

end
sgtitle('Heat Pipe Heat Transfer Coefficient');

% Create the third figure for Heat Flux (Q)
figure;
for j = 1:3
    subplot(3, 1, j);
    bar(values{3}(j, :), 'BarWidth', 0.6);  % Set the
       'BarWidth' property to 0.6
    ylabel(parameters2{3});
    title([parameters{3} '-' temperatures{j}]);
    set(gca, 'XTickLabel', heatpipes);
%     grid on;

end
sgtitle('Heat Pipe Heat Flux');


hold off

%%
% Pressure calcualtions

% % Constants
rho1 = 958;               % Density of liquid (kg/m^3)
g = 9.81;                 % Acceleration due to gravity (m/s^2)
phi = 90;                  % Angle of heat pipe relative to
   horizontal (degrees)
mu1 = 0.282e-3;           % Dynamic viscosity of liquid (Pa s)
L = 2.26e6;               % Latent heat (J/kg)
A_w = 1.32e-4;            % Cross-sectional area of wick (m^2)
K = 5.14e-9;              % Wick permeability (m^2)
dotQ = [22.79; 159.4; 378.56];  % Heat transfer values for
   THP (W)
dotQ2 = [50.39; 121.1; 463.7];  % Heat transfer values for
   BioHP (W)
l_a = 0.054;              % Length of adiabatic section (m)
l_e = 0.038;              % Length of evaporator section (m)
r_v = d_a/2;               % radius of adiabatic section (m)
rho_v = 0.597;            % Density of vapor (kg/m^3)
mu_v = 0.282e-3;          % Dynamic viscosity of vapor (Pa s)
dotm=dotQ/L
```

```
dotm2=dotQ2/L
% Calculate pressure differences
% Gravitational pressure difference (Pa)
deltaP_g = rho1 * g * l_a * sind(phi)  % Gravitational
   pressure difference (Pa)
 % Flow cross-section of wick (m^2)
A_f = pi * (r_v^2) * (1 - 0.05);
l_eff = l_a + (l_e / 2);  % Effective length (m)
% Pressure drop through the wick (Pa)
deltaP_1 = (mu1 * dotQ * l_eff) / (rho1 * L * A_w * K)
 %Total pressure difference in vapor section (Pa)
deltaP_v = ((8 * mu_v * dotm) / (pi * rho_v *
   (r_v^4)))*l_eff  % Total pressure difference in vapor
   section (Pa)



A_f = pi * (r_v^2) * (1 - 0.05);  % Flow cross-section of
   wick (m^2)

l_eff = l_a + (l_e / 2);  % Effective length (m)
% Pressure drop through the wick (Pa)
deltaP_1_bio = (mu1 * dotQ2 * l_eff) / (rho1 * L * A_w * K)
   % Pressure drop through the wick (Pa)
% Total pressure difference in vapor section (Pa)
deltaP_v_bio = ((8 * mu_v * dotm2) / (pi * rho_v *
   (r_v^4)))*l_eff


dP_total_bio=deltaP_v_bio+deltaP_1_bio+deltaP_g

dP_total=deltaP_v+deltaP_1+deltaP_g
%
%
%%
% Q_out Flow evaluation

rho_a=1.196; %Density of Air
A=0.00516128; %area of the duct in m^2
V=1.5;%(m/s) Velocity of the air
m_dot=rho_a*A*V;%kg/s mass flow rate of the air in duct
Cp=1.006 %kJ/kgK
T_fan_bio=19.88
T_duct_bio=52.17
```

```
T_fan_thp=18.24
T_duct_thp=40.2

Q_out_Bio=(T_duct_bio-T_fan_bio)*Cp*m_dot*1000

Q_out_THP=(T_duct_thp-T_fan_thp)*Cp*m_dot*1000

%%
% Limitation Analysis

innerDiameter = 0.55 * 0.0254;  % inches to meters
Length = 6 * 0.0254;  % inches to meters
wickThickness = .0009;  % inches to meters
R=461.5 %Specific gas constant of water
% Heat Pipe Temperature Range

t_w=wickThickness*3;
% Material Properties
sigma = 0.059;  % Surface tension (N/m)
rho_1 = 997;  % Liquid density (kg/m^3)
L = 2258e3%(kJ/kg)
mu_1 = 8.90e-4;  % Liquid viscosity (N-s/m^2)
k_e = 401;  % Effective thermal conductivity of the
   liquid-saturated wick (W/m-K)
gamma_v = 1.33;  % Specific heat ratio for vapor side
poreRadius = 0.00197 * 0.0254;  % inches to meters
k = 6.0e-10;  % Permeability (m^2)
r_c = poreRadius;  % Effective capillary radius (m)
A_v = pi * (innerDiameter / 2)^2;  % Cross-sectional area of
   vapor space (m^2)
z=.036e-3; %characteristic dimension of
ps=5e-6;
d=.014;%m diameter of the tube
d_a=d-t_w %diameter of adiabatic zone
Aa=pi*(d_a/2)^2;%area of adiabatic zone
Av=pi*((d/2)-t_w)^2
Atot=pi*(d/2)^2
q_crit=0.012*(L)*((rho_1-rho_v)/rho_v)^0.6
Q_b=(q_crit)*A_v
V_s=477.5%speed of sound in water

q_s = (rho_v*(L*1e-3)*V_s) / (sqrt((2 * (gamma_v + 1))));
Q_s=q_s.*A_v

```

```
Cp=1.996;%(kJ/kgK)
Cv=1.440%(kJ/kgK)
k=Cp/Cv;
lamda=t_w+ps
%%
% %pg48 of book Entrainment limitation of grav asisted HP

Q_entmax=Aa*(L*1e-3)*(((rho_v/Atot)*...
((2*pi*k/lamda)+(rho_1*9.81*d_a))))^(0.5)

qee=Aa*L*sqrt((2*pi*rho_v*sigma)/0.036e-3)


%%
% Low Temperature Gradients

Bio_low=[42.06,38.95,36.32,33.2];
x=[3, 45.33, 84.66, 126.99];
THP_low=[38.73  36.68   36.04   35.53]
x1=[3, 45.33, 84.66, 126.99];
plot(x,Bio_low,LineWidth=2)
hold on
plot(x1,THP_low,LineWidth=2)
hold on  % To keep the plot and add scatter points
scatter(x, Bio_low, 'ro', 'filled')
% plot(x1,THP_low,LineWidth=2)
hold on  % To keep the plot and add scatter points
scatter(x1, THP_low, 'ro', 'filled')
grid on
xlabel('Distance (mm)')
ylabel('Temperature (C)')
legend('Biomimetic HP','Traditional
   HP','Location','best','FontSize',18)
set(gca,'Color','none')
hold off
%%
% Middle Temperature Gradients

Bio_mid=[57.258 47.69 42.88 40.477];
x=[3, 45.33, 84.66, 126.99];
THP_mid=[61.137 56.80948 56.80539 55.71921]
x1=[3, 45.33, 84.66, 126.99];
plot(x,Bio_mid,LineWidth=2)
hold on
```

```
plot(x1,THP_mid,LineWidth=2)

hold on  % To keep the plot and add scatter points
scatter(x, Bio_mid, 'ro', 'filled')
hold on
scatter(x1, THP_mid, 'ro', 'filled')
% xlim([0 155])
% ylim([40 50])
% labels = {'Evaporator', 'Node 1', 'Node 2', 'Condenser'};
% offset = 2;  % Adjust the offset value as needed
% for i = 1:length(x1)
%     text(x1(i) + offset, THP_low(i), labels{i},
   'VerticalAlignment', 'bottom', 'HorizontalAlignment',
   'left')
% end
grid on
xlabel('Distance (mm)')
ylabel('Temperature (C)')
legend('Biomimetic HP','Traditional
   HP','Location','best','FontSize',18)
hold off

%%
% High Temperature Gradients

Bio_high=[151.82,144.8,138.16,137.34];
x=[3, 45.33, 84.66, 126.99];
THP_high=[146.03    143.16  134.59  128.47];
x1=[3, 45.33, 84.66, 126.99];
plot(x,Bio_high,LineWidth=2)
hold on
plot(x1,THP_high,LineWidth=2)

hold on  % To keep the plot and add scatter points
scatter(x, Bio_high, 'ro', 'filled')
hold on
scatter(x1, THP_high, 'ro', 'filled')
% xlim([0 155])
% ylim([40 50])
% labels = {'Evaporator', 'Node 1', 'Node 2', 'Condenser'};
% offset = 2;  % Adjust the offset value as needed
% for i = 1:length(x1)
%     text(x1(i) + offset, THP_low(i), labels{i},
   'VerticalAlignment', 'bottom', 'HorizontalAlignment',
```

```
    'left')
% end
grid on
xlabel('Distance (mm)')
ylabel('Temperature (C)')
legend('Biomimetic HP','Traditional
    HP','Location','best','FontSize',18)
hold off

%%
% Max_Q Calculations

sig=58.9e-3; %surface tension of water
L=2.258e6; %Latent heat of water
rho1=958;%density of liquid water
rho2=.5974;  %density of vapor water
l=.16;%total length of pipe
mu=.282e-3;
% numoflayers1=2
% numoflayers2=1
w_d1=0.0045% cm
w_d2=0.0025;
la=.092;
le=.034;
lc=.034;
leff=la+((lc+le)/2)
D1=1;
D2=0.7;
d=.014;%m diameter of the tube
t_1w=.0002;% Wick thickness
ps=5e-6;%poresize
e=0.05;%Porosity
layers=3%Number of layers of copper mesh
t_w=t_1w*layers%Total thickness of wick
d_a=d-t_w %diameter of adiabatic zone
rt=0.018/2%total radius submerged in oil
r_manu_t=0.09/2;%radius of manufatured HP
h=0.04;%Height submerged in tube
Aw=t_w*pi*d;%cross-sectional area of wick.
h_cyl=0.02;
At=(2*pi*rt^2)+(2*pi*rt*le)%surface area of tube submerged
    in oil
A_cone=00.0002448;%area of cone section of MHP
A_manu_t=(2*pi*r_manu_t^2)+(2*pi*r_manu_t*h_cyl)+A_cone;
```

```
Aa=pi*(d_a/2)^2%area of adiabatic zone

%%
% Calculations from page 102 and 103 of the book

ho=4100;%w/(m^2K) Thermal conductivity of Silicone Oil
K=(t_1w^2*(1-e)^3)/(66.6*(e)^2)
% K=(t_w^2*(1-e^3))/(122*(1-e)^2)
k2=20e-7;
rc1=0.0005;%thickness of mesh
% rc2=0.0001;%th=leff=0.13;%effective length of heat pip=
g=9.81;%(m/s^2)
m_max=((rho1*K*Aw)/mu*leff)*(((2*sig)/rc1)-...
(rho1*g*leff*sin(-1)))
q_max=m_max*L
q_manu_max=150; %max heat flux of manufatured HP
dT=q_max/(At*ho)
dT_manu=q_manu_max/(A_manu_t*ho)
T_hotplate=dT+20.5%temperature the hotplate needs to be at
   for maxQ
T_hotplate_manu=dT_manu+21.5%temperature the hotplate needs
   to be at for maxQ
```

A.2 All Matlab Outputs

```

w_d1 =

    0.0045


leff =

    0.1260


layers =

     3


t_w =
```

```
18
19     6.0000e-04
20
21
22 d_a =
23
24      0.0134
25
26
27 rt =
28
29      0.0090
30
31
32 Q_bio_low =
33
34     22.7862
35
36
37 Q_thp_low =
38
39     50.3948
40
41
42 Q_mhp_low =
43
44     43.7639
45
46
47 R_low =
48
49      0.3467
50      0.0549
51      0.1040
52
53
54 h_low =
55
56     1.0e+03 *
57
58      0.9809
59      6.1924
60      3.2710
61
```

```
62
63 Q_bio_mid =
64
65   159.3826
66
67
68 Q_thp_mid =
69
70   121.1405
71
72
73 Q_mhp_mid =
74
75   113.5692
76
77
78 R_mid =
79
80     0.1061
81     0.0368
82     0.0593
83
84
85 h_mid =
86
87    1.0e+03 *
88
89     3.2053
90     9.2390
91     5.7303
92
93
94 Q_bio_high =
95
96   378.5639
97
98
99 Q_thp_high =
100
101  463.6805
102
103
104 Q_mhp_high =
105
```

```
  336.3673


R_high =

    0.0452
    0.0309
    0.0881


h_high =

   1.0e+04 *

    0.7529
    1.1019
    0.3428


Q_low =

   22.7862   50.3948   43.7639


Q_mid =

  159.3826  121.1405  113.5692


Q_high =

  378.5639  463.6805  336.3673


R_values =

    0.3467    0.0549    0.1040
    0.1061    0.0368    0.0593
    0.0452    0.0309    0.0881


h_values =

   1.0e+04 *
```

```
150
151     0.0981    0.6192    0.3271
152     0.3205    0.9239    0.5730
153     0.7529    1.1019    0.3428
154
155
156 Q_values =
157
158    22.7862   50.3948   43.7639
159   159.3826  121.1405  113.5692
160   378.5639  463.6805  336.3673
161
162
163 dotm =
164
165    1.0e-03 *
166
167     0.0101
168     0.0705
169     0.1675
170
171
172 dotm2 =
173
174    1.0e-03 *
175
176     0.0223
177     0.0536
178     0.2052
179
180
181 deltaP_g =
182
183   507.4909
184
185
186 deltaP_1 =
187
188     0.3194
189     2.2338
190     5.3051
191
192
193 deltaP_v =
```

```
194
195     0.4394
196     3.0734
197     7.2990
198
199
200 deltaP_1_bio =
201
202     0.7062
203     1.6971
204     6.4983
205
206
207 deltaP_v_bio =
208
209     0.9716
210     2.3349
211     8.9406
212
213
214 dP_total_bio =
215
216   509.1687
217   511.5229
218   522.9298
219
220
221 dP_total =
222
223   508.2497
224   512.7981
225   520.0951
226
227
228 Cp =
229
230     1.0060
231
232
233 T_fan_bio =
234
235    19.8800
236
237
```

```
T_duct_bio =

   52.1700


T_fan_thp =

   18.2400


T_duct_thp =

   40.2000


Q_out_Bio =

  300.7779


Q_out_THP =

  204.5550


R =

  461.5000


L =

     2258000


d_a =

    0.0113


Av =

   5.8088e-05

```

```
Atot =

    1.5394e-04


q_crit =

    2.3248e+06


Q_b =

   356.3398


V_s =

   477.5000


Q_s =

    45.7048


Cv =

     1.4400


lamda =

     0.0027


Q_entmax =

   814.48


THP_low =

    38.7300    36.6800    36.0400    35.5300
```

```
THP_mid =

   61.1370   56.8095   56.8054   55.7192


w_d1 =

    0.0045


leff =

    0.1260


layers =

     3


t_w =

   6.0000e-04


d_a =

    0.0134


rt =

    0.0090


At =

    0.0028


Aa =
```

```
    1.32e-04


K =

    5.14e-9


m_max =

     1.31e-5


q_max =

    161.36
```

A.3 All Figures From Matlab Code

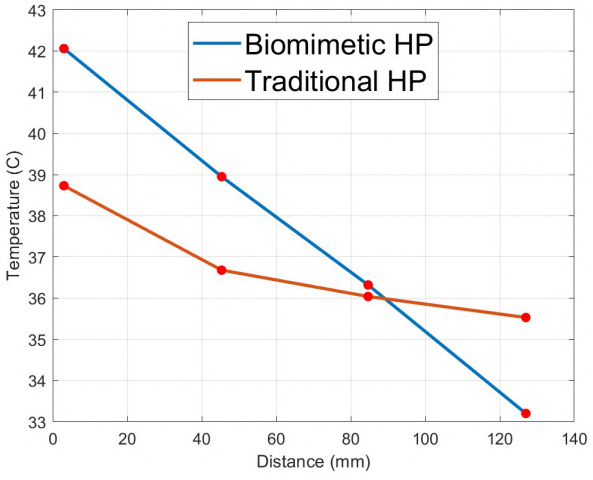

Figure A.1: Matlab Gradient Graph - Low

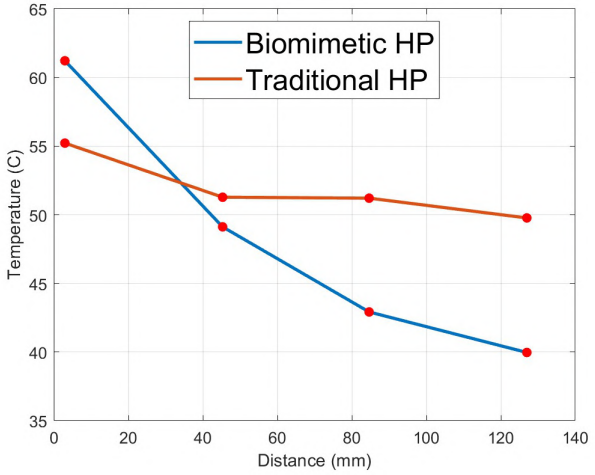

Figure A.2: Matlab Gradient Graph - Mid

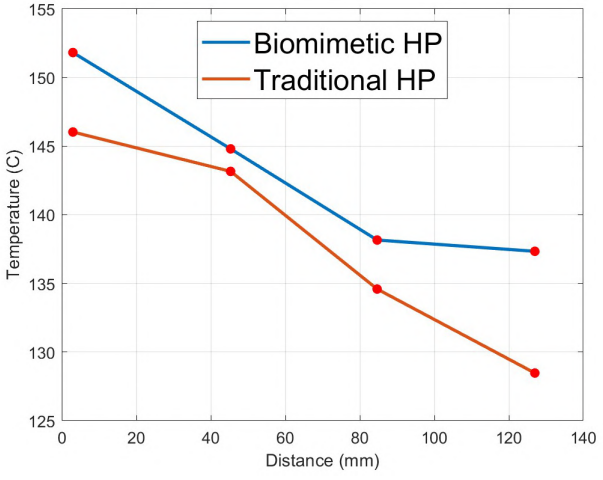

Figure A.3: Matlab Gradient Graph - High

APPENDIX B

SUPPORTIVE BIOMIMETIC HEAT PIPE DOCUMENTATION

B.1 BIOMIMETIC CONCEPT FOR THE DESIGN OF NASA'S DEEP SPACE FLIGHT RADIATORS

Proceedings of the 17th International Heat Transfer Conference,

IHTC-17 14-18 August 2023, Cape Town, South Africa

This paper provides additional context to the research as well as more comprehensive images that are referenced in the body of the thesis.

TITLE: A BIOMIMETIC CONCEPT FOR THE DESIGN OF NASA'S DEEP SPACE-FLIGHT RADIATORS

Ashok Kumar Ghosh[1]*, Owen Telford[2]

[1]Associate Professor in Mechanical Engineering, New Mexico Tech, Socorro, NM 87801, USA

[2]Graduate Student in Mechanical Engineering, New Mexico Tech, Socorro, NM 87801, USA

ABSTRACT

Traditionally, NASA has relied primarily on pumped, single-phase liquid systems to collect, transport, and reject heat via single-phase radiators. The heat-rejection system used on the space shuttle orbiters consists of over 250 small, one-dimensional tubes embedded within a honeycomb structure. Heat is transferred by convection to the tube walls, conduction through the honey-comb structure, and finally, radiation to space. NASA is currently developing nuclear electric propulsion engines to power next generation spacecrafts to transit to Mars and beyond, and these spacecrafts need heat rejection systems with performance capabilities significantly better than those provided by current systems.

The origins of a heat pipe go back over 60 years, but there is still room for new ideas to grow. While a traditional heat pipe consists of an open adiabatic zone, with a mesh wick lining the inside of the tube wall to aid in transportation of condensed liquid from the condenser side to the evaporator side. A biomimetic, multi-function composite developed at New Mexico Tech (NMT) has an architecture consisting of interconnected pores graded radially as well as longitudinally to allow heated fluid to flow radially as well as longitudinally. This configuration promotes fast convection of the heat from evaporator end to the

tube walls and dissipate heat more evenly throughout the radiator lateral surface to space by radiation.

Past experiments done at NMT using samples with biomimetic design demonstrated that upon localized heating, there can be an induced convective transport of thermal energy as fluid passes through a closed-loop porous layer. The goal of on-going investigation is to highlight how biomimetic architecture of heat pipes within a radiator panel may provide the required thermal performance simultaneously reducing heat rejection system mass.

KEY WORDS: Biomimetic Design, Heat Pipe, Deep Space, Wick Layer,

INTRODUCTION

Traditionally, NASA has relied primarily on pumped, single-phase liquid systems to collect, transport, and reject heat via single-phase radiators. The heat-rejection system used on the space shuttle orbiters consists of over 250 small, one-dimensional tubes embedded within a honeycomb structure. Heat is transferred from the coolant by convection to the tube walls, conduction through the honeycomb structure, and finally, by radiation to space. NASA is currently developing nuclear fusion engines to power the next generation of spacecrafts to transit to Mars and beyond, and these spacecrafts need heat rejection systems with performance capabilities significantly better than those provided by current systems. Designing innovative radiators is critical to advancing future deep space travel. Figure 1 shows various components of a Nuclear Electric Propulsion (NEP). Radiator manifold carries waste heat from the nuclear reactor to the heat pipe radiator to be rejected into the atmosphere.

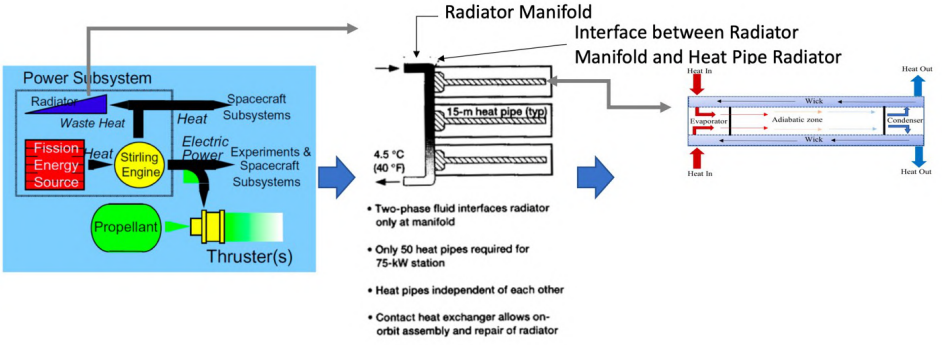

Figure B.1: (left) Schematic of Power Subsystem for NEP [taken from figure 1.6 of [1]]; (middle) Waste Heat transport from radiator manifold to heat pipe radiator; (right) Cross-section of a classical (copper/water) heat pipe showing heated region on left and transfer region on right.

Literature Research on Heat Pipe Technology

Heat pipes (HP) were first created as a concept in the early 40's [2], but the theory was not intensely investigated until the late 60's. The first published paper on design of a traditional two-phase heat pipe was shown in "Theory of Heat

Pipes" by a T.P. Cotter- A Los Alamos scientist Cotter [2]. Around decade later now, there are over 1000 references to his paper and there had been two international heat pipe conferences [2]. Since then, there has been a heat pipe conference every few years. Cotter's publication is the foundation of this large field of study. Heat pipes efficiently dissipate heat passively, reject heat without any external source needed to function properly, i.e. no external power source is required.

There are 4 main areas of the HP, the evaporator side, the condenser side, the adiabatic zone, and the wick. Heat enters the evaporator section typically through conduction. The working fluid in the evaporator absorbs the heat and the fluid changes from a liquid to a vapor. As it becomes a vapor, the fluid is transported through the adiabatic section to the condenser section. On the condenser side, the pipe is much cooler relative to the opposite side. When enough vapor is moved to this side, the vapor changes back into a liquid [3]. The wick then transports the condensed liquid back to the evaporator side. This occurs due to capillary action and pressure differences. A cyclic process will start and will continue to dissipate as long as the heat flux being added to the system is within the specifications of the HP's design. The Heat pipe process is considered adiabatic due to the liquid/vapor being fully contained within the HP. Depending on the fluid type, shape/material of the housing, type/material of wick used, and the internal structural architecture, functioning of HP requirements will change accordingly.

Wick of the Heat Pipe

A wick is a type of porous media that is designed to match the length of the tube it is used in, and is responsible for transporting fluid in a single direction. They are typically placed around the outer circumference of the heat pipe, and are directly attached to the casing. Homogeneous wicks, which are composed of various materials, all share a uniform structure throughout. On the other hand, non-homogeneous wicks have varying geometries that depend on the pore size and layering. Furthermore, heat transfer can also affect the wick in several ways. Recent research has revealed that the type of mesh used and the surface finish can significantly impact critical heat flux.

Convection at Micro-gravity

On Earth, convection is dominated by buoyancy due to gravity, and the resultant energy transport reduces the overall thermal stress upon the structure. In low gravity space environments, buoyance effects will diminish but the surface tension driven "Marangoni Effect" may play an important role in generating similar convective flow inside the porous structure. In the Japanese experiment module "Kibo", a series of experiments were performed on board International Space Station (ISS) and demonstrated the spatio-temporal flow structure in Marangoni convection. They generated Marangoni convection by applying temperature differential between the ends of a large liquid bridge. As the temperature differential is increased, the initial steady state planer flow turned to oscillatory.

State of the Art (SOA)

Traditionally, copper/water heat pipes are used in advanced spacecraft ra-

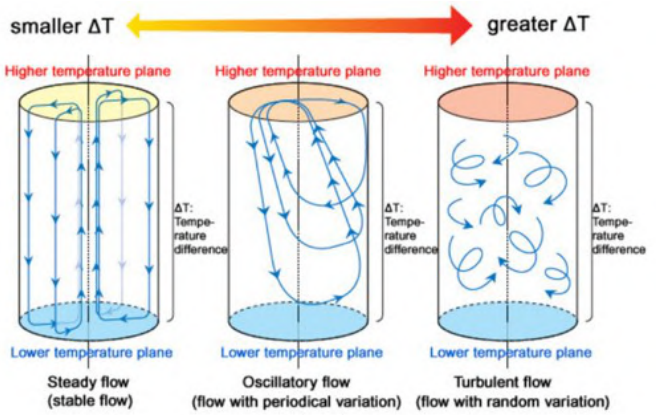

Figure B.2: "Kibo" Experiment on board ISS [4].

diator systems as shown in figure 1(right). Copper is used as the envelop next to a wick layer. Water as the working fluid at temperatures below 150ºC. Classical/ Traditional copper/water heat pipe transfers heat with no temperature change from end to end (isothermally). The heat pipe makes use of the phase change features of the fluid as it flows from evaporating end to the condensation end.

Deficiency of the SOA Design

In a traditional heat pipe, the inner face of the wick layer may be permeable or impermeable to the operating fluid in the heat pipe. When it is impermeable, operating fluid cannot flow radially to reach the wall. Thus, lateral surface does not participate directly towards heat rejection to environment through radiation. If the wick face is permeable, then the longitudinal flow will try to reach the wall radially through the wick thickness. This will give rise to two cross currents at 90º to each other. Again, heat rejection amount will decrease.

Hypothesis and the Rationale

Lesson learned from the Kibo program combined with our own experience is implemented in the design and development of the proposed biomimetic radiator system. By filling the inner volume of the heat pipe with open-cell interconnected porous structure will allow both the longitudinal as well as the radial movement of the operating fluid. This will allow the complete lateral surface to be effective.

PROPOSED BIOMIMETIC DESIGN

A biomimetic, multi-function composite is developed at New Mexico Tech (NMT) that has an architecture consisting of interconnected pores graded radially to dissipate heat as fluid travels through it. Past experiments demonstrated that upon localized heating, there can be an induced convective transport of thermal energy as fluid passes through a closed-loop porous layer. Figure 3 shows the longitudinal cross section of both the designs.

Prior Investigation

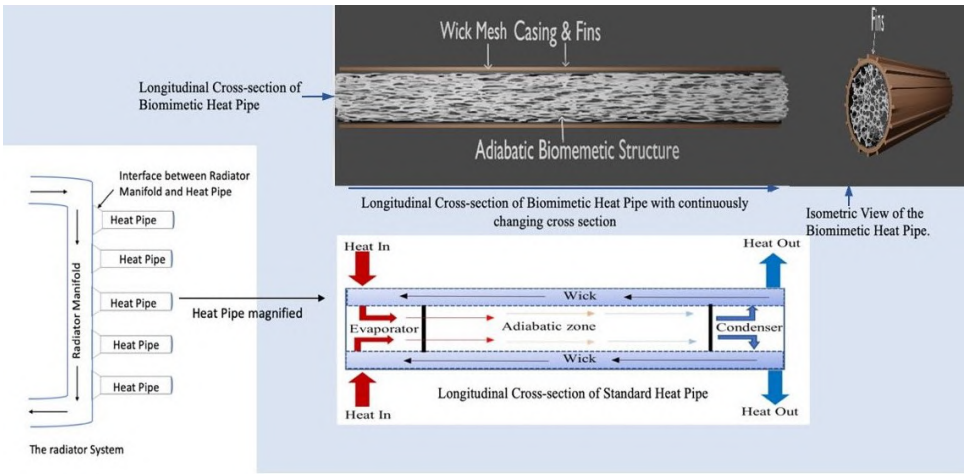

Figure B.3: Longitudinal cross-section of both the designs

Thermal management characteristics of a fluid filled porous composite (FFPC) developed for space application is studied experimentally to determine the adaptability of the composite when exposed to high thermal load. Localized heating will generate an out-flow of fluid in the interstitial pores from the hot region to cooler surroundings, resulting in dissipation of thermal energy and eventually providing a good thermal management capability to the composite. FFPC being a heterogeneous material, there exist no ASTM standards for such material. A new test method is successfully designed, developed and tested to determine the thermal management characteristics of the FFPC.

The objectives of this past study are to experimentally demonstrate the thermal management characteristics of the fluid filled porous composite (FFPC) developed for space application. The objectives also include to development of an acceptable test method for testing such heterogeneous material. Experimental results are presented and published in the Proceedings of the 23rd National Heat and Mass Transfer Conference and 1st International ISHMT-ASTFE heat and Mass Transfer Conference, IHMTC2015, 17-20 December, 2015, Thiruvanthapuram, India (paper No 2233) [5].

Current Investigation

In current analysis, there will be two types of heat pipes that will be analyzed, a classic wicked heat pipe and a biomimetic heat pipe. The former has the geometry of a traditional heat pipe. There is a wick that is lining the interior walls of the heat pipe throughout. The vapor travels through an open adiabatic zone to the condenser. As its phases change into a liquid, capillary pressure forces the liquid into the wick and brings it to the evaporator zone.

The biomimetic design has a similar geometry in the wick, but the adiabatic zone has changed to a porous media for the vapor to travel through. Instead of heat only being rejected in the condenser section, the heat pipe can dissipate laterally throughout the length of the pipe. This, along with a sectioned wick

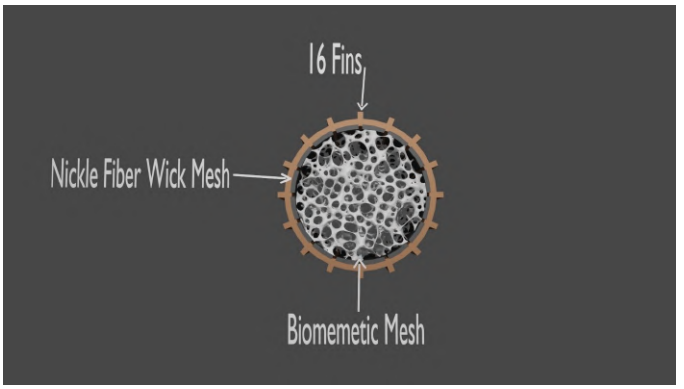

Figure B.4: Front View of the Biomimetic Heat Pipe

structure and fin attachments along the length of the pipe is hypothesized to help with heat dissipation throughout the entire heat pipe. As the vapor travels through the modified adiabatic zone, the vapor can interact with the lattice structure. Collisions between vapor molecules and the structure will cause energy transfer between them. This heat can be absorbed through conduction and if enough collisions occur, the vapor will change back into a liquid and condense on the structure. Figure 4 shows a front view of the biomimetic heat pipe. The porous media in the wick has a low porosity, while the one in the adiabatic zone has a large porosity. Materials used in their respective meshes are shown. It also shows a 16 fins to promote heat dissipation along with a cut wick design to increase internal surface area. The following analysis will consider each zone's geometry and calculate the maximum heat transport of each design.

The two heat pipe designs will be analyzed using water as the working fluid. The heat pipes are assumed to be operating at a temperature of 100 °c, with a length of 0.3m and a diameter of 0.01m. There will be two meshes that are analyzed. The mesh in the wick is two layers of Oxidized Nickle [6] and the adiabatic porous media will have 10 layers of a Nickle fiber [6]. The first selection is made based on the pore radius, which is an average size. The latter selection was chosen because it has the largest permeability in the reference, this ensures that the fluid can flow through the media with ease. Both heat pipes are also assumed to be horizontal.

The maximum heat transport can be found by using a pressure balance equation for a heat pipe.

$$\Delta P_{c,max} = \Delta P_v + \Delta P_g + \Delta P_1 \tag{B.1}$$

Where ΔP_c is the capillary pressure difference of the heat pipe, ΔP_v is the pressure difference of the vapor in the heat pipe, ΔP_1 is the pressure difference of the wick section and ΔP_g is the pressure difference due to gravity. The three pressures add up to the total capillary pressure change. If the inequality is true, a cycle occurs. It is also assumed that since the adiabatic zone is at the saturation

temperature, the phase of the fluid can change in the adiabatic zone before it reaches the condenser. This would cause the fluid to be pulled into the wick lining the wall. Each pressure can be broken down further and is shown below.

$$\Delta P_{c,max} = \frac{2\sigma cos\theta}{r_c} \tag{B.2}$$

Where σ is the value for the surface tension of water (N/m), θ is the degree of wetting of the wick (in radians), and r_c is the pore radius of the larger mesh.

The value for ΔP_v can be neglected, because, for low temperature (0-227°c), the value becomes negligible [7]. The equation for effect due to gravity is shown below in equation 3.

$$\Delta P_g = \rho_1 g l sin(\phi) \tag{B.3}$$

Where rho_1 is the density of the liquid, g is the acceleration due to gravity, l is the length of the pipe, and ϕ is the incline of the heat pipe. Since the assumption that the heat pipe is horizontal, $\phi = 1$ and thus, $\Delta P_g = 0$. The equation for ΔP_1 is shown in equation 4.

$$\Delta P_1 = \frac{\mu \cdot \dot{Q} \cdot l}{\rho_1 \cdot L \cdot A_w \cdot K_1} \tag{B.4}$$

Where μ is the dynamic viscosity of the fluid (Ns/m^2), Q is the heat transport of the heat pipe (W), rho_1 is the density of the liquid (kg/m^3), L is the latent heat of water (J/kg). A_{w1} is the area of the wick (m^2), and K_1 is the permeability of the mesh (m). Since both ΔP_g and ΔP_v approx 0, equation (1) can now be rewritten.

$$\frac{2\sigma cos\theta}{r_c} = \frac{\mu \dot{Q} l}{\rho_1 L A_w K_1} \tag{B.5}$$

Since the maximum heat transport needs to be found, Q can be solved for in equation 5 and the maximum heat transport can be found. Equation 6 shows the newly solved equation.

$$\dot{Q} = \frac{2\sigma cos\theta}{r_{c1}} * \frac{\rho_1 L\ A_w K_1}{\mu l} \tag{B.6}$$

This is used to find the maximum heat transport of the traditional heat pipe. For the biomimetic heat pipe, the equations need to be considered differently to account for the additional mesh material.

The cross-sectional area can be calculated using equation 7.

$$A_{w,a} = (2N) D_w \pi D_s \tag{B.7}$$

Where N is the number of layers of the mesh, D_w is the diameter of the wire of the mesh, and D_s is the diameter of the section being analyzed.

When accounting for the addition of the porous material an additional pressure difference needs to be accounted for. It is assumed that if the vapor in the adiabatic zone partially changes to a liquid, this pressure accounts for. This will be denoted as ΔP_2 the equation for this looks similar to equation 4 but needs to be changed based on the area of the mesh, the permeability, and the density. It is assumed that if the vapor in the adiabatic zone partially changes to a liquid, ΔP_2 accounts for it. This is shown in equation 8.

$$\Delta P_2 = \frac{\mu \dot{Q} l}{\rho_v L \ A_a K_2} \tag{B.8}$$

Where rho_v is the density of the vapor, A_a is the area of the adiabatic zone, and K_2 is the permeability of the second mesh. Now going back to our pressure balance equation, we need to account for this additional pressure difference.

$$\frac{2\sigma cos\theta}{r_{c2sa}} = \frac{\mu \dot{Q} l}{\rho_1 L \ A_w K_1} + \frac{\mu \dot{Q} l}{\rho_v L \ A_a K_2} \tag{B.9}$$

By factoring and solving for Q, we obtain equation 10.

$$\dot{Q} = \frac{2\sigma cos\theta}{r_{c2}} * \left(\frac{\rho_1 L \ A_w K_1 + \rho_v L \ A_a K_2}{\mu l} \right) \tag{B.10}$$

Dynamic viscosity is assumed to be constant for this calculation because the operation is at the saturation temperature of the fluid, there can be areas in which the adiabatic section is areas in which the water becomes liquid. This would cause the liquid portions to be pulled into the wick and transported back to the evaporator section. Now that equation 10 has been obtained, the maximum heat transport will be calculated for each of the cases and then compared.

Results

The constant values for each of the variables are shown in table 1. The r_c measurement was taken by taking a cross section of the biomimetic geometry and averaging the pore size of the cross section. The number of layers for the wick and the biomimetic structure are assumed to be two and one respectively [2,6,7,8].

Table B.1: Calculation Parameters

Parameter	Value	Unit
σ	0.0589	N/m
θ	1	-
μ	.00283	(Ns/m^2)
l	0.3	m
ρ_1	958	kg/m^3
ρ_v	0.597	kg/m^3
A_w	5.7×10^{-6}	m^2
A_a	11×10^{-6}	m^2
K_1	$.302 \times 10^{-10}$	m^2
K_2	20×10^{-6}	m^2
r_{c1}	2×10^{-5}	m
r_{c2}	1×10^{-4}	m

The degree of wetting on both meshes are assumed to be perfectly wetted. In this case, Equation 6 is used to find the maximum heat transport of the standard heat pipe using the values that are shown above. Equation 9 finds the maximum heat transport for the biomimetic heat pipe. To distinctly compare the two heat pipes, Q is assumed to be a function of the length of the heat pipe and is iteratively calculated. The heat pipe (l) length is increased to 1 m and incrementally reduced to the target length of 0.3 cm. A MATLAB code was created for this analysis to calculate the iterated heat transport values. Figure 5 shows this analysis.

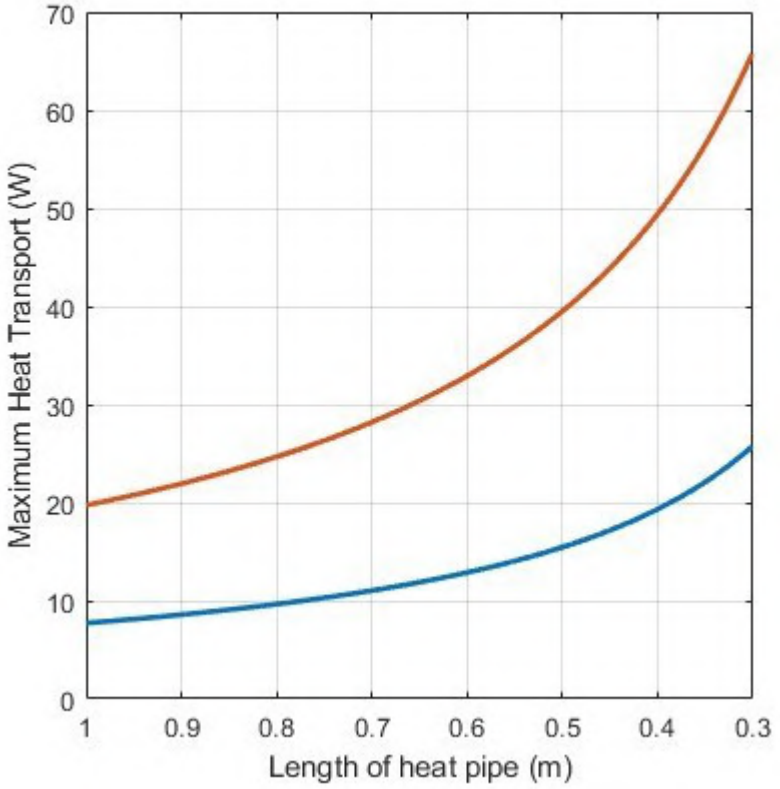

Figure B.5: Q values for each Heat Pipe as it reaches the target length.

The maximum value for the traditional heat pipe is 25.72 W and the biomimetic heat pipe has a maximum heat transport value of 65.1 W.

Discussion and Conclusion

This analysis reveals that the biomimetic heat pipe exhibits enhanced heat transport capabilities as the length of the heat pipe is reduced. This suggests that if the biomimetic heat pipe were to be shortened by half of its targeted length, it would still dissipate heat equivalent to that of a conventional heat pipe operating at its current length. This show, the biomimetic heat pipe achieves this without sacrificing its lightweight design, despite the additional material introduced into the system. It is worth noting that this analysis does not account for lateral dissipation arising from the incorporation of the wick and fins. Further investigation are underway to fully validate the efficacy of the biomimetic design, including utilization of simulation software to compare results and physical testing. A comprehensive testing procedure will be conducted, and all relevant results will be presented in the final presentation. It is important to note that the mesh quantities and geometry constants used in this analysis are subject to further optimization.

REFERENCES

[1] Briana N. Tomboulian, "Lightweight, High-Temperature Radiator for In-Space Nuclear-Electric Power and Propulsion", Doctoral Dissertations,

November 2014, U. of Massachusetts, Amherst.
https://doi.org/10.7275/5972048.0

[2]. Reay, David, et al. *Heat Pipes: Theory, Design and Applications*. 6th ed., Elsevier Science, pp.74 & 75 2013.

[3]. Cotter, T. P., "Theory of Heat Pipe", Los Alamos Scientific Laboratory, LA-3246-MS, 1965

[4]. https://iss.jaxa.jp/en/kiboexp/theme/first/marangoni/index.html

[5]. Ghosh, A.K., "Thermal Management Characteristics Of A Fluid Filled Porous Composite - An Experimental Investigation", Proceedings Of The 23rd National Heat And Mass Transfer Conference And 1st International ISHMT-ASTFE Heat And Mass Transfer Conference, IHMTC2015, 17-20 December, 2015, Thiruvanthapuram, India (Paper No 2233)

[6] Shishido, I. Oishi, and S. Ohtani, "Capillary Limit in Heat Pipes," J. Chem. Eng. Japan, vol. 17, no. 2, pp. 179–186, 1986.

[7] "Surface Tension." *Engineering ToolBox*, https://www.engineeringtoolbox.com/surface-tension-d_962.html.

[8] "Water - Heat of Vaporization vs. Temperature." *Engineering ToolBox*, https://www.engineeringtoolbox.com/water-properties-d_1573.html.

APPENDIX C

RAW DATA FIGURES

C.1 Real-time Temperature Readings From Pico Data Logger

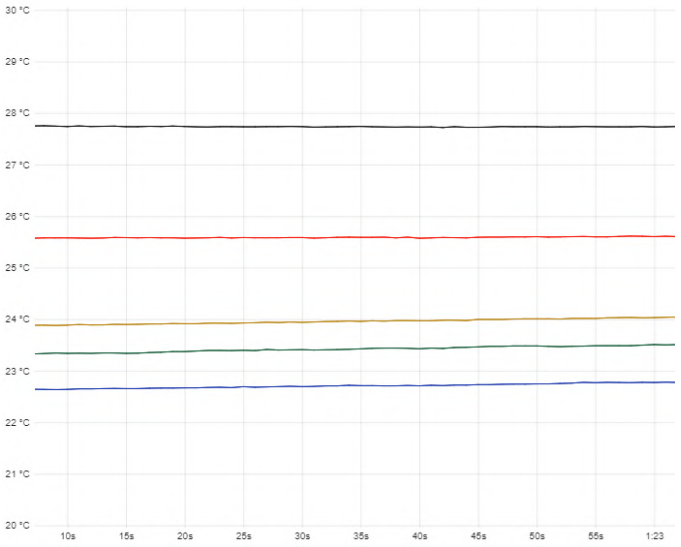

Figure C.1: BioHP Low Test 1

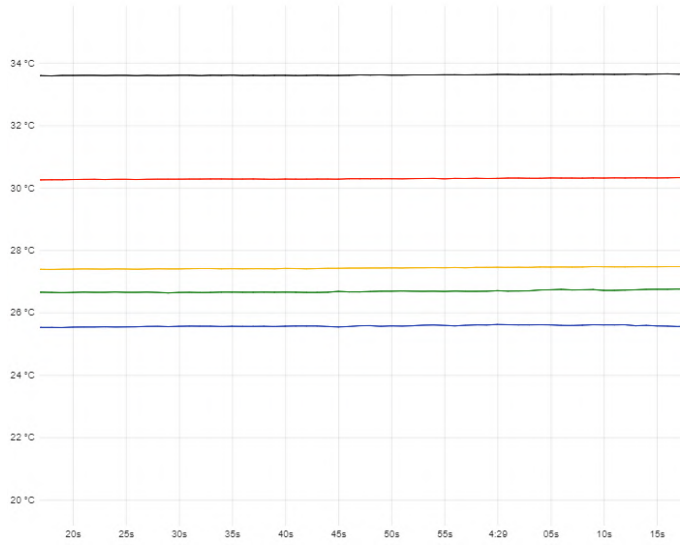

Figure C.2: BioHP Low Test2

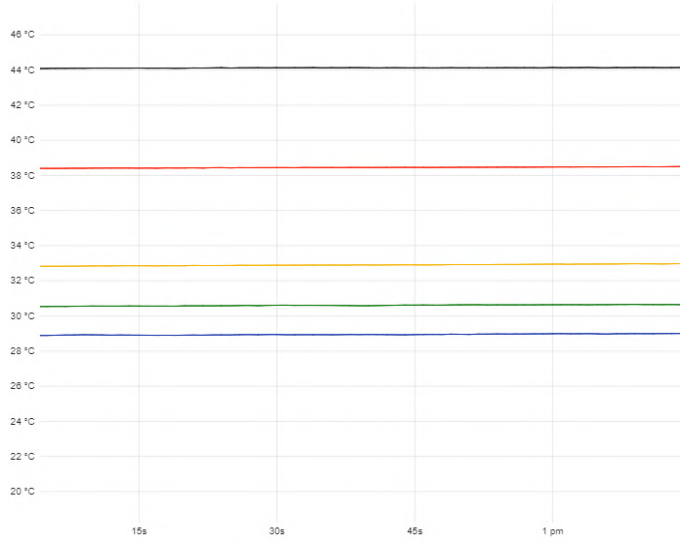

Figure C.3: BioHP Low Test 3

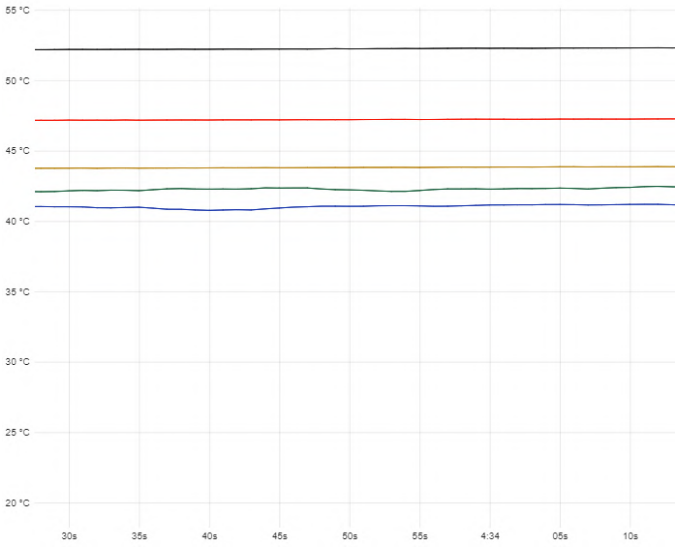

Figure C.4: BioHP Mid Test 4

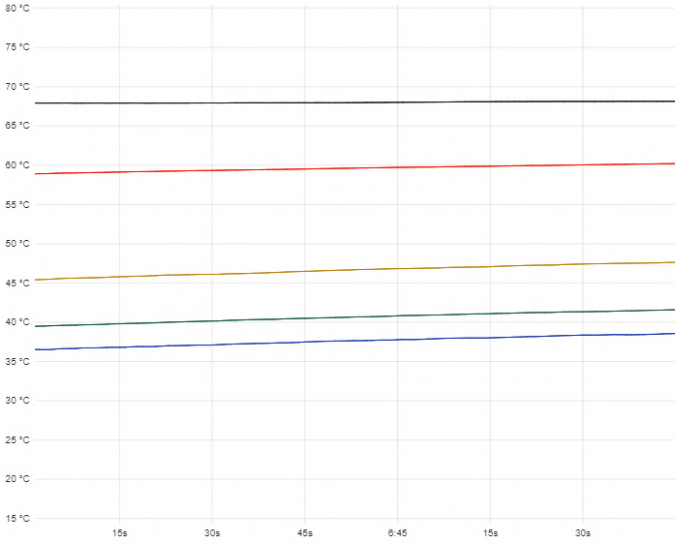

Figure C.5: BioHP Mid Test 5

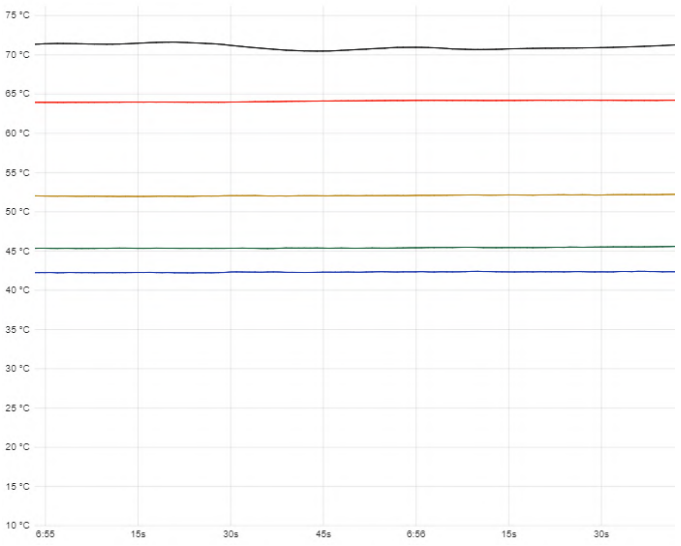

Figure C.6: BioHP Mid Test 6

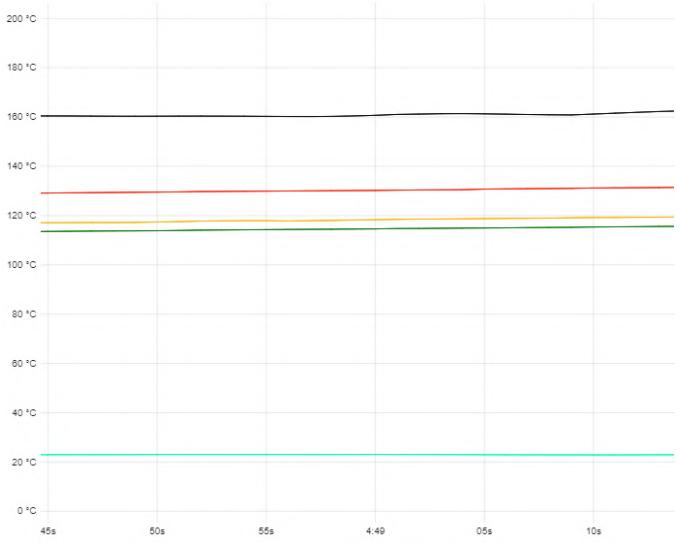

Figure C.7: BioHP Mid Test 7

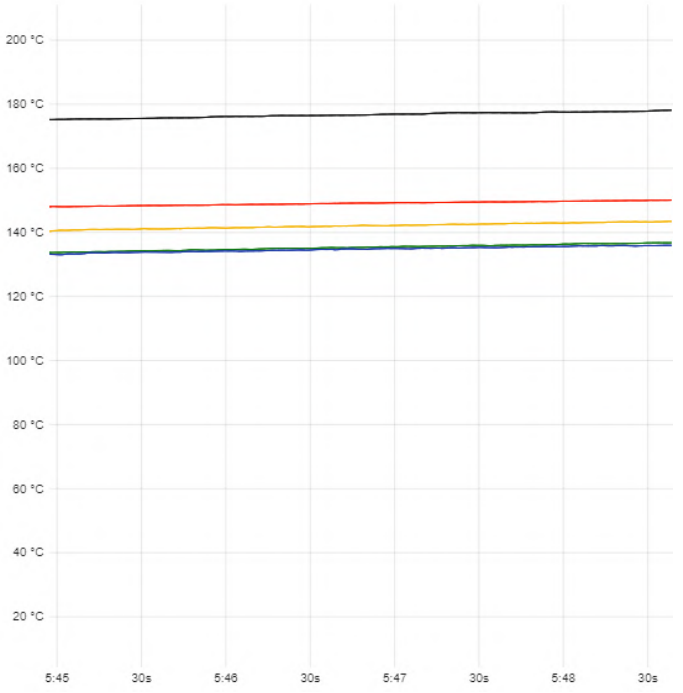

Figure C.8: BioHP High Test 8

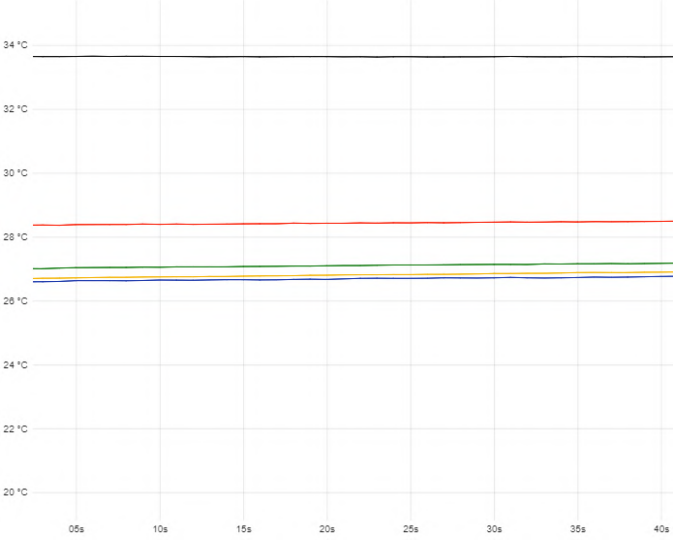

Figure C.9: MHP Low Test 1

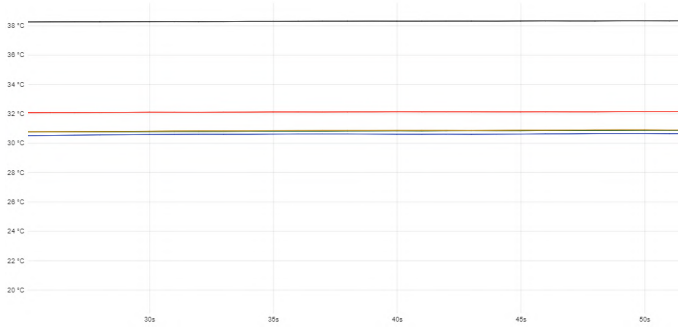

Figure C.10: MHP Low Test 2

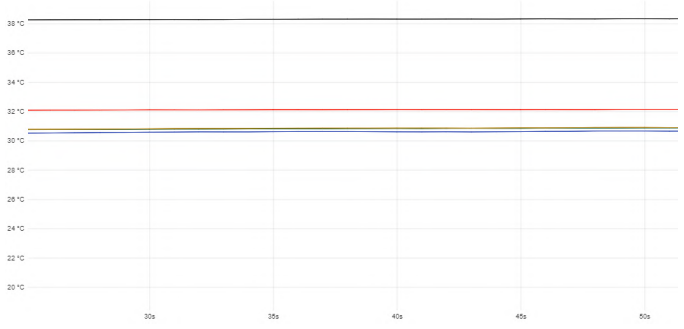

Figure C.11: MHP Low Test 3

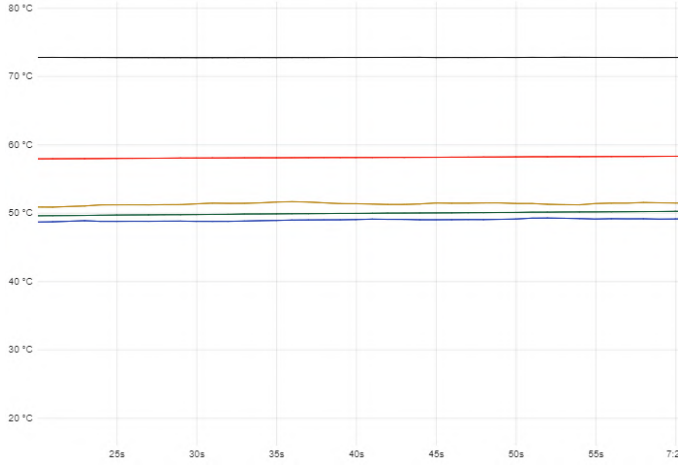

Figure C.12: MHP Mid Test 4

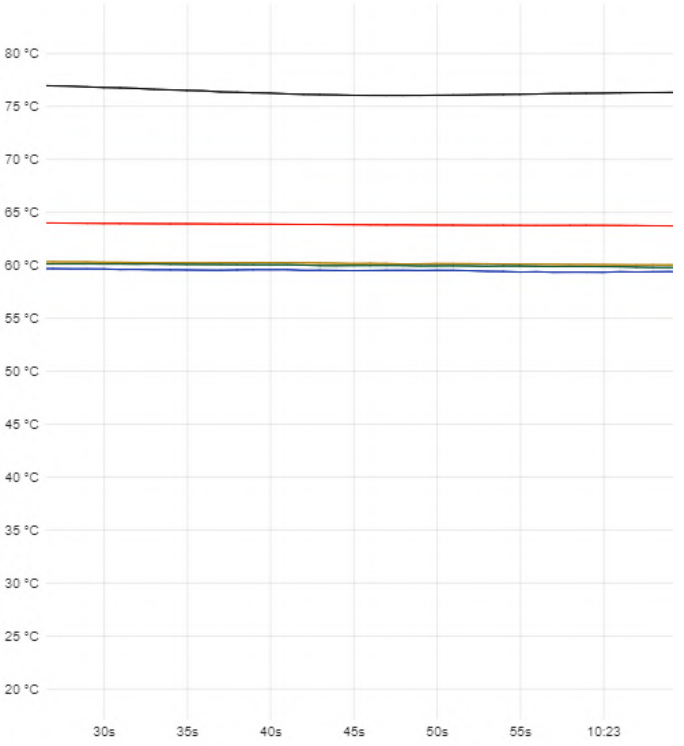

Figure C.13: MHP Mid Test 5

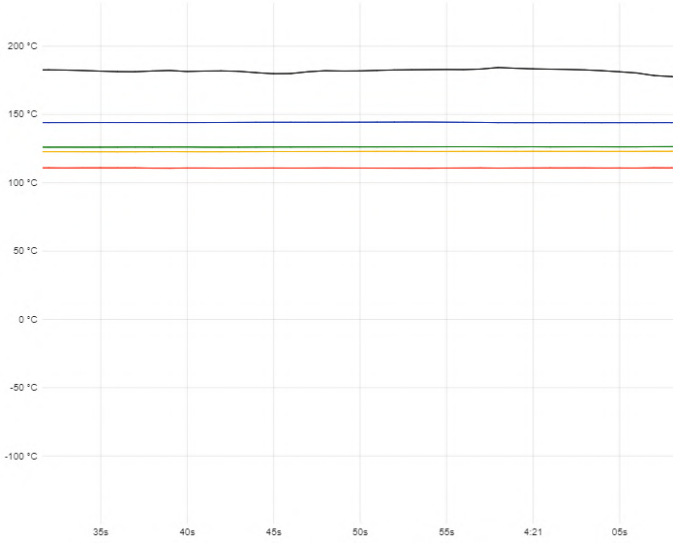

Figure C.14: MHP High Test 6

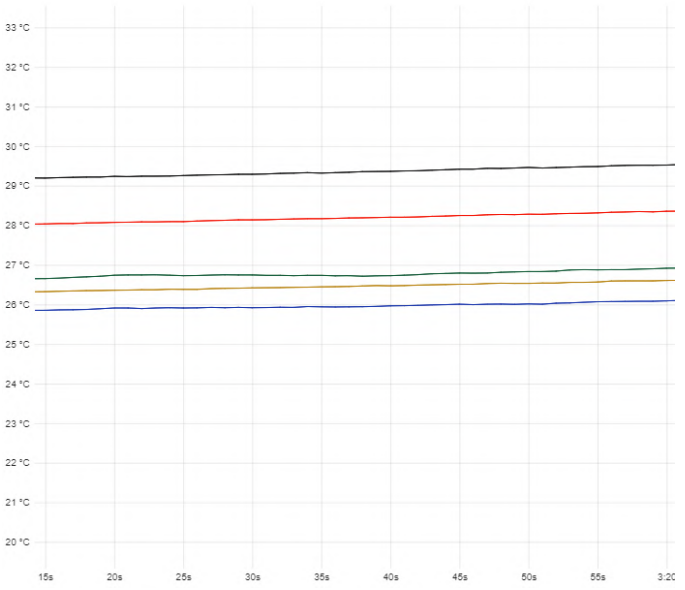

Figure C.15: THP Low Test 1

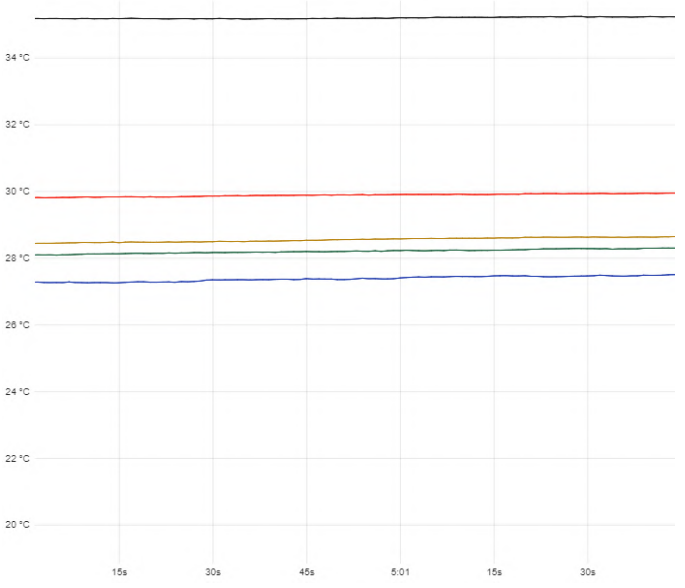

Figure C.16: THP Low Test 2

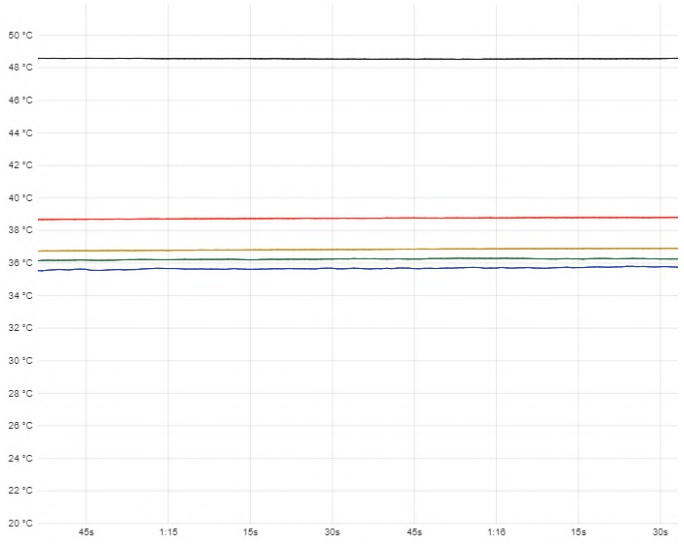

Figure C.17: THP Low Test 3

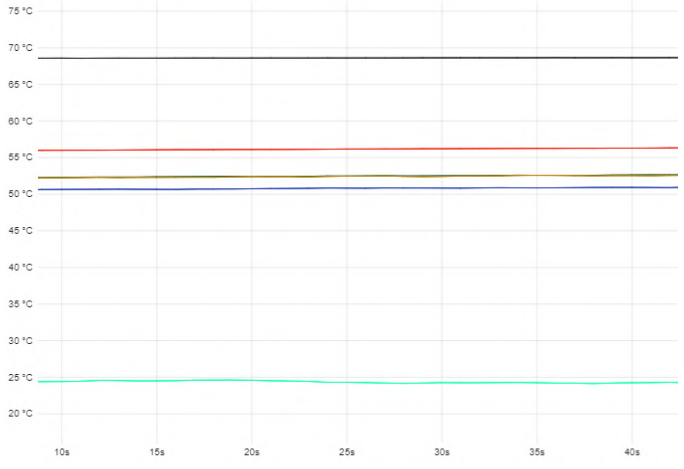

Figure C.18: THP Mid Test 4

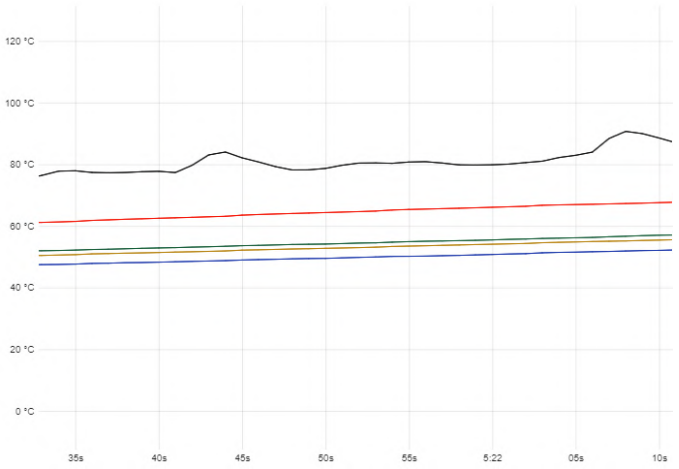

Figure C.19: THP Low Test 5

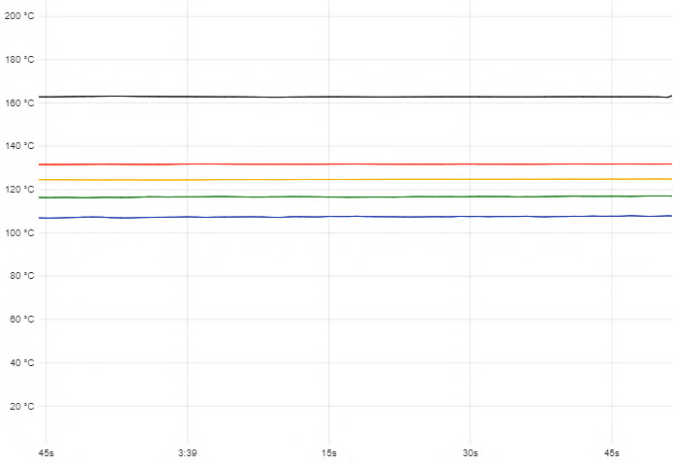

Figure C.20: THP High Test 6

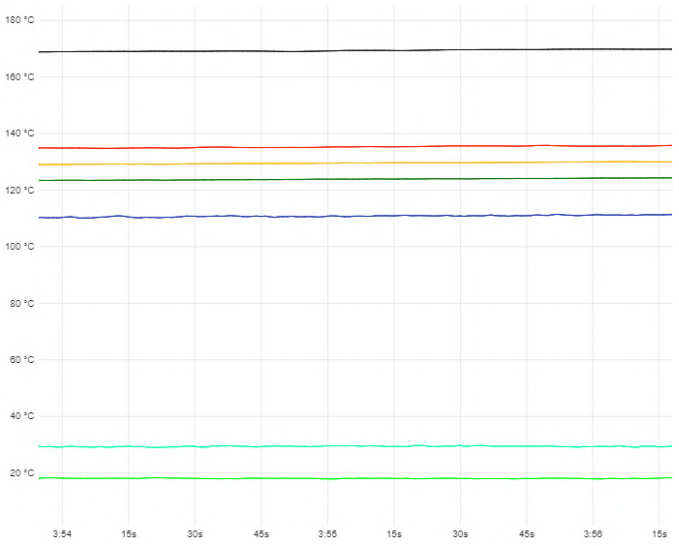

Figure C.21: THP High Test 8

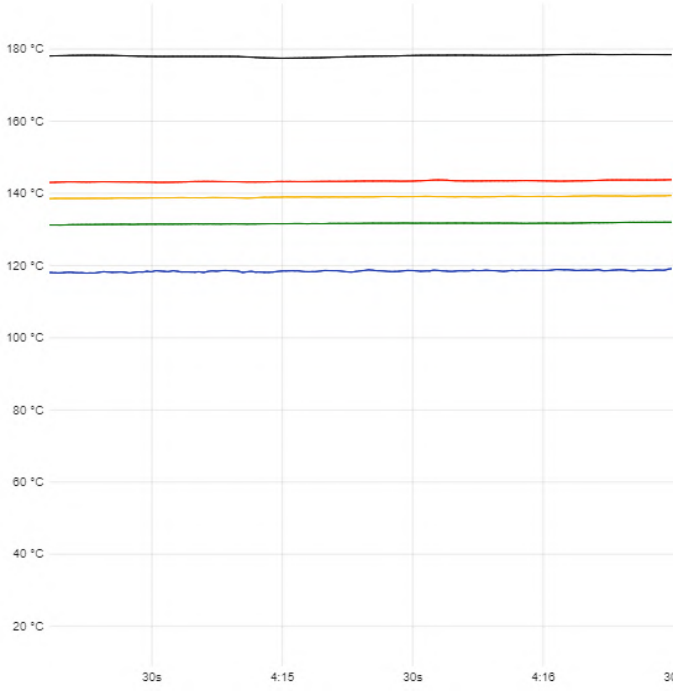

Figure C.22: MHP High Test 7

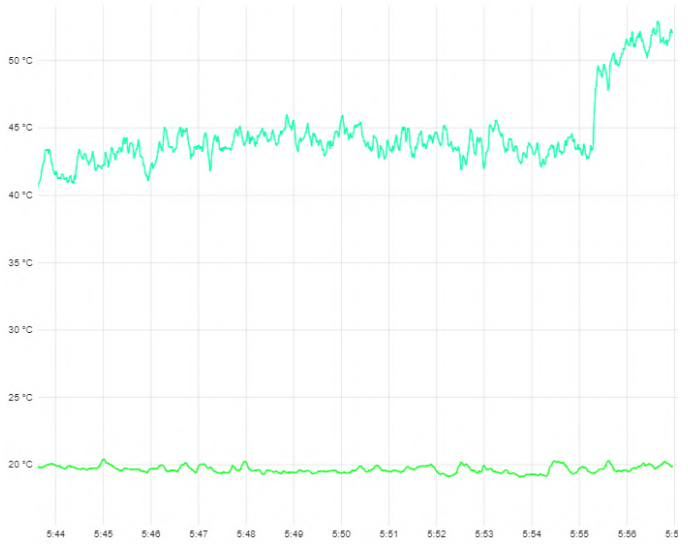

Figure C.23: BioHP High Level Fan Data

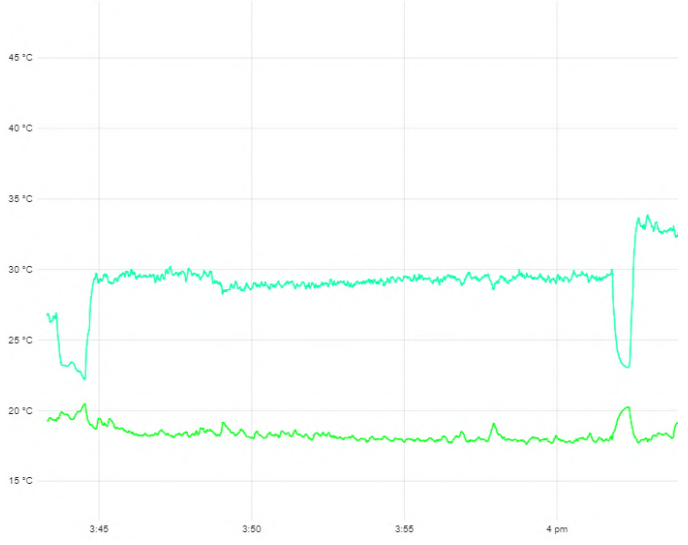

Figure C.24: THP High Level Fan Data

INVESTIGATION OF A BIOMIMETIC HEAT PIPE DESIGN FOR IMPROVED HEAT TRANSFER IN SPACE RADIATORS

by

Owen Telford